

Study of Hybrid Semiconductor Nanoclusters and Hydrogen Storage Materials by using Density Functional Theory

Thesis

Submitted in partial fulfillment of the requirements for the degree of

Doctor of Philosophy

by

Ravi Kumar Trivedi

2011PHXF029P

Under the Supervision of

Prof. Debashis Bandyopadhyay



**BIRLA INSTITUTE OF TECHNOLOGY & SCIENCE PILANI
PILANI (RAJASTHAN) INDIA**

2016

dedicated to

my parents

&

those from whom I have learnt

BIRLA INSTITUTE OF TECHNOLOGY AND SCIENCE, PILANI

CERTIFICATE

This is to certify that the research work presented in the thesis entitled “Study of Hybrid Semiconductor Nanoclusters and Hydrogen Storage Materials by using Density Functional Theory” by Ravi Kumar Trivedi, Department of Physics, BITS Pilani, Pilani campus for the award of the degree of Doctor of Philosophy (Ph.D.), is carried out under my guidance and supervision and is fit to be considered for the award of the degree of Ph.D. No part of the present thesis work has ever been submitted in part or in full to any other university or institution for the award of any other degree or diploma.

Date:

Supervisor

(Prof. Debashis Bandyopadhyay)
Department of Physics
BITS, Pilani Pilani Campus
Rajasthan- 333031, INDIA

ज्ञानं परमं बलम्

Acknowledgement

It is a great pleasure for me to acknowledge the assistance and contributions of many individuals in making this dissertation a success.

First and foremost, I would like to thank my supervisor, Professor Debashis Bandyopadhyay, for his assistance, ideas, and feedbacks during the process in doing this dissertation and also for encouraging my research and allowing me to grow as a research scientist. Your advice on both research as well as on my career have been priceless. Without his guidance and support, this dissertation cannot be completed on time.

Besides my advisor, it is a pleasure to express my heartfelt thanks to my DAC members Dr. Jayendra Nath Bandyopadhyay and Dr. Srijata Dey for sparing their time to participate in this study. I deeply appreciate their helpfulness and willingness in providing the useful information for this study.

I am grateful to Prof. V. S. Rao, acting Vice-Chancellor and Director Prof. A. K. Sarkar (Pilani campus), for allowing me to carry out my doctoral research work in this privileged institute.

I am thankful to Prof. Sanjay Kumar Verma, Dean, Academic research (Ph.D. programme), BITS, Pilani, for his co-operation and encouragement at every stage of this research work.

I would like to express my deep gratitude to Dr. D.D. Pant, Head of Physics department, for providing me all the necessary departmental facilities at various stages of my research work. It has been my pleasure to be taught by the excellent teachers like Dr. Subhash karbelkar, Dr. Rajkumar gupta, Dr. Kunal Bhattacharya and Dr. Rakesh choubisa during the course work. I am heartily thankful to all of them for helping me in understanding the concept of physics.

I am deeply grateful to Dr. Prasenjit sen, for allowing me to use their computational facilities at HRI Allahabad and for his valuable suggestions during all phases of my work.

A deep gratitude to Prof. Hemant Jadhav (Associate Dean: Academic Research), for his encouragement and support during this Ph.D. tenure.

I am thankful to the office staff of Research and Consultancy Division Mr. Mahipal, and Mr. Raghuvir for all the help and good wishes.

I express my deep thanks to the office staff of Physics Group, BITS Pilani, including Mr. Srikant Sharma and Mr. Rajiv Gaur for providing all the necessary support whenever needed.

I would like to acknowledge research scholar, Munesh Rathore, Amar Singh, Sunita Joshi, Jitendra Kumar, Keerti Choudhary, Monika Poonia, Surender, Tridev Mishra, Aashis Pal, Sumita, Shivani Choudhary, Tej Varma, Mandeep Singh and Sachin for their friendship, love and valuable time spent with me to make this duration memorable.

Special thanks to my colleague Kapil, who did a lot of help to me during this entire research work. At hard times we did a valuable and numerous discussions related to the research work that has supported a lot.

A special thanks to my family. Words cannot express how grateful I am to My mother and father for all of the sacrifices that they've made on my behalf, My sisters for supporting me spiritually throughout writing this thesis and my life in general.

Last but not the least I would like express appreciation to my beloved wife Varsha, who entered in my life at the initial stage of the Ph.D work, was always my support and help as well as encouragements.

Ravi Kumar Trivedi

ABSTRACT

Nanostructures of silicon and germanium are currently of great interest because of its future applications in nanodevices, sensors, germanium and silicon based optoelectronics, biological systems, and possibilities of cluster assembled materials and superatoms. A detailed research has been done on silicon and germanium based clusters. The thesis sheds light onto these systems from a theoretical perspective. The density functional theory, a successful material specific theory is used for describing the structure, growth, stability, electronic, chemical and physical properties of pure and transition metal doped germanium nanoclusters. In the present research work, first the method is applied for the pure and transition metal doped germanium nanoclusters of different size and shape, and then optimized through the interaction between the atoms in the clusters to search for the stable cluster of different sizes. The accepted optimized model of different structures is then critically examined using comparisons of energetic stability and types of chemical bonding present in the clusters. To check the structural and chemical stabilities of the optimized nanoclusters, different parameter like binding energy (BE), Fragmentation energy (FE), Vertical ionization potential (VIP), Vertical electron affinity (VEA), IR and Raman spectrum and nucleus independent chemical shift (NICS) have been calculated. After the confirmation of the stability of some of the structures, few selected transition metal doped germanium clusters are used to form superatom which are useful from application point of view.

In the later part of the thesis, we applied first principle method for hydrogen storage materials which is future energy solutions. Hydrogen is a promising clean energy carrier, and thereby it has attracted lot of interest among scientific communities, government organizations and industries. One of the primary technical challenges is the lack of economic, effective and safe hydrogen storage medium, Therefore, storage of hydrogen in solid-state materials offers an alternative way. The use of magnesium based system is considered as one of the promising hydrogen storage material, which leads to lightweight materials, low cost and having high hydrogen storage capacity. In this research work we found some transition metal doped magnesium based nanoclusters which can store hydrogen as an energy source. Based on the calculated parameters like chemisorptions and physisorption energy, reaction energy and the relaxation of H-H bond length, the most suitable size and composition have been identified as the most specific hydrogen storage element in the nano-order dimensions.

TABLE OF CONTENTS

	<i>Page No.</i>
<i>Acknowledgement</i>	<i>IV</i>
<i>Abstract</i>	<i>VI</i>
<i>Table of contents</i>	<i>VII</i>
<i>List of tables</i>	<i>X</i>
<i>List of figures</i>	<i>XI</i>
<i>List of abbreviations</i>	<i>XII</i>
Ch. 1 - Introduction	1-11
1.1 Permeable	1
1.2 Clusters, properties and the goal of the cluster science	2
1.3 Literature review and research gap	4
1.4 References	9
Ch. 2 – Theoretical background of DFT	12-26
2.1 Foundation of density functional theory	12
2.1.1 Hartree Fock approximation	12
2.1.2 Hohenberg- Kohn thorem	13
2.1.3 Kohn-Sham approach	15
2.1.4 Schrodinger equation	16
2.1.4 Born-Oppenheimer approximation	18
2.1.5 Principle of anti-symmetry	19
2.1.6 Variational principle	19
2.1.7 Functional	19
2.2 Basic machinery of DFT	20
2.2.1 Local density approximation (LDA)	20
2.2.2 Slater determinant	21
2.2.3 Basis sets	22
2.2.4 Self consistent field procedure	23
2.2.5 Exchange-correlation functional	24
2.3 Methodology	25

2.4 References	26
Ch. 3 - Study of electronic properties, stabilities and magnetic quenching of MoGe_n (n = 1-20) clusters: A density functional investigation	27-51
3.1 Introduction	27
3.2 Computational details	28
3.3 Results and discussions	29
3.3.1 Electronic structure and stabilities	34
3.3.2 Nucleus-independent chemical shift (NICS)	46
3.4 Conclusions	47
3.5 References	50
Ch. 4 - Role of NICS and shell closing model in the stability of neutral and cationic NbGe_n (n = 7-18) clusters: A density functional investigation	52-67
4.1 Introduction	52
4.2 Computational details	53
4.3 Results and discussion	53
4.3.1 Electronic structure and stability	54
4.3.2 NICS and orbital of neutral NbGe ₁₂ and cationic NbGe ₁₆	60
4.3.3 IR and Raman spectrum	63
4.4 Conclusions	65
4.5 References	76
Ch. 5 - Hydrogen storage in small size Mg_nCo (n = 1-10) clusters: A density functional study	68-86
5.1 Introduction	68
5.2 Computational details	71
5.3 Results and discussions	71
5.3.1 Minimum energy structures and stability	76
5.3.2 Physisorptions and chemisorptions energy	79
5.3.3 H ₂ dissociation mechanism (IRC path)	81
5.4 Conclusions	83
5.5 References	84
Ch. 6 - Study of adsorption and dissociation path way of H₂ molecule on Mg_nRh (n = 1-10) clusters: A first principle investigation	87-104
6.1 Introduction	87
6.2 Computational details	89

6.3 Results and discussions	89
6.3.1 Energetics and stability	90
6.3.2 Physisorptions and chemisorptions energy	96
6.3.3 Activation path for hydrogen dissociation	99
6.4 Conclusions	101
6.5 References	102
Ch. 7 - Summary and Future scope	115-109
<i>Appendix (A-C)</i>	110-121
<i>List of relevant Publications</i>	122
<i>List of conference and workshop attended</i>	122
<i>Biography of the supervisor</i>	123
<i>Biography of the candidate</i>	124

List of Tables

Table No.	Title of Table	P.No.
Table 3.1	Bond length (Å) and lowest frequencies (cm ⁻¹) of Ge-Ge, Mo-Mo and Ge-Mo dimer	29
Table 3.2	Natural electronic configuration [NEC] in MoGe ₁₂ cluster	39
Table 4.1	Bond length (Å) and lowest frequencies (cm ⁻¹) of Ge-Ge, Nb-Nb dimer	51
Table 4.2	IR and Raman spectra of NbGe _n (n = 10-15) clusters	64
Table 5.1	Bond lengths (Å) and frequencies (cm ⁻¹) of Mg-Mg, Co-Co and H-H dimer	71
Table 5.2(a)	Bond lengths (Å) of Mg _n , Mg _n Co, Mg _n Co-H ₂ and H ₂ -Mg _n Co clusters	75
Table 5.2(b)	Binding energy (BE), Fragmentation energy (FE) and HOMO-LUMO gap (eV) Mg _n , CoMg _n , Mg _n Co-H ₂ and H ₂ -Mg _n Co clusters	75
Table 5.3	Vertical ionization potential (VIP) and Vertical electron affinity (VEA) of clusters	78
Table 5.4	Adsorption energy, H-H bond length (Å), Co-H bond length (Å) and HOMO-LUMO gap (eV) of physisorption system	80
Table 5.5	Location of H, Multiplicity, H-H Bond length (Å), HOMO-LUMO gap (eV) and chemisorptions energy is shown	80
Table 5.6	Reaction energy (ΔE ₀) including zero point energy (kcal/mol), activation barrier (kcal/mol) and frequency (cm ⁻¹)	82
Table 6.1	Bond lengths (Å) and frequencies (cm ⁻¹) of Mg-Mg, Rh-Rh and H-H dimer	90
Table 6.2(a)	Bond lengths (Å) of Mg _n , RhMg _n , Mg _n Rh-H ₂ and H ₂ -Mg _n Rh clusters	94
Table 6.2(b)	Binding energy (BE), Fragmentation energy (FE) and HOMO-LUMO gap (eV) Mg _n , RhMg _n , Mg _n Rh-H ₂ and H ₂ -Mg _n Rh clusters	94
Table 6.3	Vertical ionization potential (VIP) and Vertical electron affinity (VEA) of clusters	96
Table 6.4	Adsorption energy, H-H bond length (Å), Rh-H bond length (Å) and HOMO-LUMO gap (eV) of physisorption system	97
Table 6.5	Location of H, Multiplicity, H-H Bond length (Å), HOMO-LUMO gap (eV) and chemisorptions energy is shown	98
Table 6.6	Reaction energy (ΔE ₀) including zero point energy (kcal/mol), activation barrier (kcal/mol) and frequency (cm ⁻¹)	99

List of Figures

Figure No.	Figure Title	P.No.
Figure 3.1(a)	Optimized ground state structures of MoGe _n (n=1-20) clusters with point group symmetry. Blue balls are Ge and yellow balls are Mo atoms.	31-33
Figure 3.1(b)	Different valence orbital's of MoGe ₁₂ in neutral and different charged state	33
Figure 3.2	Variation of average binding energy of the MoGe _n clusters with the cluster size (n)	34
Figure 3.3	Variation of (a) embedding energy (EE) and ionization potential (IP), (b) stability, and (c) fragmentation energy (FE) of neutral and cationic MoGe _n clusters with the cluster size (n)	37
Figure 3.4	Density of states of ground state MoGe ₁₂ cluster and it's orbital with their position in DOS	40
Figure 3.5	Variation of (a) chemical potential and chemical hardness and (b) polarizability and electrostatic dipole moment of MoGe _n clusters with the cluster size	45
Figure 3.6	NICS plot of MoGe ₁₂ cluster	47
Figure 4.1	Optimized ground state structures of NbGe _n (n=1-20) clusters with point group symmetry. Blue balls are Ge and yellow balls are Nb atoms.	55-56
Figure 4.2	Variation of (a) Binding energy, (b) stability, (c) fragmentation energy (d) HOMO-LUMO gap and of NbGe _n ⁺ and NbGe _n with the number of germanium atom.	59
Figure 4.3	Variation of Vertical ionization potential (VIP), Adiabatic ionization potential (AIP) and Vertical electron affinity (VEA), Adiabatic electron affinity (AEA) with number of germanium atom.	60
Figure 4.4	NICS plot of NbGe ₁₂ cluster	61
Figure 4.5	Orbital plot cationic NbGe ₁₆ cluster	62
Figure 5.1	Optimized ground state isomers of CoMg _n , Mg _n Co-H ₂ and H ₂ -Mg _n Co clusters (n=1-10). Dark purple balls are Mg atom, green balls are Co atom and small red balls are H atoms. Superscript indicates the multiplicity of the clusters.	73
Figure 5.2	Variation of Binding energy and stability of CoMg _n and H ₂ -Mg _n Co clusters with the number of magnesium atom	76
Figure 5.3	Variation of chemical potential and chemical hardness; VIP and VEA of different clusters with number of magnesium atom	79
Figure 5.4	Potential energy surface of H ₂ -Mg ₅ Co clusters	82
Figure 6.1	Optimized ground state isomers of RhMg _n , Mg _n Rh-H ₂ and H ₂ -Mg _n Rh clusters (n=1-10). Dark purple balls are Mg atom, green balls are Rh atom and small red balls are H atoms. Superscript indicates the multiplicity of the clusters.	91
Figure 6.2	Variation of Binding energy and stability of RhMg _n and H ₂ -Mg _n Rh clusters with the number of magnesium atom	93
Figure 6.3	Variation of chemical potential and chemical hardness; VIP and VEA of different clusters with number of magnesium atom	95
Figure 6.4	Potential energy surface of H ₂ -Mg ₉ Rh clusters	100

List of Abbreviations

η	Chemical hardness
$\bar{h}_c(r'/r)$	Coupling constant averaged correlation hole
$\bar{h}_{xc}(r' r)$	Coupling constant averaged exchange-correlation hole
$\hat{V}_\lambda[\rho]$	Modified standard potential operator
$h_c(r' r)$	Correlation hole
$h_x(r' r)$	Exchange hole
$h_{xc}(r' r)$	Exchange-correlation hole
V_{xc}	Exchange-correlation potential energy
$V_{int}^{(S)}$	Non-interacting internal potential energy
$v_{xc}(r)$	Exchange-correlation potential energy per electron
$v_{int}(r)$	Internal potential energy per electron
$\varepsilon_{xc}(r)$	Exchange-correlation energy per electron
$\mu_H(r)$	Hartree Potential
$\mu_{KS}(r)$	Kohan-Sham potential
$\mu_{loc}(r)$	local potential
$\mu_\lambda[\rho](r_n)$	Fictitious external potential
ΔE	HOMO-LUMO gap
ΔE_2	Stability
<i>B3LYP</i>	Becke, three-parameter, Lee-Yang-Parr
<i>B3PW91</i>	Becke, three-parameter, Perdwe-Wang 91
<i>BE</i>	Binding energy
<i>CI</i>	Configuration interaction
<i>DFT</i>	Density functional theory
<i>EAs</i>	Electron affinities
<i>E_c</i>	Correlation energy
<i>ECP</i>	Effective core potential
<i>EE</i>	Embedding energy
<i>E_{GS}</i>	Ground state energy

E_{var}	Variational energy
E_{xc}	Exchange-correlation energy
$F[\rho]$	Functional of densities
$FE/\Delta(n,n-1)$	Fragmentation energy
FK	Frank-Kasper
$GGAs$	Generalised gradient approximations
HEG	Homogeneous electron gas
$HOMO$	Highest occupied molecular orbital
IP	Ionization Potential
IR	Infrared
LDA	Local density approximation
$LUMO$	Lowest unoccupied molecular orbital
$P_n(i)$	Permutation operator
QMC	Quantum Monte-Carlo
SCF	Self-consistent-field
T_C	Correlation kinetic energy
T_S	Non-interacting kinetic energy
V_C	Correlation potential energy
V_{ext}	External potential energy
V_H	Hartree energy
V_{int}	Internal potential energy
V_X	Exchange energy
WW	Wigner-Witmer
A	Electron-electron coupling constant
M	Chemical potential
$\rho(r)$	Density of electrons
ρ_{GS}	Ground State density
Ψ_S	Full wave function

CHAPTER 1

1.1 Preamble

Nanoclusters, consisting of a few to a few hundreds of atoms have attracted attention because of their importance in nanoscience and nanotechnology. The nanoclusters are considered as the new phase of matter where the properties are very much sensitive to the size and composition. Effectively nanoclusters are a bridge between bulk materials and atomic or molecular structures. The physical and chemical properties of bulk material are independent of its size, whereas, at the nanoscale stage, the size-dependent properties are often observed. Hence, tailoring of their electronic properties is easy to achieve by varying the composition, size, and structures. After the advent of laser vaporization techniques, studies of metal and semiconductor nanoclusters are becoming more interesting. The present high performance characterization experimental tools have been applied to determine the structures of nanoclusters and it has contributed important information in nanotechnology and nanoscience. To understand the science behind their electronic structures and properties, the computational modeling using different quantum mechanical techniques have been developed. Due to quantum confinement effect, the physical and chemical properties of nanoclusters are different from those of bulk materials as we mentioned. Ab-initio first principle quantum mechanical calculation of theoretically predicted optimized nanoclusters motivates experimentalists to produce nanostructures of particular interest on the basis of the theoretical understanding. Over the last several years, different metal and semiconductor binary nanoclusters have been studied [1-7] using small atomic clusters as constituent elements to build up relatively bigger and well-controlled nanostructure. To reduce the size of the devices, silicon and germanium nanoclusters have been extensively investigated, both experimentally and theoretically [4-7]. Sometimes it is found that chosen stable clusters with a specific composition can mimic the chemical property of an atom or a group of elements in the periodic table. This major finding, known as the superatom concept, came from the study of aluminum clusters [8-9] where interesting size-dependent reactivity is noted. On the other hand, to solve problems in renewable energy field, metal clusters are very much useful as hydrogen storage elements. In both cases, theoretical predictions of the nanoclusters are very much important to model and design the appropriate materials based on demand. These are not always possible only experimentally in a controlled manner because of high probability of reaction affinity of the small size clusters. So, theoretical prediction of hybrid nanoclusters and their characterization are very hot topic of research at the present age.

Therefore, both experimental as well as theoretical research in the field of nanoscience and technology are essential in the development of this field.

1.2 Clusters, properties and the goal of the cluster science

In the last few decades, cluster science has become a rapidly growing interdisciplinary field of study with the advancement of experimental, theoretical and computational techniques. Therefore, research on the cluster science has increased rapidly. There are several reasons for that. Firstly, clusters provide a bridge between the limits of isolated atoms, molecules and bulk matter. Therefore, it is interesting to study the evolution of the cluster properties with size in a particular composition. Such knowledge provides a new viewpoint and this would improve the understanding of the behavior that occurs at the more familiar limits. This enthusiasm is still a primary influential force for cluster science and also this thesis will touch upon some aspects of the size evolution of cluster properties. A second motivation in the cluster science is to study the reasons behind the nucleation at an atomistic level, which can form thermodynamically and chemically stable structures. Most of the current works in this area is now no longer directed at clusters as a model of a (critical) nucleus, but instead of clusters as an environment in which nucleation can occur on faster time scales and for which only a single nucleation event is required to transform the cluster.

As we have mentioned that nanoclusters are mesoscopic particles ranging from few to few hundreds of atoms in size. In contrast to the free molecule in gases, the condensed phases of matter are called as liquid, crystalline, solids and glasses depending on their properties on the constant proximity of all their constituent atoms. Weakly bound solids, such as solid carbon dioxide or their liquid counterparts, are made up of molecules whose properties differ a little from the properties of the same molecules in gaseous phase. These are called Van der Waals solids. Another type of bonding found in condensed matter where ionic compounds are held together by the mutual attraction of the opposite charged ions. Further, metallic bonding is another type in which electrons moving between the positive atomic cores form an electron cloud. The attraction between the positive cores and the negative charges is responsible for holding metals together. Clusters are aggregates of atoms, molecules or ions that adhere together under forces is mentioned above that bind the atoms, ions or molecules. The difference is due to the most stable structure in small size clusters and bulk solids which is their most stable form. In the small sized clusters and nanoclusters, the structural periodicity is absent which is must in crystal lattice in i.e. in bulk. The most common geometries that are present in the nanoclusters are in the form of icosahedrons, incomplete icosahedrons, hexagonal prism structures, or anyother polyhedral structures. In general, these clusters cannot grow in the form of periodic lattices. But appropriate modeling can form cluster assembled materials in the form of 1-D nanotubes or 2-D planer

structures using these nanoclusters. Some properties of these clusters reflect their quantum confinement effect, which is rarely found in bulk. One such property is the nature of the energy levels occupied by the electrons. Clusters containing only a small number of metallic atoms have very few available discrete quantum states. In this sense, small stable clusters of metal atoms are sometimes look like a molecule with much bigger size and having specific important character, such as, magnetic moment, ionization potential, etc. These clusters are known as the superatomic clusters.

In the cluster science, study of the electronic and thermodynamic stability, electronic, magnetic and optical properties are of main interest. In a particular size and composition, there may be a number of isomers, and among these isomers, one would be the most stable which is known as ground state isomer. Such unusual stability suggests that its interpretation should be associated with the closing of electronic shells or energy levels. The overall structure that determines the clusters stability is generally called its shell structure. When atoms form a lattice, the discrete energy levels of the atoms are smudged out into energy bands. The term density of states refers to the number of energy levels in a given interval of energy. For a metal, the top band is not totally filled, in the case of a semiconductor the top occupied band called the valence band, is filled and there is a small energy separation referred to as the band gap between it and the next higher unfilled band. When the size of bulk metal is reduce in the size to a few hundred of atoms, the density of states in the conduction band, and the top band containing electrons change dramatically. The continuous density of states in the band is obtained by introducing finite width to a set of discrete energy levels, spacing larger than the thermal energy. A small cluster is analogous to molecule having discrete energy levels with bonding and antibonding orbitals, and the size is of the order of the wavelength of an electron. In this situation, the energy levels can be modeled by quantum mechanically treating a particle in a box. This is referred to as the quantum size effect. Cluster of atoms bound by Vander Waals force or by other simple forces depending only on the distance between each pair of atoms have unusual stability when the cluster has exactly the number of atoms needed to form regular icosahedrons. The shell structure, that provides special stabilities in this class of clusters, is determined by the individual stability of the shells of the atoms themselves. In simple metal clusters, the electrons and the filling of those shells that have energy states available to the electrons, determine the shell structure. The numbers of electrons corresponding to closed electron shells in metal clusters are 2, 8, 20, 40, 58, 68, 92, and 126. The electronic shell structure can be modeled by assuming that the positively charged cores consisting of the protons and inner-shells electrons of all the clusters which smeared out into a continuous shell structure. Here, the electron-counting rule plays an important role to understand the stability of the clusters.

The significant properties of clusters are their electric, magnetic, and optical behavior where the size and composition of cluster plays an important role. As we know, quantum mechanics predict the wavelike character of matter. This wavelike behavior is detectable only when the matter is examined on the scale of nanometer or less. In fact, we can say that quantum properties play a major role in determining the electronic behavior of the cluster. In particular, since the size of the clusters is so small, the energy levels or quantum states of the electrons are not close enough to permit the cluster to behave like a bulk. Magnetic properties of cluster depend only on the number of unpaired electrons, holding by the clusters. The optical properties of the weakly bound clusters are much like those of their component atoms or molecules. The small differences in frequencies between the component elements and the clusters are frequently used to analysis of how the cluster is bound and what its structure may be. However, the optical properties of metal clusters are similar to the corresponding bulk metals than its constituent atoms. Sometimes, these properties help to identify the stable clusters.

Much work has been reported on the properties of the nanoclusters. However, it is still driven by the prospect that a fundamental understanding of the properties, particularly the chemical reactivity of metal clusters, could have far-reaching consequences for catalysis. Small metal particles and clusters (supported, for instance, within a zeolite) could provide both a large surface area to volume ratio and the properties, such as activity and selectivity, which have been tailored to catalyze a specific reaction [10-11]. With this background of understanding of cluster, the present thesis focuses on the main two research fields in the cluster science.

The thesis consists into seven chapters. First and second chapters discuss introduction and methodology. In the following chapters (chapter 3 to chapter 6) the research works have been described. In chapters 3 and 4, the work related to the investigation and analysis of the inherent science of the stability of the clusters and super atoms are presented. The next two chapters (chapters 5 and 6) are practical application oriented, where the possibility of metal clusters have been investigated to use it as an effective nanocluster based hydrogen storage elements to solve the possible fuel problems. The last chapter describes the summery and future scope of the present work.

1.3 Literature review and research gap

The major thrust of cluster science is to produce a wide variety of nanostructure materials and understand their properties. Metal clusters, which are studied theoretically and experimentally, have drawn extensive attention in different field because of their attractive physical and chemical properties [12-15]. Recent finding of Os cluster [16] can be used as catalysts for methane dissociation and hydrogenation, which act as an aid in further experimental

and theoretical studies. Low lying structure of small iridium clusters have been investigated by Chen et al. [17]. Zhang et al. [18] identified the geometrical and magnetic properties of Tb_n cluster and found that local spin magnetic moment exhibits a weak dependence on the cluster size. In particular, research on mixed metal clusters has become an advanced topic in cluster science [19]. The structural, electronic and magnetic properties of Sc, Ti doped Au cluster shows that the electronic properties of the golden cage can be systematically tuned through doping. It can be used in electronic devices for tuning [20]. Investigation of the Cr doped Au cluster by Dong et al. [21] found that the cluster has magnetic moment which can be used as a magnetic storage device. Magnetic properties of small sized Pt capped Fe, Co and Ni clusters have been studied by Sahoo et al. [22]. Current findings of uranium encapsulated Au_{14} [23] cage provide a theoretical basis for future synthesis and further study of mixed cluster, which might subsequently facilitate application of radio-labeling which is another biomedical application.

Among the clusters of different compositions, study of pure and hybrid semiconductor nanoclusters has attracted a lot of theoretical and experimental attention due to their potential applications in the electronic industries [24-27]. However, pure semiconductor clusters are chemically reactive due to the presence of unsaturated dangling bonds on the cluster surface. There are two ways to saturate the dangling bonds on Si and Ge cluster, first encapsulation of transition metal (TM) in the cage [28], and second, the addition of hydrogen atoms exohedrally [29]. Involving these two, it has been observed that, encapsulation of transition metal in semiconductor cage cluster is very effective for saturating the dangling bonds of Si and Ge cage clusters [30]. The first experimental contribution to this field was made by Beck [31] who found that the transition metals (TM) such as Cr, Mo, W etc in silicon cluster enhance the stability of the doped cluster. Recent reports on metal encapsulated caged cluster of silicon [32-33] and germanium [34-35] have opened new avenues to develop different nanostructures which may have many applications in the field of electronics and luminescence. The transition metal doping has proven to be effective to tune the optoelectronic, magnetic properties and stability of the host clusters [36]. The structural, optical, and magnetic properties of Cu, Ag and Au doped silicon clusters have been investigated systematically by Ma et al. [37] and found that the clusters have potential application in magneto-optics and photovoltaic cells. Recent study suggests that the physical and chemical properties of silicon cluster can be easily adjusted by changing their sizes, and shapes [38, 39]. The role of the d shell and the atomic radii of the dopant atoms in the cage formation of the transition metal doped Si cluster have been investigated by Li et al. [40]. A theoretical study of Yang et al. [41] predicts the lowest energy structure of Au_nSi ($n = 16-20$) has the Si atom bound to the exterior surface of an Au_n cage. The structural, electronic, and magnetic properties of $TMGe_n$ ($TM = Mn, Co, \text{ and } Ni$) have been studied by

Neha et al. [42] which showed that the TM atom always prefers to occupy surface position for $n < 9$ and endohedral position for $n \geq 9$. The magnetic properties of TM doped germanium clusters offer a new direction for further improvements. Study of lowest energy structure of neutral and cationic transition metals Au, Ag, Yb, Mn, Fe doped germanium cluster can be altered by varying the element of the cage itself or transition metal atom. It also suggests that Ge_9Fe and Ge_{10}Fe would be useful as the building blocks in cluster assembled nanomaterials due to their high stability [43]. The findings of metal encapsulated germanium cage clusters led to a renewed interest. Recent theoretical investigation on Cr doped germanium cluster [44] explains the origin of magnetic moment in the clusters which is mainly localized at the Cr atom. Kapil et al. [45] performed a systematic study on Ni doped germanium clusters within the frame work of linear combination of atomic orbital shed light on the design of Ge based superatom. To explain the relative stability, chemical, and vibrational properties of cluster, Manish et al. [46] performed a theoretical calculation on transition metal (TM = Ti, Zr and Hf) doped cluster and found that the metal doped fullerene like clusters are chemically stable. Jorg et al. [47] presented a combined theoretical and experimental study on lithium doped germanium cluster and analyzed the chemical properties in detail using density of states and molecular orbitals. Effects of size selectivity on the geometry and electronic properties of bimetallic Au-Ge nanocluster has been studied by Xiaojun et al. [48], and demonstrated that the induced effect by an additional electron in the neutral cluster enhances their stabilities. Deng et al. [49] have studied the structural, electronic and magnetic properties of VGe_n ($n = 3-12$) cluster using anion photoelectron spectroscopy in combination with DFT and gave a detail description on charge transfer mechanism and the minimization of the clusters. They have [50] also investigated the structural and magnetic properties of Co doped germanium anion clusters using photoelectron spectroscopy. Recently Ravi et al. [51] investigated the stability, electronic and magnetic quenching of Mo doped Ge_n cluster using density functional theory and found that the MoGe_{12} with hexagonal prism-like structure is the most stable isomer and possesses strong aromatic character. Magnetic quenching of the Mo atom with increase of the clusters explained by means of strong hybridization between d orbital of Mo with p and s orbitals of Ge cage. Recently, the atomic and electronic structure of both neutral and negatively charged ZrGe_n ($n = 1-21$) cluster have been studied by Vijay et al. [52], this study provides a platform for further study of charged germanium cluster. These studies of transition metal encapsulated clusters of germanium have shown that, in general, the growth behavior, electronic and magnetic properties are very sensitive to transition metal doping as well as the size of the cluster.

One of the major elaborations of the past few decades was the identification of cluster science as a field that has a huge impact on science and technology. Attributable to the reduced size and related phases of quantum confinement, an exciting achievement in cluster science is the realization that chosen stable clusters can mimic the chemical property of an atom or a group of elements in the periodic table. This major finding, known as the superatom concept is explained by the Zhixun and Castelman [8-9]. Torres et al. [53] have studied the structural and electronic properties of MSi_{16} ($M = \text{Sc}, \text{Ti}, \text{V}^+$) superatom which can serve to grow low dimensional system. Shell magnetism in transition metal doped calcium superatom has been investigated by Vikas et al. [54]. They reported a stable magnetic FeCa_8 cluster with 24 valance electrons distributed following a closed shell sequence. The last four electron occupying the majority $2D_{xy}$, $2D_{x^2-y^2}$, $2D_{xz}$ and $2D_{yz}$ levels while the unfilled $2D_z^2$ level is separated by a large energy due to atomic deformation and exchange splitting. A study on 4d transition metal doped Mg_n clusters (TcMg_n) was reported by Xian et al. [55], where they explained the enhanced stability of TcMg_8 cluster with high magnetic moment having a closed shell electronic configuration $1S^2, 2P^6, 1D^{10}$. A recent [56] theoretical study of the doping of Zn_{17} nanoparticle with transition metal impurity ($\text{TM} = \text{Sc}, \text{Ti}, \text{V}, \text{Cr}, \text{Mn}, \text{Fe}, \text{Co}, \text{Ni}$ and Cu), has investigated and Zn atomic environment found to be spin polarized and modulates the total spin moment of these molecular magnets depending on the induced moments and magnetic coupling. The existence of designer magnetic superatom VNa_8 has been studied by Khanna et al. [57], and they have found that VNa_8 is a magnetic superatom with a filled d-subshell and magnetic moment of $5\mu\text{B}$. This opens a pathway to investigate the spin dependent electronics of the new magnetic motifs. Its low electron affinity is consistent with filled subshell and enhanced stability. Recent finding of Al_{12}Cu superatom by Reveles et al. [58] can be used as stable building blocks of ionic salt. Zhang et al. [59] have demonstrated a first principle investigation for magnetic superatom in the vanadium doped lithium clusters. Molecular orbitals analysis shows that VLi_8 has an electronic configuration $1S^2 1P^6 1D^5$, exhibiting Hund's rule that can be used for magnetic building blocks for nanomaterials. Similarly, using an ab-initio computational technique on cluster, Acevedo et al. [60] have studied the gold, aluminium, and gallium superatom complexes, that gives further insight into the superatom analogy in the class of ligand metal clusters. The superatom may be used to create molecular electronic devices for the next generation of faster computers with large memory storage. Using magnetic superatom, it is expected to develop volatile data storage, denser integrated devices, and higher data processing.

The exploration of transition metal doped magnesium cluster for hydrogen storage has been an important and active area of research. So hydrogen storage in metal hydride is the focus of chapters 5 and 6. Varano and

Henery have [61] investigated the hydrogen adsorption on magnesium doped aluminium clusters using DFT method. Recent study on small metal clusters [62, 63] shows that they can be used as a process of hydrogen dissociation. These theoretical studies have shown that how the number of atoms, shape, and the particular electronic spin state in small clusters can drastically change the ability to dissociate hydrogen molecule from the clusters surface. A DFT approach has been studied for use some metal clusters as hydrogen storage materials in detail by Giri et al. [64]. They have explained the capacity of metal cluster to trap hydrogen molecules. Theoretical investigation of adsorption and dissociation of H₂ on (ZrO₂)_n (n= 1-6) clusters have been investigated by the Jin et al. [65] They have found that the absorption favors the sites with low coordinate number and increasing H-H bond length that helps to dissociate hydrogen molecule on the surface. Srinivasu et al. [66] have performed a systematic study on molecular hydrogen adsorption in binary metal system using ab initio quantum mechanical calculation. Stability of transition metal on Mg surface and their effect on hydrogen adsorption have been studied by Chen et al. [67] and they have found that TMs doping with second layer on Mg surface is generally more stable than that on clean Mg but weaker than TMs in the first layer. This favors the peripheral positions of TMs atom. Fanjie and Yanfei [68] have reported the electronic, structural and magnetic properties of Mg_nX cluster (X= Fe, Co, Ni) and they have found that TMs atom is endohedrally localized in Mg_nX clusters. Recently, Guo [69] has investigated the possible dissociation mechanism and dissociation pathway of H₂ on Al_nCr (n = 1-13) clusters, and characterizes the hydrogen dissociation behavior by the activation number and reaction energy. This study provides a theoretical approach of TM metal doped clusters as highly efficient and cost effective catalysts for hydrogen dissociation. Mananghaya [70] has reported the implementation and effectiveness of the ability of nitrogen doped carbon nanotube (4ND-CN_xNT) decorated with Sc for hydrogen storage under the spin-unrestricted density functional theory. Detailed structural and electronic properties are reported starting from one to five hydrogen molecules absorbed by the system.

Investigation of nano clusters have been carried out experimentally and theoretically in numerous ways. As a results ,wide variety of materials are found with wide range of structural,optical,electroni can dmagnetic properties.

[1] No systematic investigation on the growth pattern mechanism for TM metal doped germanium and silicon nanoclusters were reported in the literature.

[2] It is quite important to study the electronic, thermodynamic and chemical behavior of different TM doped germanium and silicon nanoclusters to predict the superatom.

[3]Study of small sized metal clusters that can be used as effective nanocluster based hydrogen storage elements to solve the possible fuel problems.

1.4 References

- [1] Khanna SN, Rao BK, Jena P, Phys Rev Lett, **2002**; 89: 016803.
- [2] Jarrold MF, Constant VA, Phys Rev Lett, **1991**; 67: 2994.
- [3] Ho KM, Shvartsberg AA, Pan B, Lu ZY, Wang CZ, Wacker J G, Fye JL, Jarrod MF, Nature, **1998**; 392: 582.
- [4] Shvartsberg AA, Jarrod MF, Phys Rev A, **1999**; 60: 1235.
- [5] Benedict LX, Puzer A, Willimson AJ, Grossman JC, Galli G, Klepeis JE, Raty JY, Pankratov O, Phys Rev B, **2003**; 68: 85310.
- [6] Hiura H, Miyazaki T, Kanayama T, Phys Rev Lett, **2001**; 86: 1733.
- [7] Brown WL, Freeman RR, Raghavachari K, Schluter M, Science, **1987**; 235: 860.
- [8] Zhixun L, Castelman AW, Article, Acc Chem Res, **2014**; 47: 2931-2940.
- [9] Iwasa T, Nakajima A, J Phys Chem C, **2013**; 117: 21551-21557.
- [10] Klacar S, Hellman A, Panas I, Gronbeck H, J Phys Chem C, **2010**; 114: 12610-12617.
- [11] Liu C, Yang B, Tyo E, Seifert S, Debartolo J, Von IB, Zapol P, Vajda S, Curtis LA, J Am Chem Soc, **2015**; 137: 8676-8679.
- [12] Sun WM, Li Y, Wu D, Li ZR, Phys Chem Phys Chem, **2012**; 14: 16467-16475.
- [13] Van Dijk CN, Rasing T, Kirilyuk A, Bowlan J, Liang A, Heer WA, J App Phys, **2010**; 107: 09B526-529.
- [14] Bhattacharya, Nguyen TT, Haeck JD, Hansen K, Lievens P, Janssens E, Phys Rev B, **2013**; 87: 054103.
- [15] Zheng BX, Dong D, Wang L, Yang JX, J Phys Chem, **2014**; 118: 4005-4012.
- [16] Takahashi K, Isobe S, Ohnuki S, Chem Phys Lett, **2013**; 555: 26-30.
- [17] Chen M, Dixon DA, J Phys Chem A, **2013**; 117: 3676-3688.
- [18] Zhang GL, Yuan HK, Chen H, Kunag AL, Tian CL, Wang JZ, **2014**; 118: 1936-1947.
- [19] Kaydashev VE, Janssens E, Lievens P, J Chem Phys, **2015**; 142: 034310-034317.
- [20] Li HF, Wang HQ, Phys Chem Chem Phys, **2014**; 16: 244-254.
- [21] Die D, Kuang XY, Guo JJ, Zheng BX, Physica A, **2010**; 389: 5216-5222.
- [22] Sahoo S, Hucht A, Gruner ME, Rollmann G, Entel P, Phys Rev B, **2010**; 82: 054418.
- [23] Gao Y, Dai X, Kang S, Cruz CAJ, Xin M, Meng Y, Han J, Wang Z, Zhou R, Scinetific Report, **2014**; 4: 5862-5867.
- [24] Negishi Y, Kawamata H, Hayakawa F, Nakajima A, Kaya, Chem Phys Lett, **1998**; 294: 370.
- [25] Atobe, J., Koyasu, K., Furusea, S. & Nakajima, A. Phys Chem Chem Phys, **2012**; 14, 9403-9410.

- [26] Ngan VT, Gruene P, Claes P, Janssens E, Fielicke A, Nguyen MT, Lievens P, *J Am Chem Soc*, **2010**; 132: 15589-15602.
- [27] Claes P, Janssens E, Ngan VT, Gruene P, Lyon JT, Harding DJ, Fielicke A, Nguyen MT, Lievens P, *Phys Rev Lett*, **2011**; 107: 173401.
- [28] Bandopadhyay D, Sen P, *J Phys Chem A*, **2010**; 114: 1835-1842.
- [29] Kumar M, Singh BJ, Kajjam S, Bandopadhyay D, *J Comp Theo Nanoscience*, **2010**; 7: 296-301.
- [30] Bandopadhyay D, *J Mol Model*, **2012**; 18: 3887-3902.
- [31] Beck SM, *J Chem Phys*, **1987**; 87: 4233.
- [32] Wang J, Liu Y, Li YC, *Phys Lett A*, **2010**; 374: 2736-2742.
- [33] Cao Y, Linde VD, Hockendrof RF, Beyer MK, *J Chem Phys*, **2010**; 132: 224307.
- [34] Atobe J, Koyasu K, Furuseand S, Nakajima A, *Phys Chem Chem Phys*, **2012**; 14: 9403.
- [35] Mondal K, Ghanty TK, Banerjee A, Chakarabarti A, Kamal C, *Mol Phys*, **2013**; 111: 725-734.
- [36] Dhaka K, Bandopadhyay D, *RSC Adv*, **2015**; 20: 83004-83012.
- [37] Ma W, Chen F, *J Mol Model*, **2013**; 19: 4555-4560.
- [38] Lin CS, Cheng WD, Wang JY, Zhang RQ, *Chem Phys Lett*, **2011**; 509: 124.
- [39] Zhao RN, Han JG, Bai JT, Liu FY, Sheng LS, *Chem Phys*, **2010**; 372: 89.
- [40] Li Y, Lyon JT, Woodham AP, Lievens P, Fielicke A, Janssens E, *J Phys Chem C*, **2014**; 119: 10896-10903.
- [41] Yang HW, Lu WC, Zhao LZ, Qin W, Yang WH, Xue XY, *J Phys Chem A*, **2013**; 117: 2672-2677.
- [42] Kapila N, Jindal V, Sharma H, *Physica B*, **2011**; 406: 4612-4619.
- [43] Qin W, Lu WC, Xia LH, Zhao LZ, Zang QJ, Wang CZ, Ho KM, *AIP advance*, **2015**; 5: 067159-067167.
- [44] Kapila N, Garg I, Jinal V, Sharma H, *J Magne Mag Materials*, **2012**; 324: 2885-2893.
- [45] Dhaka K, Trivedi R, Bandyopadhyay D, *J Mol Model*, **2012**; 19: 1473-1488.
- [46] Kumar M, Bhattacharya N, Bandyopadhyay D, *J Mol Model*, **2012**; 18: 405-418.
- [47] Haeck JD, Tai TB, Bhattacharya S, Le HT, Janssens E, Nguyen MT, Lievens P, *Phys Chem Chem Phys*, **2013**; 15: 5151-5162.
- [48] Li X, Su K, Yang X, Song L, Yang L, *Computaional and theoretical Chemistrtr*, **2013**; 1010: 32-337.
- [49] Deng XJ, Kong XY, Xu HG, Xu XL, Feng G, Zheng WJ, *J Phys Chem C*, **2015**; 119: 11048-11055.
- [50] Deng XJ, Kong XY, Xu HG, Xu XL, Feng G, Zheng WJ, *Phys Chem Chem Phys*, **2014**; 15: 3987-3993.
- [51] Trivedi R, Dhaka K, Bandopadhyay D, *RSC Adv*, **2014**; 4: 64825-64834.
- [52] Jaiswal S, Kumar V, *Computational and theoretical chemistrtr*, **2016**; 1075: 87-97.

- [53] Torres MB, Fernandez EM, Balbas LC, **2011**; 111: 444-462.
- [54] Chouhan V, Medel VM, Reveles JU, Khanna SN, Chem Phys Lett, **2012**; 528: 39-43.
- [55] Ge GX., Han Y, Wan J G, Zhao JJ, Wang GH, J Chem Phys, **2013**; 139: 174309-174317.
- [56] Lebon A, Aguado A, Vega A, J Phys Chem C, **2015**; 119: 27838-27847.
- [57] Zhang X, Wang Y, Wang H, Lim A, Gantfoer G, Bowen KH, Reveles JU, Khanna SN, J Amer Chem Soc, **2013**; 135: 4856-4861.
- [58] Reveles JU, Baruah T, Zope RR, J Phys Chem, **2015**; 119: 5129-5137.
- [59] Zhang M, Zhang J, Feng X, Zhang H, Zhao L, Luo X, Cao W, J Phys Chem A, **2013**; 117: 13025-13036.
- [60] Acevedo OL, Clayborne PA, Hakkinen H, Phys Rev B, **2011**; 84: 035434.
- [61] Varano A, Henry DJ, J Phys Chem A, **2010**; 114: 3602 -3608.
- [62] Pino I, Kroes GJ, Hemert MC, J Chem Phys **2010**; 133: 184304-18318.
- [63] Kuang XJ, Wang XQ, Liu GB, J Chem Sci, **2011**; 123: 743-754.
- [64] Giri S, Charaborty A, Chattaraj PK, J Mol Model, **2011**; 17: 777-784.
- [65] Jin R, Zhang S, Zhang Y, Huang S, Wang P, Tian H. Int J Hydrogen Energy, **2011**; 36: 9069-9078l.
- [66] Srinivasu K, Ghosh SK, Das R, Giri S, Chattaraj PK, RSC Adv, **2012**; 2: 2914-2922.
- [67] Chen M, Yang XB, Cui J, Tang JJ, Gan LY, Zhu M, Zhao YJ, Int J Hydrogen Energy, **2012**; 37: 309-317.
- [68] Fanjie K, Yanfei H, J Mol Model, **2012**; 20: 2087-2093.
- [69] Guo L, J Phys Chem, **2013**; 117: 3458-3466.
- [70] Mananghaya M, Int J Hydrogen Energy, **2015**; 40: 9352-9358.

CHAPTER 2

THEORETICAL BACKGROUND OF DENSITY FUNCTIONAL THEORY

2.1 Foundation of Density functional theory

Hartree introduced a quantum mechanical method to calculate approximate wave function and energies of atoms, and ions which are called Hartree function [1]. Fock and Slater individually proposed a self consistent procedure with consideration of Pauli Exclusion Principle and the multi-electron wave function in the form of a determinant of one particle orbitals known as Slater determinant. In the same time 1927 Fermi and Thomas [2] proposed a statistical model to calculate the energy of atoms by approximate the distribution of electron in atoms. They expressed the kinetic energy of an atom by the functional of electron density. In starting this part did not contain any information regarding exchange energy, which is a conclusion of Pauli Exclusion Principle and in 1930 Dirac add this term [3]. In fact the Thomas Fermi theory was the first predecessor step towards the density functional theory. In 1964 Hohenberg-Kohn made the foundation of DFT and solves the complicated many electron wave function introducing the functional [4]. These functional only deals with the 3 variable which is easy to handle rather than $3N$ variables (N is the number of electrons and each electron has 3 spatial variables). The Hohenberg and Kohn theorems deal with the central quantity of DFT known as exchange correlation functional. The Hohenberg-Kohn first theorems point out the ground state energy is uniquely determined by the electron density. The second theorem states that by minimizing the energy of the system, ground state energy can be obtained. The electron density of any system determines all ground state properties of the system. In this case the total ground state energy of a many-electron system is a functional of the density. So if we know the total energy of system, we can obtain all the information related to system at hand.

2.1.1 Hartree fock approximation

Finding and describing complete solution to the Schrödinger equation of electrons in solids it is necessary to obtained the many electron wave functions for the system at hand. Except for the very simple case like H_2^+ quantum mechanics are faced with many electron problems. To solve such type of problem is the Hartree fock approximation. It has played very important role in quantum chemistry. Hartree simplified the problem by making an assumption about the form of the many electron wave-function, namely that it was just the product of set of parameter values which most correctly describe the ground state of the system is just the set of values which minimizes the total energy. So using Hartree fock approximation [1] it is possible to solve the N electron wave function. Defining a suitable subset, this gives a reasonable approximation to the exact wave function. In this

scheme it consist approximation of the N electron wave function by an antisymmetrized product of N one electron wave function. This product is known as Slater determinant. We are representing Slater determinant by φ_{SD}

$$|\Psi_0\rangle = |\chi_1, \chi_2, \dots \dots \chi_N\rangle \quad (2.1)$$

This one electron function χ_i are known as are called spin orbital's, and are composed of spatial orbital $\varphi_i(r)$ and one of the two spin functions, $\alpha(s), \beta(s)$.

$$\chi(x) = \varphi_i(r) \sigma(s), \sigma = \alpha, \beta \quad (2.2)$$

The spin functions have important property that they are orthonormal. In the Hartree fock approximation these spin orbital's χ_i varied under some condition that they will remain orthonormal such that the energy obtained from the corresponding Slater determinant is minimum

$$E_{HF} = \min_{\varphi_{SD \rightarrow N}} E[\varphi_{SD}] \quad (2.3)$$

Here the expectation value can be obtained by extending the determinant. The HF energy is given by

$$E_{HF} = \sum_I^N \langle i | \hat{H} | i \rangle + \frac{1}{2} \sum_i^N \sum_j^N (ii|jj) - (ij|ji) \quad (2.4)$$

Where $(ii|jj)$ and $(ij|ji)$ defines like

$$(ii|jj) = \iint |\chi_i(\vec{x}_1)|^2 \frac{1}{r_{12}} |\chi_j(\vec{x}_2)|^2 d\vec{x}_1 d\vec{x}_2$$

$$(ij|ji) = \iint \chi_i(\vec{x}_1) \chi_j^*(\vec{x}_1) \frac{1}{r_{12}} \chi_j(\vec{x}_2) \chi_i^*(\vec{x}_2) d\vec{x}_1 d\vec{x}_2$$

Where the first term give the kinetic energy and electron nucleus attraction and second terms giving the coulomb and exchange integrals. Now in this equation the spin orbital's remain orthonormal that must be satisfied throughout the minimization which give the Lagrangian multipliers ε_i . Using these Langragian multipliers we can define fock operator which is an effective one electron operator

$$\hat{f}_i = -\frac{1}{2} \nabla_i^2 - \sum_N^M \frac{Z_A}{r_{iA}} + V_{HF} \quad (2.5)$$

In this equation kinetic energy and electron nucleus interaction is defined by first two terms and VHF is the Hartree fock potential. It is the average repulsive potential experienced by the i^{th} electron due to the remaining N-1 electrons.

2.1.2 Hohenbeg-Kohn theorems

In the ground state DFT, we can describe the N electron system by the Hamiltonian

$$\hat{H} = \hat{T} + \hat{V} + \hat{V}_{ee} \quad (2.6)$$

$$= - \sum_{i=1}^N \frac{\nabla_i^2}{2} + \sum_{i=1}^N v(r_i) + \frac{1}{2} \sum_{i=1}^N \sum_{\substack{j=1 \\ i \neq j}}^N \frac{1}{|r_i - r_j|} \quad (2.7)$$

with the kinetic, potential and interaction energy operators. The central statement of formal density functional theory is the Hohenberg Kohn theorem [4] can be written by these two statements:

1. The external potential $v(r)$ of N interacting electron uniquely determines by the ground state electron density $n(r)$, in which the electrons move and thus the Hamiltonian and all physical properties of the system formally determined by the ground state density.
2. The ground state density $n(r)$ and the ground state energy of a system characterized by the potential $V_0(r)$ which can be obtained by the variational principle. It involve only the density i.e. ground state energy can be written as a functional of the density. This gives the ground state energy E_0 if and only if the true ground state density $n_0(r)$ is inserted. For other densities $n(r)$, the inequality

$$E_0 = E_{\vartheta_0}[n_0] < E_{\vartheta_0}[n] \quad (2.8)$$

holds. There exists a functional $F[n]$ such that the energy functional can be written as

$$E_{\vartheta_0}[n] = F[n] + \int d^3 r \vartheta_0(r) n(r) \quad (2.9)$$

This functional is universal because it is independent of the potential $\vartheta_0(r)$ of the particular system for a given particle- particle interaction. The proof of the Hohenberg-Kohn theorem is based on the Rayleigh-Ritz variational principle. From the Hohenberg- Kohn variational principle, i.e. in the second statement, the ground state density $n(r)$ corresponding to the external potential $\vartheta(r)$ can be obtained as solution of the Euler equation:

$$\frac{\delta E_{\vartheta}[n]}{\delta n(r)} = \frac{\delta F[n]}{\delta n(r)} + \vartheta(r) = 0 \quad (2.10)$$

So the formal definition of the Hohenberg-Kohn functional is given by

$$F[n] = T[n] + V_{ee}[n] = \langle \Psi[n] | \hat{T} | \Psi[n] \rangle + \langle \Psi[n] | \hat{V}_{ee} | \Psi[n] \rangle \quad (2.11)$$

Where $\Psi[n]$ is the N electron wave function which yields the density n and minimizes the expectation value of $\hat{T} + \hat{V}_{ee}$. Approximation have been suggested, the oldest one is very well known Thomas- Fermi [2] approximation which precedes the Hohenberg Kohn theorem.

2.1.3 Kohn-Sham approach

Kohn-Sham suggest [5] a wonderful idea that how the universal functional can be approached. They realized the most of the problems with direct density functional like the Thomas Fermi method. Kohn Sham introduced the concept of a non-interacting reference system built from a set of orbitals where the major part of the kinetic energy can be computed to good accuracy. In this theory Kohn-Sham proposed a way of approximating the universal functional $F_{HK}[\rho]$. Kohn and Sham divided the kinetic energy functional $T[\rho]$ into the kinetic energy of a hypothetical non-nteracting system of electrons $T_S[\rho]$ and an unknown part $T_e[\rho] = T[\rho] - T_S[\rho]$ which contains the correction due to interaction between the electrons in the real system.

Kohn-Sham equations – Here we have to use the expression of the exact kinetic energy of the non-interacting reference system with the same density as the real, interacting one

$$T_S = -\frac{1}{2} \sum_i^N \langle \Phi_i | \nabla^2 | \Phi_i \rangle \quad (2.12)$$

This is not equal to the true kinetic energy, even if the system shares the same density. Kohn-Sham introducing the following separation for the functional this is

$$F[\rho(\vec{r})] = T_S[\rho(\vec{r})] + J[\rho(\vec{r})] + E_{XC}[\rho(\vec{r})] \quad (2.13)$$

Where E_{XC} , the so called exchange-correlation energy is defined like

$$E_{XC}[\rho] = (T[\rho] - T_S[\rho]) + (E_{ee}[\rho] - J[\rho]) = T_C[\rho] + E_{nuc}[\rho] \quad (2.14)$$

So the exchange correlation energy E_{XC} is the functional which contains everything that is unknown. E_{XC} Contains not only the non classical effects of self interaction correction, exchange and correlation which are contribution to the potential energy of the system, but also a portion belonging to te kinetic energy. T_S is expected to be a functional of ρ . Here we can see that the energy expression of the non-interacting system contains only two components: the kinetic energy and the energy due to the interaction with the external potential. But the problem is that how we can determine the orbital's in our non-interacting system. Following this approach the many electron problem is again mapped onto an effective 1-electron problem and all unknown terms are merged into exchange-correlation part. The one particle wave function can now be determined by solving the 1-particle equations under the constraint to reproduce the density of the real interacting system. This yields the so-called Kohn-Sham (KS) equations.

$$\left[-\frac{1}{2} \nabla^2 + V_{eff}(f) \right] \Psi_i = E_i \Psi_i \quad (2.15)$$

Where the effective potential $V_{eff}(r)$ contains external potential, the classical columbic potential due to electron-electron repulsion V_H and exchange-correlation potential $V_{xc}(r)$,

$$V_{eff}(r) = V_{ext} + \int \int \frac{\rho(1)\rho(2)}{r_{12}} d_{r_1} d_{r_2} + V_{xc}(r) \quad (2.16)$$

The density $\rho(r)$ of the real system can be given in the terms of Kohn–Sham orbitals

$$\rho(r) = \sum_{i=1}^N |\Psi_i(r)|^2 \quad (2.17)$$

And the exchange-correlation potential $V_{xc}(r)$ is given by the derivative of the $E_{xc}[\rho]$

$$V_{xc}(r) = \frac{\delta E_{xc}[\rho(r)]}{\delta \rho(r)} \quad (2.18)$$

Kohn-Sham equation has same structure as Hartree-fock equation. Since the effective potential depends on the density itself, the equation has to be solved by self-consistent method. Initially we guess the electron density. By using some approximation for the functional dependence of E_{xc} on the density, we compute V_{xc} as a function of r . The set of Kohn-Sham equation is then solved to obtain an initial set of K-S orbital (Ψ_i). The set is used to compute an improved density by using above equation. The process is repeated until the ρ and the E_{xc} converge to within certain tolerance. The electronic energy is then calculated from the above equation.

2.1.4 Schrodinger equation

This part begins with the definition of the electron density given by Schrödinger in 1926 [6] and traces its use and many applications directed at the understanding of the properties of matter to its present day role in density functional theory and the development of the quantum mechanics of an open system. The material world which we experience everyday, as studied by chemistry and condensed matter physics. It is built up from electrons and a few kinds of nuclei. The basis interaction is electrostatic or Columbic: An electron at position r is attracted to a nucleus of charge Z at R by the potential energy $[-Z / r-R]$, a pair of electrons at r and r_+ repels one another by potential energy $[1/ (r-r_+)]$, and two nuclei at R and R_+ repel one another as $[ZZ_+ / (R-R_+)]$. The electron must be described by quantum mechanics, while the more massive nuclei can sometime regarded as classical particle. All of the electrons in the lighter elements and the chemically important valance electrons in most elements move at speed much less than the speed of light, and so are non- relativistic. Different chemical theories had the ambition to rationalize those experimental facts. The most fruitful and promising framework so far is probably the Density Functional Theory of quantum mechanics. Quantum mechanics is the only theory we have why electrons and nuclei combine to form atoms, and why atoms form chemical bond to form molecules. We can say quantum mechanics is a

set of equations that tells us how to compute the energy and position of a wave with mass and a charge. The key equation of quantum chemistry is the “Schrodinger equation”. The simplest wave is one that is moving in one dimension (x) and does not interact with anything:

$$\Psi(x) = \sin\left(\frac{2\pi}{\lambda}x\right) \quad (2.19)$$

here λ is the wavelength and $\Psi(x)$ is known as the wave-function. The energy of this wave function can be obtained from its second derivative with respect to “x”, and the equation is:

$$\frac{d^2x}{dt^2} = -\left(\frac{2\pi}{\lambda}\right)^2 \Psi = -\frac{2M}{\hbar^2} T\Psi \quad (2.20)$$

where T is the kinetic energy. Since the wave is not interacting with anything, there is no potential energy and the total energy $E = T$, so it gives:

$$\hat{H}\Psi(x) = E\Psi(x) \quad (2.21)$$

This is the Schrödinger equation for an isolated electron, where H is known as Hamiltonian operator. As is well known the ultimate aim of most quantum chemical scheme is the solution of the time independent, non relativistic Schrodinger equation. The key problem in the structure of matter is to solve the Schrödinger equation for a system of N interacting electrons in the external columbic field created by a collection of atomic nuclei. It is very difficult problem in much body theory and in fact the exact solution is known only in the case of uniform gas for atom with a small number of electrons and molecules. Since the exact many electron wavefunction cannot be obtained, one tries to get accurate approximate solutions of the Schrödinger equation. An intuitive approach to do this first we write the Hamiltonian of such a system in the following general form:

$$\hat{H} = -\frac{1}{2\sum_{l=1}^N \nabla_l^2} - \frac{1}{2\sum_{A=1}^M \frac{1}{M_A} \nabla_A^2} - \sum_{i=1}^N \sum_{A=1}^M \frac{Z_A}{r_{iA}} \sum_{i=1}^N \sum_{J>i}^N \frac{1}{r_{ij}} + \sum_{A=1}^M \sum_{B>A}^M \frac{Z_A}{R_{AB}} \frac{Z_B}{R_{AB}} \quad (2.22)$$

Here H is the Hamiltonian operator for a molecular system consisting of M nuclei and N electrons in the absence of magnetic or electric field. The wave function contains all the information that can possibly be known about the system at hand. Again here H is a differential operator representing the total energy. In this equation A and B run over the M nuclei while i, j denote the N electrons in the system. The first two terms describe the kinetic energy of the electrons and nuclei respectively, M is the mass of nucleus ‘A’ in multiples of the mass of an electron, here the laplacian operator ∇_q^2 is defined as a sum of differential operator

$$\nabla_q^2 = \frac{\partial^2}{\partial x_q^2} + \frac{\partial^2}{\partial y_q^2} + \frac{\partial^2}{\partial z_q^2} \quad (2.23)$$

In the remaining three terms define the potential part of the Hamiltonian and indicating the attractive electrostatic interaction between the nuclei and the electrons and the repulsive potential due to the electron-electron and nucleus-nucleus interactions, respectively. So electrons are fermions, so that the total electronic wave function must be anti-symmetric with respect to exchange of two electrons. Nuclei can be fermions, bosons or distinguishable particles, according to the particular problem under consideration. All the ingredients are perfectly known and in principle all the properties can be derived by solving the many body Schrödinger equation. But this problem is almost impossible to treat in a full quantum mechanical framework. This Schrödinger equation can be further simplified if we take the advantages of the differences between the masses of nuclei and electrons. This is the famous Born-Oppenheimer approximation.

2.1.5 Born-Oppenheimer approximation

Unfortunately we are not able to solve the Schrödinger equation for a wave function with more than one particle. So equation can be further simplified if we take advantage of the differences between the masses of nuclei and electrons. Electron are so much lighter than nuclei, we can assume that the nuclei appear stationary to the electron. In the practical point of view we can consider the electron as moving in the field of fixed nuclei and we can take the position of the nucleus and electrons separately. This is Born- Oppenheimer approximation [7]. So if the nuclei are stationary in space and do not move, than the kinetic energy of the nuclei is zero and the potential energy is merely constant. Thus the Hamiltonian equation reduces to the so called electronic Hamiltonian.

$$\hat{H}_{elec} = -\frac{1}{2} \sum_{i=1}^N \nabla_i^2 - \sum_{i=1}^N \sum_{A=1}^M \frac{Z_A}{r_{iA}} + \sum_{i=1}^N \sum_{j>i}^N \frac{1}{r_{ij}} = \hat{T} + \hat{V}_{Ne} + \hat{V}_{ee} \quad (2.24)$$

In this condition the total energy E_{total} is then the sum of E_{elec} and the constant nuclear repulsion term

$$E_{nuc} = \sum_{A=1}^M \sum_{B>A}^M \frac{Z_A}{r_{AB}} \frac{Z_B}{r_{AB}} \quad (2.25)$$

$$\hat{H}_{elec} \Psi_{elec} = E_{elec} \Psi_{elec} \quad (2.26)$$

$$E_{total} = E_{elec} + E_{nuc} \quad (2.27)$$

the expectation value of the second operator V_{Ne} is also termed the external potential, V_{ext} , in Density functional theory.

2.1.6 Principle of anti-symmetry

In this situation the wave function Ψ itself is not observable. A physical interpretation can only be associated with the square of the wave function in that represent the probability that electrons 1, 2 ...N are found simultaneously in volume elements dx_1, dx_2, \dots, dx_n . Since electrons are indistinguishable, this probability must not change if the coordinates of any two electrons are switched, it can be shown that the only possibilities occurring in nature are that either the two functions are identical or that the interchange leads to a sign change. Electrons are fermions and Ψ must therefore be anti-symmetric with respect to interchange of the spatial and spin coordinates of any two electrons.

2.1.7 Variational principle

Now to solve the Schrodinger equation for any molecule, first we have to set up the specific Hamiltonian operator. For this end we should know about those parts of Hamiltonian that are specific for system. If we inspection of equation (2.20) we get only the information about the number of electrons, N, and the external potential V_{ext} . Further remaining parts like operator of kinetic energy or the electron repulsion are independent of the molecule. In the second step we have to find out the eigenfunctions and eigenvalues. Once the wave function is determined, all the interested properties can be found out. Apart from trivial exceptions, we don't have any strategy to solve the Schrödinger equation exactly for atomic and molecular system. There is a method for systematically approaching the wave function of the ground state Ψ_0 . This is the variational principle, which holds a very important role in quantum chemical application. As we know by fundamental quantum mechanics law that the expectation value of a particular observable represented by the appropriate operator O using any, possibly complex, wave function Ψ_{trial} that is given by

$$\langle \hat{O} \rangle = \langle \Psi_{trial} | \hat{O} | \Psi_{trial} \rangle \quad (2.28)$$

Here the bracket notation used for integrals known as Dirac notation.

So the variational principle says that the energy computed via equation as the expectation value of the Hamiltonian operator H from any guessed Ψ_{trial} will be an upper bound to the true energy of the ground state, i.e.

$$\langle \Psi_{trial} | \vec{H} | \Psi_{trial} \rangle = E_{trial} \geq E_0 = \langle \Psi_0 | \vec{H} | \Psi_0 \rangle \quad (2.29)$$

Here the equality holds if and only if Ψ_{trial} is identical to Ψ_0 . Now to solve this equation we will introduce functional.

2.1.8 Functional

A function maps one number to another. A functional assigns a number to a function. Here we encounter for the first time the main mathematical concept of density functional theory. A rule which assigns a number to a

function is called a functional. To distinguish a functional from a function in writing, we use square brackets for the argument. Hence $f(x)$ is a function of the variable x while $F[f]$ is a functional of the function. So when we show that the ground state energy of a quantum mechanical system is a functional of the density, we will then want to minimize that energy to find ground state density. To do this we must know how to differentiate functional. So for beginning we must define a functional derivative. As we know the key insight that makes DFT awesome is the Hohenbeg-Kohn theorem, which says that instead of trying solving this really hard 3N dimensional problem of finding the wave-function, there exist a 3 dimensional problem for finding the electron density. So to put this a little concretely, after doing some math we get an equation like

$$V[\rho(X)] = e \cdot \rho(x) \quad (2.30)$$

Where $\rho(x)$ is the electron density throughout space and V is a functional (mathematical object that takes as an argument a function and returns a new function). A lot of different approximate functional exist. They trend to vary along a computational accuracy. That is, the functional that are more accurate take more time to compute. So now for finding the ground state energy and wave function we will have to minimize the functional $E[\Psi]$ by searching through all acceptable N electron wave function. The function which gives the lowest energy will be Ψ_0 and the energy will be the true ground state energy E_0 . This equation can be expressed as

$$E_0 = \min_{\Psi-N} E[\Psi] \quad (2.31)$$

Here $\Psi-N$ indicates that Ψ is an allowed N electron wave function. So in DFT the functional is the electron density which is a function of space and time. The electron density is used in DFT as the fundamental property unlike Hartree fock theory which deals directly with the many body wavefunction.

2.2 Basic machinery of DFT

Now we will turn to the more complicated problem of how the strategies developed so far can be mapped onto computational schemes. To this end we will introduce LDA (Local density approximation), Slater determinant, Exchange correlation energy functional, and Basis set (one of the main part). Briefly LDA make the iterative self-consistent field procedure for solving the one electron Kohn-Sham equations computationally accessible. This leads immediately to the problem of which kinds of basis set are suitable in order to expand the Kohn-Sham orbitals in such calculation and according to which criteria should choose a particular set of orbitals.

2.2.1 Local density approximation

The LDA has been for a long time the most widely used approximation to the exchange correlation energy. It has been proposed in the seminal paper by Kohn-Sham. This approximation [8] is based on the assumption that a

system of electrons in molecules or atoms is like an electron gas. In the homogeneous electron gas model the electrons move in an infinite region of space with uniform positive charge background to preserve charge neutrality. For an inhomogeneous system it is then assumed that the exchange correlation energy can be obtained by approximating the density of the inhomogeneous system locally by the density of the homogeneous system of electron gas. This means that

$$\tilde{\rho}_{xc}^{LDA}(r, r') = \rho(r)(\tilde{g}^h[|r - r'|, \rho(r)] - 1) \quad (2.32)$$

With $\tilde{g}^h[|r - r'|, \rho(r)]$ the pair correlation function of the homogenous gas, which depends only on the distance between r and r' evaluated at the density ρ^h , which locally equal $\rho(r)$. Within this approximation, the exchange – correlation energy density is defined as

$$\varepsilon_{xc}^{LDA}[\rho] = \frac{1}{2} \int \frac{\tilde{\rho}_{xc}^{LDA}(r, r')}{|r - r'|} dr' \quad (2.33)$$

And the exchange correlation energy becomes

$$E_{xc}^{LDA}[\rho] = \int \rho(r) \varepsilon_{xc}^{LDA}[\rho(r)] dr \quad (2.34)$$

Where $\varepsilon_{xc}[\rho(r)]$ is the exchange correlation energy per electron of the homogeneous electron gas? The $\varepsilon_{xc}[\rho(r)]$ can be written as the sum of exchange and correlation part as

$$\varepsilon_{xc}(\rho(r)) = \varepsilon_x(\rho(r)) + \varepsilon_{xc}(\rho(r))$$

The exchange part has been expressed explicitly as

$$\varepsilon_x(\rho(r)) = -\frac{3}{4} \sqrt{\frac{3\rho(r)}{\pi}} \quad (2.35)$$

But there is no expression for the correlation part of energy. In general the exchange correlation energy density is not a local functional of ρ . From its definition it is very clear that it has to be a non-local object because it reflects the fact that the probability of finding an electron at r depends on the presence of other electrons in the surroundings, through the exchange-correlation hole.

2.2.2 Slater Determinant

We will lay down the general procedure for constructing anti-symmetric wave function for a multi-electron atom. But with increasing in the number of electrons, the number of terms increases in such large proportions that we must find an abbreviated form to represent a wave function. A short hand form is determinant in which spin orbitals are the elements; each row in this determinant is labeled with an electron and each column with a spin orbital. The normalized wave function of an n electron atom, there are n rows and m columns

$$\Psi_- = \frac{1}{\sqrt{n!}} \begin{vmatrix} A(1) & B(1) & \dots \\ A(2) & B(2) & \dots \\ \dots & \dots & \dots \\ \dots & \dots & \dots \\ A(n) & B(n) & \dots \end{vmatrix} \quad (2.36)$$

Such determinants of spin orbitals are called Slater determinants [9]. It consists of approximating the N electron wave function by an antisymmetric product of N one electron wave function. The Hartree product does not satisfy the antisymmetric wave function. We consider a two electron case in which we occupy the spin orbital's χ_i and χ_j . If we put electron one in χ_i and electron two in χ_j , we have

$$\Psi_{12}^{HP}(X_1 X_2) = \chi_i(X_1) \chi_j(X_2) \quad (2.37)$$

On the other hand if we changed the position of electron then,

$$\Psi_{21}^{HP}(X_2 X_1) = \chi_i(X_2) \chi_j(X_1) \quad (2.38)$$

Each of these Hartree products clearly distinguishes between electrons. So here we can obtain that wave function which will satisfy anti-symmetric condition. By combining these two equation

$$\Psi(X_1, X_2) = 2^{-\frac{1}{2}} [\chi_i(X_1) \chi_j(X_2) - \chi_j(X_1) \chi_i(X_2)] \quad (2.39)$$

The factor $2^{-\frac{1}{2}}$ is a normalization factor. The minus sign insures those wave functions anti-symmetric with respect to the interchange of the coordinates of electrons one and two. From above equation it is clear that wave function vanishes if both electrons occupy the same spin orbitals. If these anti-symmetric wave function can be written as above equation then it is known as Slater determinant form of many body problems.

2.2.3 Basis sets

In order to compute the energy, we need to define mathematical functions for the orbitals. In the case of atoms we can simply use the solution to the Schrodinger equation, But what about molecular orbitals. So expanding an unknown function like molecular orbitals in a set of known functions is not an approximation if the basis set is complete. A complete basis set means that an infinite number of functions must be used. The expansion of the molecular orbitals leads to the integrals of quantum mechanical operators over a basis set and the ease with which these integrals can be calculated also depends on the type of basis function. Thus the one way of constructing molecular orbitals is as a linear combination of atomic orbitals, we can write like

$$\Phi_i = \sum_{\mu=1}^k C_{\mu i} \chi_{\mu} \quad (2.40)$$

The approximation becomes better and better if the K increases. Here χ_μ is a mathematical function that looks like an atomic orbital and it is called a basis function. A collection of basis functions for various atoms is called a basis set. $C_{\mu i}$ is a number that indicates how much basis function contributes to molecular orbitals and it is determined for each system via the variational principle. Here every molecular orbital is expressed in terms of all basis functions and therefore extends over the entire molecule. There are two types of basis functions commonly used in electronic structure calculation [10-11]

(i) Slater type orbital

(ii) Gaussian type orbitals

Slater type orbitals have the functional form like

$$\chi_{\zeta,n,l,m}(r, \theta, \Phi) = NY_{l,m}(\theta, \Phi)r^{n-1}e^{-\zeta r} \quad (2.41)$$

Where N is the normalization constant and $Y_{l,m}$ is spherical harmonic functions. STO (Slater type orbitals) do not have any analytical solution. Again Gaussian type orbitals can be written as

$$\chi_{\zeta,l,n,m}(r, \theta, \Phi) = NY_{l,m}(\theta, \Phi)r^{2n-2-l}e^{-\zeta r^2} \quad (2.42)$$

The sum of l_x, l_y, l_z determines the type of orbital. Here the r^2 dependence in the GTO (Gaussian type orbitals) makes the GTOs inferior to the STOs. The Gaussian functions are called primitives. Generally three primitives are sufficient to represent an STO, and this basis set is known as the STO-3G basis set. Minimal basis sets are usually not sufficiently accurate to model reaction energy. This is due to the fact that the atomic basis functions cannot change size to adjust to their bonding environment. It can be made possible by using some of the contraction coefficients and this will increase the basis set size. In similar manner 3-21G (Three-Two-One G) [12] which denotes that core basis functions are described by three Gaussians, while the basis functions are split into two basis functions, described by two and one Gaussian each. Further such functions are called as polarization functions and denoted like 6-31G(d) [13] denotes d polarization functions and can also be written as 6-31G*. Similarly 6-31G(d, p) is a basis set where p functions have been also added for polarization and can be written as 6-31G**. So there are many other basis functions but they have the same kind of attribute.

2.2.4 Self consistent field procedure

In very simple words the solution for the molecular orbitals and the total energy has to be carried out iteratively starting from the initial guess. Each MO (Molecular orbital) depends on the repulsion of the electron in the orbitals with all other electrons in the system. We cannot optimize the molecular orbitals unless we already know this field experienced by the electron. So we have to use an iterative method. This method is called the self

consistent field method. This allows us to obtain the density functional energy. In the Hartree fock equation the Fock operator depends on the HF potential on the spin orbital's i.e. we need to solve the eigen value problem and it can be solved out iteratively and this technique known as self consistent field procedure since the orbitals are derived from their own effective potential. This procedure starts with a guessed set of orbital's, for which the HF equations are solved. The resulting new set of orbitals is then used in the next iteration and so on until we did not get lowest ground state energy.

2.2.5 Exchange- correlation Functional

Let us briefly review what we have seen, we would like to find the ground state energy of the Schrödinger equation, but it is difficult because this is an N body problem. But by the beautiful results of Kohn, Hohenberg and Sham found that the ground state energy can be obtained by minimizing the energy of energy functional, and that this can be achieved by Self consistent solution as described above. There is one critical complication in this: to solve the Kohn- Sham equation we must specify the exchange correlation function $E_{xc}[\Psi_i]$. As we know defining this term is very difficult. In face the true form of the exchange correlation functional whose existence is taken by H-K theorem is not known. So there is one case where this functional can be derived exactly that is uniform electron gas. In this situation, the electron density is constant at all points in space that is $n(r) = \text{constant}$. This situation may appear to be of limited bonds and generally make materials interesting. But the uniform electron gas provides a practical way to actually use the Kohn-Sham equation. To do this we set the exchange correlation potential at each position from the uniform electron gas at the electron density observed at that position.

$$V_{xc}(r) = V_{xc}^{electron\ gas}[n(r)] \quad (2.43)$$

This approximation uses only the local density to define the approximate exchange-correlation functional, so it is called the local density approximation. The LDA gives us a way to completely define the Kohn-Sham equations. As mentioned, the Kohn-Sham kinetic energy is not the true kinetic energy; we may use this to formally the exchange-correlation energy

$$E_{xc}[n(r)] = T[n(r)] - T_s[n(r)] + E_{ee}[n(r)] - E_H[n(r)] \quad (2.44)$$

Where $T_s[n(r)]$ and $E_{ee}[n(r)]$ are the exact kinetic and electron-electron interaction energies respectively. Physically this term can be interpreted as containing the contributions of detailed correlation and exchange to the system energy. This explanation ensures that the Kohn-Sham is exact. However the exact form of E_{xc} is not known; thus we must introduce approximate functional based upon the electron density to describe this term. There are two common approximations in use: the LDA (Local density approximation) and GGA (Generalized gradient

approximation) [14-16]. The simplest is LDA: assumes that the exchange correlation energy at point r is simply equal to the exchange-correlation energy of a uniform electron gas that has the same density at the point r , so we can write

$$E_{xc}[n(r)] = \int \epsilon_{xc}(r)n(r)dr \quad (2.45)$$

So that the exchange correlation potential may be written as

$$v_{xc}(r) = \frac{\delta E_{xc}[n(r)]}{\delta n(r)} \quad (2.46)$$

Where in the last equation the assumption is that the exchange correlation part is purely local.

2.3 Methodology

In this thesis, we performed all calculation within the framework of linear combination of atomic orbital. The exchange correlation potential contributions are incorporated into the calculation using the spin polarized generalized gradient approximation (GGA), popularly known as B3LYP [17]. All geometry optimization are performed with no symmetry constraints in the Gaussian' 03 [18] program based on Gaussian basis sets which is widely for isolated molecules. It is very flexible in the choice of basis sets, effective core potentials and density functional. It has excellent geometry optimizers and initial guesses for the self consistent field iterations. We also used VASP [19-20] program package to optimize the initial geometry and determine the density of states of particular cluster. It is always possible during optimization that a cluster with particular guess geometry is trapped in local minima of potential energy surface. To avoid this we used a global search method using USPEX [21] to get all possible optimized geometric isomers for each size of clusters.

2.4 References

- [1] Hartree DR, Math Proc Cmabridge Philos Soc, **1928**; 24: 89-110.
- [2] Fermi E, Rend Accad Nat Lincei, **1927**; 6: 602-607.
- [3] Dirac PAM, Proc Cmabridge Philos Soc, **1930**; 26: 376-385.
- [4] Hohenberg P, Kohn W, Phys Rev B, **1964**; 136: 864-871.
- [5] Kohn W, Sham LJ, Phys Rev A, **1965**; 140: 1133-1138.
- [6] Schrodinger E, Ann Physik, **1926**; 79: 361-376.
- [7] Born M, Oppenheimer JR, Ann Physik, **1930**; 84: 718.
- [8] Stevens P, Devlin JF, Chabolowski CF, Frish MJ, J Phys Chem, **1994**; 98: 11623-11627.
- [9] Slater JC, Phys Rev, **1951**; 81: 385-390.
- [10] Slater JC, Phys Rev, **1930**; 36: 57.
- [11] Boys SF, Proc R Soc London Ser A, **1950**; 200: 542.
- [12] Binkley JS, Pople JA, Hehre WJ, J Am Chem Soc, **1980**; 102: 939-47.
- [13] Ditchfield R, Hehre WJ, Pople JA, J Am Chem Soc, **1971**; 54: 724
- [14] Perdew JP, Wang Y, Phys Rev B, **1992**; 45: 13244-13249.
- [15] Perdew JP, Phys Rev Lett, **1985**; 55: 1665-1668.
- [16] Perdew JP, Burke K, Wang Y, Phys Rev B, **1996**; 54: 16533-16539.
- [17] Lee C, Yang W, Parr RG, Phys Rev B, **1988**; 37: 785.
- [18] Frisch MJ, Trucks GW, Schlegel HB, Scuseria GE, Robb MA, Cheesemen JR, Zakrzewski VG, Montgomery jr JA, Stratmenn RE, Burant JC, Dapprich S, Millam JM, Daniels AD, Kudin KN, Strain MC, Farkas O, Tomasi J, Barone V, Cossi M, Cammi R, Mennucci B, Pomelli C, Adamo C, Clifford S, Ochtrski J, Petersson GA, Ayala PY, Cui Q, Morokuma K, Malick DK, Rabuck AD, Raghavachari K, Foresman JB, Cioslowki J, Ortiz JV, Baboul AG, Stefanov BB, Liu B, Liashenko A, Piskorz P, Komaromi I, AL-Laham MA, Peng CY, Nanayakkara A, Challacombe M, Gill PMW, Johnson B, Chem W, Wong MW, Andress JL, Gonzalez C, Head-Gordon M, Replogle ES, Pople J A, 2004; Gaussian 03, revision E 01 Gaussian, Wallingford.
- [19] Kresse G, Furthmüller, Phys Rev B, **1996**; 54: 1169.
- [20] Kresse G, Joubert D, Phys Rev B, **1999**; 59: 1758.
- [21] Glass CW, Oganov AR, Hansen N, Compu Phys Commu, **2006**; **175**: 713

CHAPTER 3

STUDY OF ELECTRONIC PROPERTIES, STABILITIES AND MAGNETIC QUENCHING OF MoGe_n ($n = 1-20$) CLUSTER: A DENSITY FUNCTIONAL INVESTIGATION

3.1 Introduction

The number of electrons involved in the growth of the nanoclusters and cluster-assembled materials by forming chemical bonds is the fundamental concept to explain and understand the electronic properties and stabilities of the nanomaterials. In last few decades, searching of stable hybrid nanoclusters, specially, transition metal-doped semiconductor nanoclusters are extremely active area of research for their potential applications in nanoscience and nanotechnology. One of the challenges in the computational materials design or synthesis of such materials is to search for the clusters that are likely to retain their properties and structural reliability during the formation of cluster assembled materials [1]. Among these materials, in the transitional metal-doped semiconductor clusters and cluster-assembled materials are interesting and also it is important to understand the physical and chemical processes taking places at the metal-semiconductor interface for their application as nano-devices [2]. Pure semiconductor nanoclusters are not really stable and it is a challenging job to make them stable. Among different possibilities of stabilizing the semiconductor nanoclusters, encapsulation of a transition metal (TM) in pure semiconductor cage is one of the most effective methods. Many insights of the transition metal doped Si and Ge clusters were reported in literature and also explained their stabilities on the basis of electron counting rules [3-11]. The existence of several stable transition metal doped semiconductor nanoclusters have already experimentally verified by Beck et al. [12, 13] using lasers vaporization techniques. Recently, Atobe et al. [14] investigated the electronic properties of transition metal and lanthanide-metal doped MGe_n ($M = \text{Sc, Ti, V, Y, Zr, Nb, Lu, Hf, and Ta}$) and MSn_n ($M = \text{Sc, Ti, Y, Zr, and Hf}$) by anion photoelectron spectroscopy and explained the stability of the clusters using electron-counting rule. In a theoretical study Hiura et al. [15] argued that the magic nature of WSi_{12} cluster is because of the 18 electron shell fill structure assuming each silicon atom donates one valence electron to the encapsulated transition metal which is donating six valence electrons in hybridization. Wang et al. [16] found that the encapsulation of Zn atom in germanium cage starts from $n=10$ whereas, ZnGe_{12} is the most stable species which is not an 18-electron cluster. In another study Guo et al. [17] explained the stability of MSi_n ($M=\text{Sc, Ti, V, Cr, Mn, Fe, Co, Ni, Cu, Zn; } n=8-16$) nanoclusters using shell filling model where the d-shell of the transition metals plays an important role in hybridization to make a closed shell structure. In this context, more corrected information

was reported by Reveles and Khanna [18, 19]. They considered that the valence electrons in TM-Si clusters behave like a nearly free-electron gas and one needs to invoke the Wigner-Witmer (WW) spin conservation rule [19] while calculating the embedding energy of the clusters to explain its stability. It is worth mentioning here that the one-electron levels in spherically confined free-electron gas follow the sequence $1S^2 1P^6 1D^{10} 2S^2 \dots$. Thus, 2, 8, 18, 20, etc. are the shell filling numbers, and clusters having these numbers of valence electrons attain enhanced stability. But in some cases this theory is not valid. As example, by applying Wigner-Witmer (WW) spin conservation rule [19] and without applying that Revelese and Khanna [18, 19] found that CrSi_{12} and FeCr_{12} in neutral state exhibit highest binding energy, whereas, anionic MnSi_{12} , VSi_{12} and CoSi_{12} show maximum embedding energy which is one of the most important parameter to understand the stability of the nanoclusters. Therefore, both 18- and 20-electron counting rules are valid for different clusters and in different charged states to explain the stability. Experiments also supported the validity of these electron-counting rules in some of the charged clusters. Koyasu et al. [20] studied the electronic and geometric structures of transition metal (Ti, V and Sc) doped silicon clusters in neutral and different charged states by mass spectroscopy and anion photoelectron spectroscopy. They found that the neutral TiSi_{16} , cationic VSi_{16} and anionic ScSi_{16} clusters were produced in greater abundance, which follows the validity of 20-electron counting rule. In summary, it was found that in most of the research transition metal-doped semiconductor clusters show maximum stability in closed-shell electron configuration with 18 and 20 valence electrons in the cluster by taking into account the fact that each germanium or silicon atoms contributes one electron to the bonding with the transition metal atom. In the present study we make an effort to explain the enhanced stability of MoGe_{12} in MoGe_n ($n=1-20$) by following the behavior of different physical and chemical parameters of the ground state clusters in each size using density functional theory (DFT). Detailed studies on this system are important to understand the science behind the cluster stability and its electronic properties. DOS plots of different clusters are also discussed to explain the role of d-orbital's of Mo atom in the hybridization and in the quenching of magnetic moment of Mo atom in germanium cluster. In addition, to understand the enhance stability of MoGe_{12} isomer, distance dependence nucleus independent chemical-shift (NICS), which is the measure of the aromaticity of the cluster is calculated and discussed its role in stability. Finally, electron-counting rule is applied to understand the stability of the MoGe_{12} cluster and the possibility of Mo-based cluster assembled materials.

3.2 Theoretical and Computational details

All calculations were performed within the framework of linear combination of atomic orbital's density functional theory (DFT). The exchange-correlation potential contributions are incorporated into the calculation using

the spin-polarized generalized gradient approximation (GGA) proposed by Lee, Yang and Parr popularly known as B3LYP [21]. Different basis sets were used for germanium and molybdenum with effective core potential using Gaussian' 03 [22] program package. The standard LanL2DZdp and LanL2DZ basis sets were used for germanium and Molybdenum to express molecular-orbitals (MOs) of all atoms as linear combinations of atom-centered basis functions. LanL2DZdp. This is a double- ζ , 18-valence electron basis set with a LANL effective core potential (ECP) and with polarization function [23-24]. All geometry optimizations were performed with no symmetry constraints. During optimization, it is always possible that a cluster with particular guess geometry can get trapped in a local minimum of the potential energy surface. To avoid this, we used global search method by using USPEX [25] and VASP [26, 27] to get all possible optimized geometric isomers in each size from n=5 to 20. The optimized geometries were then again optimized in Gaussian 03 [22] program using different basis sets as mentioned above to understand the electronic structures. In order to check the validity of the present methodology, a trial calculation is carried out on Ge-Ge, Ge-Mo and Mo-Mo dimers using different methods and basis sets. Detailed result of the outputs is presented in Table 3.1 The bond length of germanium dimer at triplet spin state (ground state) is found 2.44Å (with a lowest frequency of 250 cm⁻¹) in the present calculation, which is within the range of the values obtained theoretically as well as experimentally reported by several groups (see Table 3.1). The bond length and the lowest frequency of the Ge-Mo dimer in the quintet spin state (ground state) were obtained in the present calculation as 2.50 Å and 207.82 cm⁻¹ respectively. The values reported by other groups are 2.50 Å and 208 cm⁻¹ as shown in table 3.1. The optimized electronic structure is obtained by solving the Kohn-Sham equations self-consistently [33] using the default optimization criteria of the Gaussian 03 program [22]. Geometry optimizations were carried out to a convergence limit of 10⁻⁷ Hartree in the total optimized energy. The optimized geometries as well as the electronic properties of the clusters in each size were obtained from the calculated program output.

Table 3.1 – Bond length and lowest frequencies of Ge-Ge, Ge-Mo and Mo-Mo dimer

Dimer	Bond length (Å)	Lowest frequencies (cm ⁻¹)
Ge-Ge	2.44 ^a , 2.44 ^b , 2.44 ^c , 2.39 ^d , 2.3 ^e , 2.36-2.42 [28, 29], 2.46 [32]	250.63 ^a , 261 ^b , 263 ^c , 282 ^d , 317.12 ^e , 258 [28]
Ge-Mo	2.5 ^a , 2.48 ^b , 2.51 ^c , 2.41 ^d , 2.43 ^e , 2.50 [29]	202.56 ^a , 218 ^b , 198 ^c , 251.78 ^d , 252.53 ^e , 287.82 [29]
Mo-Mo	1.97 ^a , 2.5 ^b , 2.5 ^c , 1.88 ^d , 1.89 ^e , 1.98 [30]	561.79 ^a , 567.24 ^b , 570.36 ^c , 582.1 ^d , 583.07 ^e , 562 [30], 477 [31]

^a B3LYP/Lanl2dz-ECP, ^b B3LYP/aug-cc-pvdz, ^c B3LYP/aug-cc-pvtz-pp, ^d M06/aug-cc-pvtz-pp

^e M06/Lanl2dz-ecp

3.3 Results and Discussions

Molybdenum atom, a typical 4d transition metal, has electronic configuration of [Kr] 4d⁵5s¹ where 'd' and 's', both the shells are half filled. Optimized ground state clusters with the point group symmetry are shown in

fig. 3.1a. Following the growth pattern of Ge_nMo clusters from $n=1$ to 10, the Mo is absorbed on the surface of the Ge_n cluster or replace a Ge atom from the surface of Ge_{n+1} cluster to form Ge_nMo cluster where Mo atom in all clusters are exposed outside. In the next stage of the growth pattern, Mo is absorbed partially by the Ge_n clusters in $n=8$ and $n=9$. Complete encapsulation starts from $n=10$. The low energy structures within the size range $n = 10$ to 16 are all very known in most of the transition metal doped silicon and germanium clusters and also reported by others [34-38]. The first encapsulated ground state isomer MoGe_{10} is icosahedral, where; the Mo atom makes hybridization with all ten-germanium atoms in the cage. Addition of one germanium atom on the surface of ground state MoGe_{10} isomers gives endohedral Mo doped MoGe_{11} cluster. Endohedrally absorbed Mo in hexagonal prism kind structure MoGe_{12} is the ground state isomer at $n=12$ size. Here Mo bonded with all twelve germanium atoms in the cage. In this structure Mo atom is placed between two parallel benzene likes hexagonal Ge_6 surfaces. The ground state isomer of MoGe_{13} structure is a Mo encapsulated hexagonal capped bowl kind of structure.

Fig.3.1a Optimized ground state structures of MoGe_n (n=1-20) clusters with point group Symmetry. Blue balls are Ge and yellow balls are Mo atoms.


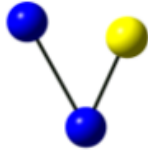
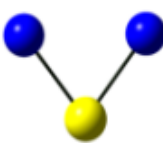

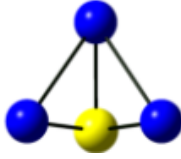
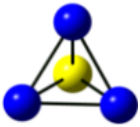

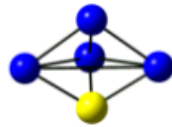
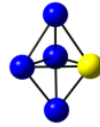
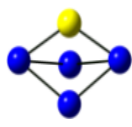
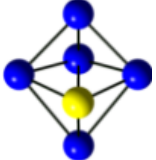
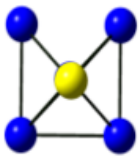
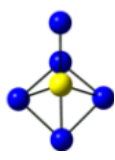
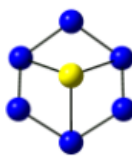
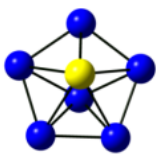
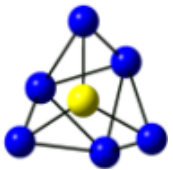
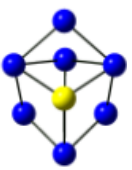
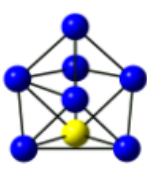
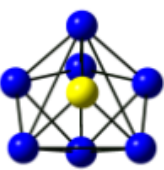
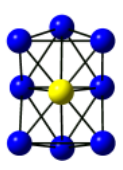
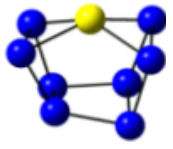
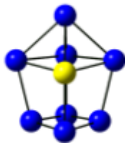
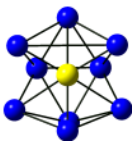
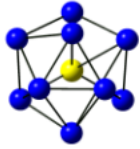
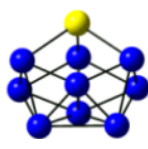
				
1A^{GS}: C_V	2A^{GS}: C_{2V}	2B : C_{2V}:0.069	2C: C_{2V}:0.092	3A^{GS}: C_{2V}
				
3B: C_s:0.23	3C: C₁:.46	4A^{GS}: C_{2V}	4B: C_{2V}:0.023	4C: C_{2V}:0.27
				
5A^{GS}: C_s	5B: C_s:0.0	5C: C_{2V}:0.23	6A^{GS}: C_s	6B: C_s:0.39
				
6C: C₁:0.46	7A^{GS}: C_s	7B: C₁:0.52	7C: C_s:0.53	8A^{GS}: 2V
				
8B: C₁:0.00	8C: C_{2V}: 0.56	9A^{GS}: C₂	9B: C₁:0.002	9C: C₂:0.004

Fig.3.1a- Continue....

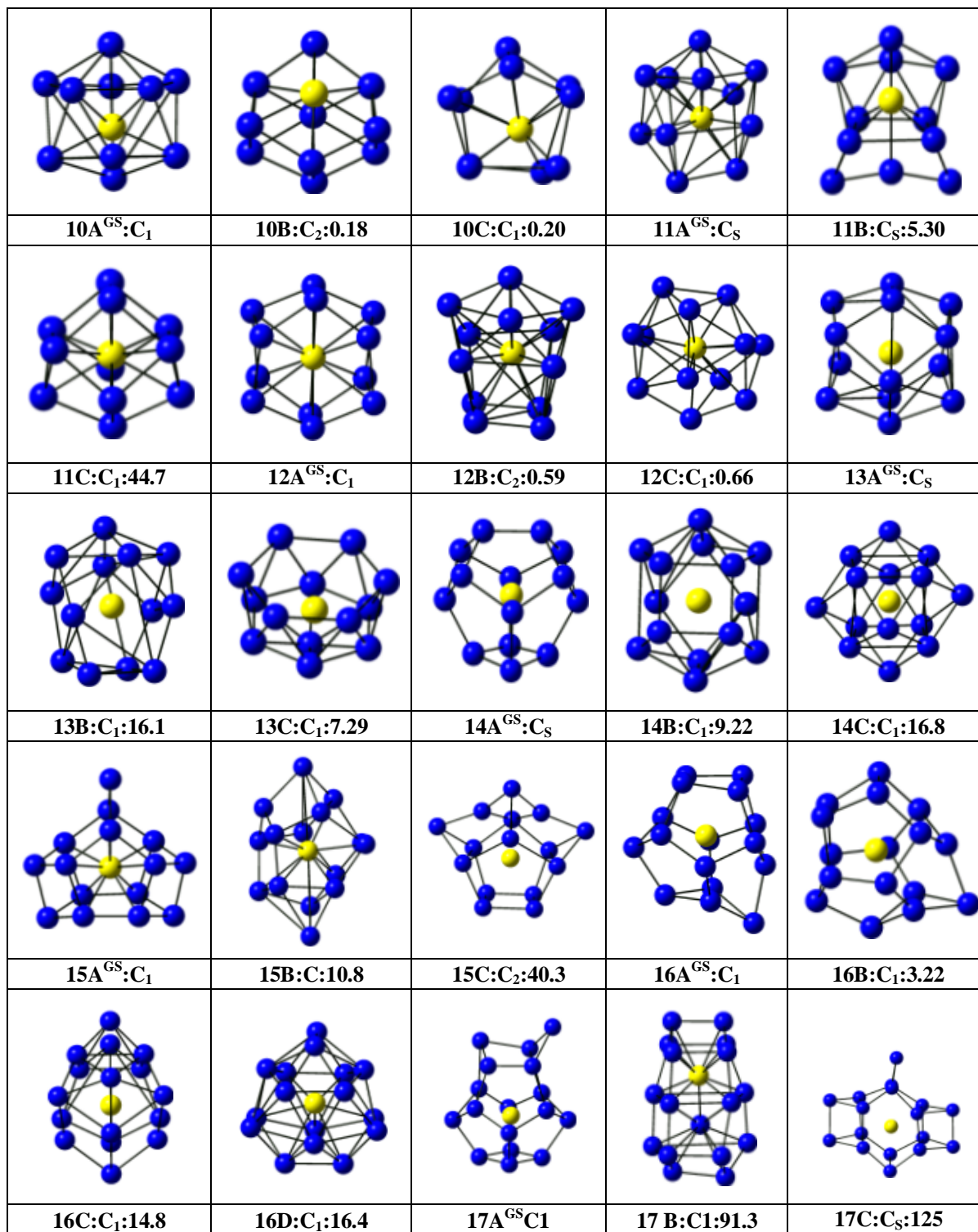


Fig.3.1a Continue....

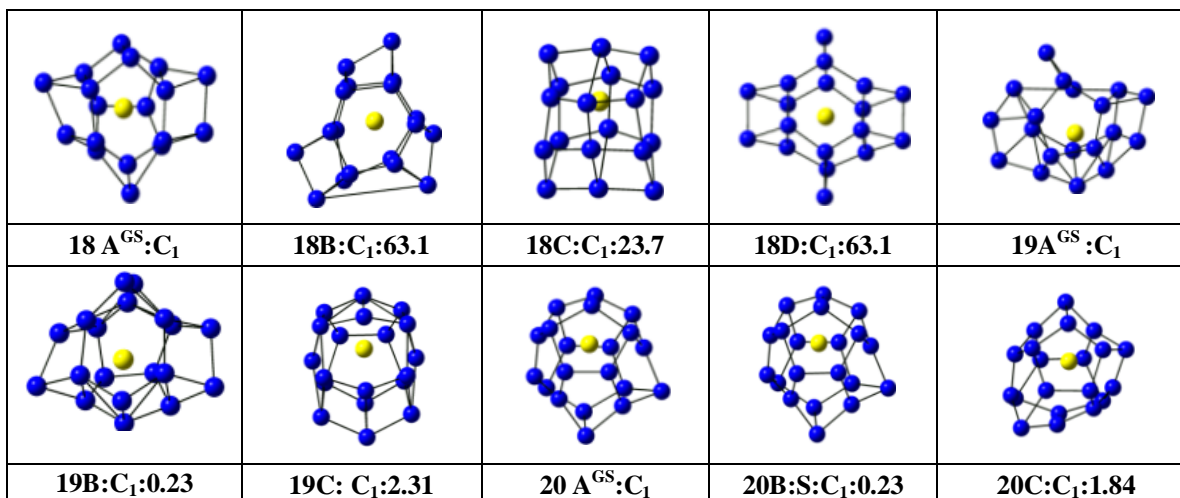
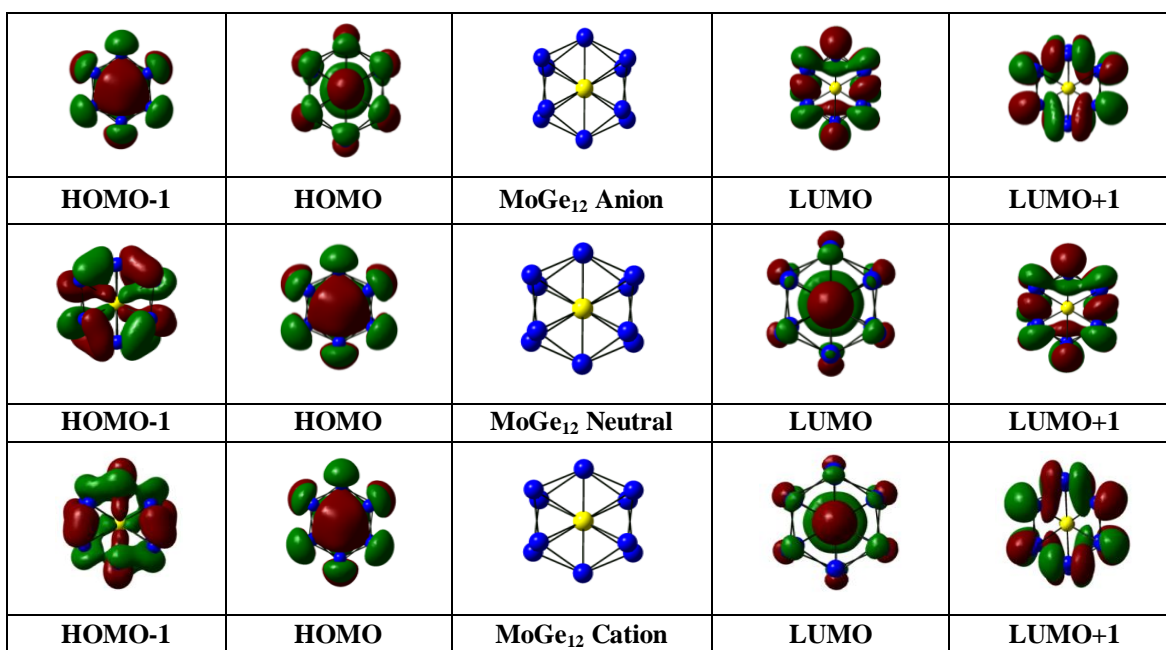


Fig.3.1b Different valence orbital's of MoGe₁₂ in neutral and different charged state



The structure can be understood by capping one germanium atom with the hexagonal plane of n=12 ground state isomer. The ground state structure of MoGe₁₄ is a combination of three rhombus and six pentagons, where, rhombuses are connected only with the pentagons. It is a threefold symmetric structure. The other bigger structures can be understood by adding a single Ge or a Ge-Ge dimer with the lower sizes. In all ground state Ge_nMo clusters from n=10 to 14, Mo atoms takes an interior site of the Ge_n cage and make the cages more symmetric compare to the

pure Ge_n cages. This continued up to the end size range in the present study. Among all these nanoclusters between $8 \leq n \leq 20$, the ground state MoGe_{12} is the most symmetric.

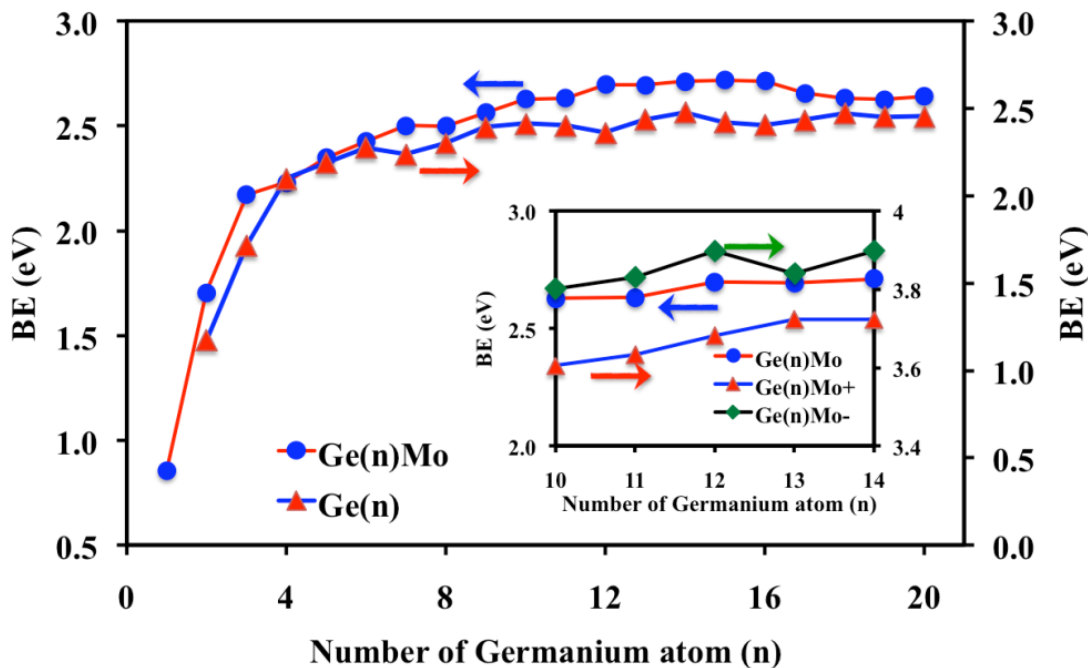
3.3.1 Electronic structure and properties

We first studied the energetic of pure Ge_n and MoGe_n clusters. Then we explored the electronic properties and stabilities of the MoGe_n clusters, by studying the variation of different thermodynamic parameters of the clusters, like, average binding energy (BE), embedding energy (EE), fragmentation stability (ΔE) and second order change in energy (Δ_2) with the increase of the cluster size following the reported work [7-11]. The average binding energy per atom of MoGe_n clusters here is defined as:

$$BE = (E_{\text{Mo}} + nE_{\text{Ge}} - E_{\text{MoGe}_n}) / (n + 1) \quad (3.1)$$

and by definition it is always positive. The variation of the binding energy of the clusters with the cluster size is presented in fig.3.2. For pure germanium clusters E_{Mo} in the above equation is taken as zero and $n+1$ is replaced by n . Following the graph, the binding energy of small sized clusters in the size ranges from 1 to 5 increases rapidly. This is an indication of thermodynamic instability of these clusters (both pure and doped Ge_n).

Fig.3.2 Variation of average binding energy of the MoGe_n clusters with the cluster size (n)



For the sizes $n > 5$ the binding energy curve increase with relatively slower rate. Binding energy of the Mo doped clusters is always higher than the same size pure germanium cluster for $n > 6$ indicate that the doping of transition metal atom helps to increase the stability of the clusters. It is to be noted that there are two local maxima in the binding energy graph at $n=12$ and 14 . According to the 18- or 20-electron counting rule, the binding energy and other thermodynamic parameter should show a local maxima (or minima) at $n=12$ and 14 for neutral clusters respectively. Other 18 and 20 electron clusters are at $n=13$ and 15 in cationic and $n=11$ and 13 in anionic states assuming each germanium atom is contributing one valance electron in the hybridization with the Mo following our previous work [10]. Following the fig.3.2, the behavior of the neutral and anionic clusters is same and both of them show a peak at $n=12$ in the binding energy graph. However, the cationic cluster shows a peak at $n=11$ and it follows the demand of the 18-electron counting rule. Because of the anomalous behavior of the anionic clusters, in the present study we considered only neutral and cationic clusters. Another important parameter that explains thermodynamic stability of the nanoclusters is embedding energy (EE). In the present study, the embedding energy of a cluster after imposing Wigner-Witmer spin-conservation rule [19] is defined as:

$$\begin{aligned}
 EE^{WW} &= E\left({}^M Ge_n\right) + E\left({}^0 Mo\right) - E\left({}^M Ge_n Mo\right) \\
 \text{or,} & \\
 EE^{WW} &= E\left({}^0 Ge_n\right) + E\left({}^M Mo\right) - E\left({}^M Ge_n Mo\right)
 \end{aligned}
 \tag{3.2}$$

where, M is the total spin of the cluster or the atom in units of $h/2\pi$. Following this definition EE is positive, which means addition of transition metal atom to the cluster, is favorable. In the above embedding energy expressions, we have chosen the higher of the resulting two EEs. In the present calculation, ground states for $n=1$ and 2 are quintet and triplet respectively. For $n > 2$, all ground states are in singlet state. Therefore, to calculate the EE according to the WW spin-conversation rule, pure Ge clusters were taken to be in either the triplet or the singlet state. For cationic $MoGe_n$ clusters the EE can be written as:

$$\begin{aligned}
 EE^{WW} &= E\left({}^M Ge_n^\pm\right) + E\left({}^0 Mo\right) - E\left({}^M Ge_n Mo^\pm\right) \\
 \text{or,} & \\
 EE^{WW} &= E\left({}^0 Ge_n\right) + E\left({}^M Mo^\pm\right) - E\left({}^M Ge_n Mo^\pm\right)
 \end{aligned}
 \tag{3.3}$$

Variation of EE and ionization potential with the size of cluster is shown in fig. 3.3a. Both neutral and cationic clusters show maxima at $n=12$ and 13 respectively. Both the clusters are 18-electron clusters.

To check whether the neutral and cationic clusters are following 20-electron counting rule, we studied the BE and EE values at n=14 and 15. In the BE graph, at n=14, there is no relative maxima. At n=14, EE shows a local minima. Hence it clearly shows that n=14 ground state clusters does not follow 20-electron counting rule. To further check the stability of the clusters during the growth process by adding germanium atom one by one to Ge-Mo dimer, fragmentation energy (FE), $\Delta(n, n-1)$ and 2nd order difference in energy (Δ_2 or stability) are calculated following the relations given below:

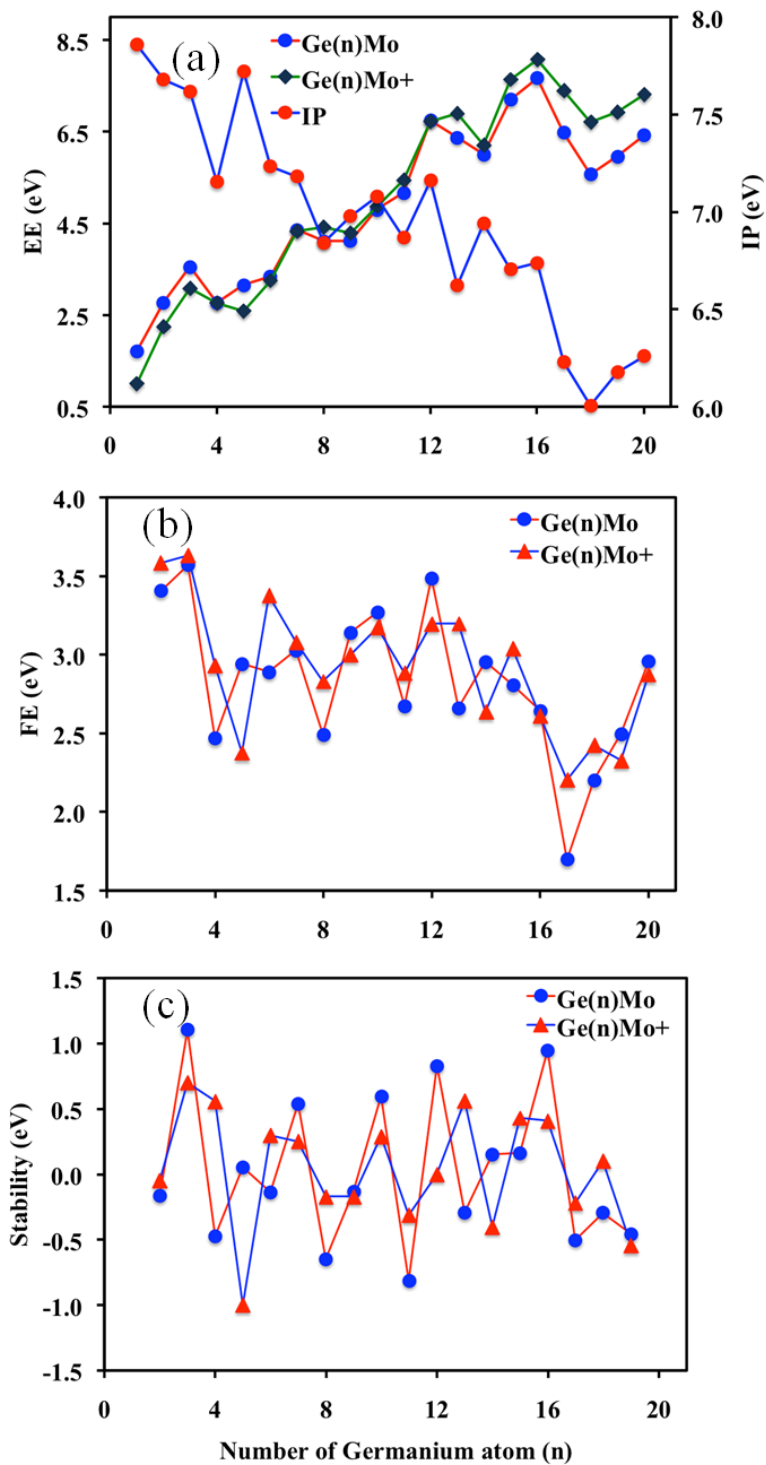
$$\Delta(n, n - 1) = -(E_{Ge_{n-1}Mo} + E_{Ge} - E_{Ge_nMo}) \quad (3.4)$$

$$\Delta_2(n) = -(E_{Ge_nMo} + E_{Ge_{n-1}Mo} - 2E_{Ge_nMo}) \quad (3.5)$$

means, higher positive values of these parameters indicate the higher stability of the clusters compare to its surrounding clusters during growth process. Variations of fragmentation energy and stability with the size for neutral and cationic clusters are shown in Figs. 3.3b and 3.3c respectively. The sharp rise in FE from n=11 to 12 and sharp drop in the next step from n=12 to 13 during growth process indicates that in neutral state MoGe₁₂ size is favorable compare to its neighboring sizes. The same is true for cationic clusters at n=13. This is an indication of higher stability of neutral MoGe₁₂ and cationic MoGe₁₃ clusters. There is a sharp rise in Δ_2 when 'n' changes from 11 to 12 and from 12 to 13 in neutral and cationic states respectively as shown in Fig. 3.3c. This is an indication of higher stability of the clusters at n=12 and 13 in neutral and cationic states respectively. Drastic drop in Δ_2 from n=12 to 13 in neutral and from n=13 to 14 in cationic clusters respectively are again indication of the enhanced stability of these clusters. Both of these parameters are again supporting the enhanced stability of ground state neutral n=12 and cationic n=13 clusters during the growth process and follow 18-electron counting rule. The binding energy of the clusters, both in pure Ge_n and Ge_nMo, first increases rapidly and then saturates with a small fluctuation. However, the variation of Δ_2 and Δ , is oscillatory in nature. We also measured the gain in energy in pure germanium clusters. The gain in energy (2.83 eV) in pure Ge₁₃ cluster is higher than Ge₁₂ (2.68 eV) and Ge₁₄ (2.80 eV). The gain in energy is even more in doped clusters. For MoGe₁₁, MoGe₁₂ and MoGe₁₃ these values are 2.33 eV, 3.13 eV and 2.30 eV respectively. Though the FE and stability are oscillatory in nature, but from the systematic behavior of these two parameters at n=12 (neutral) and 13 (cationic) sizes we can take these two 18-electron clusters as the most stable clusters in the neutral and cationic MoGe_n series. Therefore, it is clear that BE, EE, FE and Δ_2 (n)

parameters support relatively higher thermodynamic stability of MoGe_{12} in neutral and MoGe_{13} in cationic states where both the clusters have closed shell filled 18-electron structure.

Fig. 3.3 Variation of (a) embedding energy (EE) and ionization potential (IP), (b) stability, and (c) fragmentation energy (FE) of neutral and cationic MoGe_n clusters with the cluster size (n)



To understand the stability of the MoGe_{12} cluster we further studied the charge exchange between the germanium cage and the embedded Mo atom in hybridization during the growth process using Mulliken charge population analysis and shown in fig.3SID (Appendix A). As like the other thermodynamic parameters, the charge on the Mo and Ge atoms show a global maximum and minimum respectively at $n = 12$. The electronic charge transfer is always from germanium cage to Mo atom in different MoGe_n clusters. In the figure the charge on Mo is plotted in units of 'e', the electronic charge. Since the average charge per germanium atom and the charge on molybdenum atom in MoGe_{12} cluster are minimum and maximum respectively, therefore the electrostatic interaction increases and hence improve the stability of MoGe_{12} cluster. The effect of ionization (neutral to cation or anion of $n=12$ ground state) that gives redistribution of electronic charge density in the orbital's can be seen from the orbital plot in the Fig 3.1 (b), addition of one electron to Ge_{12}Mo neutral cluster, the higher order orbital's just shifts to one step down and holds the orbital's similar to the neutral cluster. As example, the HOMO, LUMO and LUMO+1 orbital's of neutral MoGe_{12} shifts to anionic Ge_{12}Mo HOMO-1, HOMO and LUMO respectively. However, the HOMO and LUMO orbital's remains unchanged when neutral Ge_{12}Mo cluster ionized to cationic cluster. Details of the natural electronic configuration (NEC) for Ge_{12}Mo ground state cluster is shown in Table 3.2. Combining the fig. 3SID (Appendix A) and Table 3.2, it is seen that when the charge transfer takes place between the germanium cage and the Mo atom, at the same time there is rearrangement of electronic charge in 5s, 4p and 4d orbital's in Mo; and 3d, 4s and 4p orbital's of Ge to make the cluster stable. According to the Table 3.2, the main change contribution in hybridization between Mo and Ge are from d-orbital's of Mo and s, p orbitals of Ge atoms in the ground state MoGe_{12} cluster. The average charge contribution from s, p and d orbitals of Ge are in the ratio of 1.22:1.04:0.05, whereas, in Mo the ratio is 0.37:0.48:4.28. In Ge_{12}Mo cage Mo atom gain about 4.0 electronic charges from the cage where average charge contribution from the Ge atoms is 0.34e, means the Mo atom behaves as a bigger charge receiver or as superatom. It enhances the electrostatic interaction between the cage and the Mo atom, which plays an important role in stabilizing MoGe_{12} cage.

Similar information we obtained from the total density of states plot with s-, p-, d- site projected density of state contribution of Mo atom in different clusters in the size range $n=10$ to 14 and in different charged states shown in fig. 3SIE (Appendix A). The PDOS is calculated using Mulliken population analysis. The DOS illustrates the presence of an electronic shell structure in MoGe_{12} where the shapes of the single electron molecular orbitals (MOs) can be compared with the wave functions of a free electron in a spherically symmetric potential. The broadening in DOS occurs due to the high coordination of the central Mo atom. According to the phenomenological shell model in

simple way assumes that the valence electrons in a cluster usually delocalized over the surface of the whole cluster whereas the nuclei and core electrons can be replaced by their effective mean-field potential. Therefore, the molecular orbitals (MOs) have the shape similar to those of the s, p, d, ...etc atomic orbitals which is labeled as S, P, D, ... etc.

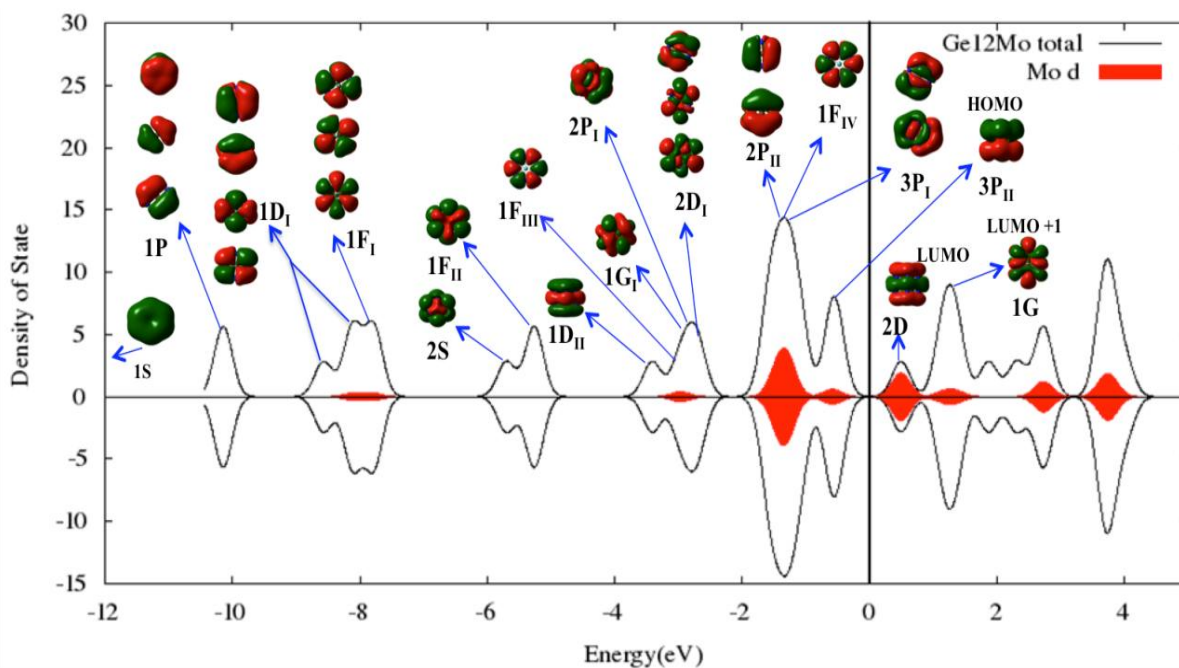
Table 3.2 Natural electronic configuration (NEC) in MoGe₁₂ cluster

Atom	Orbital charge contribution			Total Charge	NEC
	s	p	d		
Ge	1.220	1.052	10.002	12.274	3s ^{1.220} 4p ^{1.052} 4d ^{10.002}
Ge	1.218	1.057	10.002	12.277	3s ^{1.218} 4p ^{1.057} 4d ^{10.002}
Ge	1.219	1.054	10.002	12.275	3s ^{1.219} 4p ^{1.054} 4d ^{10.002}
Ge	1.219	1.053	10.002	12.274	3s ^{1.219} 4p ^{1.053} 4d ^{10.002}
Ge	1.221	1.049	10.002	12.271	3s ^{1.221} 4p ^{1.049} 4d ^{10.002}
Ge	1.217	1.058	10.002	12.277	3s ^{1.217} 4p ^{1.058} 4d ^{10.002}
Ge	1.219	1.051	10.002	12.272	3s ^{1.219} 4p ^{1.051} 4d ^{10.002}
Ge	1.221	1.046	10.001	12.268	3s ^{1.221} 4p ^{1.046} 4d ^{10.001}
Ge	1.219	1.050	10.002	12.271	3s ^{1.219} 4p ^{1.050} 4d ^{10.002}
Ge	1.219	1.053	10.002	12.273	3s ^{1.219} 4p ^{1.053} 4d ^{10.002}
Ge	1.217	1.054	10.002	12.273	3s ^{1.217} 4p ^{1.054} 4d ^{10.002}
Ge	1.221	1.045	10.001	12.268	3s ^{1.221} 4p ^{1.045} 4d ^{10.001}
Mo	0.375	0.484	4.273	5.1320	5s ^{0.375} 4p ^{0.484} 4d ^{4.273}

Enhanced stability of the clusters is expected if the number of delocalized electrons corresponds to a closed electronic shell structure. The sequence of the electronic shells depends on the shape of the confining potential. For a spherical cluster with a square well potential, the orbital sequence is 1S²; 1P⁶; 1D¹⁰; 2S²; 1F¹⁴; 2P⁶; 1G¹⁸; 2D¹⁰; 1H²²; ..., corresponding to shell closure at 2, 8, 18, 20, 34, 40, 58, 68, 90, ... roaming electrons. There are 54 valence electrons in MoGe₁₂. By comparison of the wave functions, the level sequence of the occupied electronic states in Ge₁₂Mo can be described as 1S²; 1P⁶; 1D⁸ (1D_I⁸ + 1D_{II}²); 1F¹⁰ (1F_I⁶ + 1F_{II}² + 1F_{III}² + 1F_{IV}²); 2S²; 1G²; 2P⁶ (2P_I² + 2P_{II}⁴); 3P⁶ (3P_I² + 3P_{II}²); 2D². Their positions in the DOS plot are shown in Fig. 3.4. Due to the crystal field splitting, which is related to the non-spherical or distorted spherical symmetry of the cluster some of the orbitals with higher angular momentum lifted up [39]. As example, 2P orbital of MoGe₁₂ cluster splitted into two as mentioned above. The most important difference with the energy level sequence of free electrons in a square well potential is the lowering of the 2D level. Examination of the 2D molecular orbitals show that they are mainly composed of the Mo

3d AOs, representing the strong hybridization between the central Mo with the Ge cage. The strong hybridization of the Mo 4d electrons with the Ge valence electrons (evidenced by the PDOS shown in fig. 3SIE (Appendix A) has implications for the quenching of magnetic moment of Mo. According to Hund's rule, the electronic configuration in molybdenum is $([Kr] 5s^1 4d^5)$. As per this arrangement Mo should pose a very high value of magnetic moment equal to $6 \mu_B$. The local magnetic moment of Mo in $Ge_{12}Mo$ is zero as well as in all the ground state isomers (except ground states quintet Ge-Mo dimer and triplet Ge_2Mo). The quenched magnetic moment can be attributed to the charge transfer and the strong hybridization between the Mo 4d orbitals and Ge 4s, 4p orbitals. Mixing of d-orbital of transition metal is the main cause of stability enhancement in the cluster here.

Fig. 3.4 Density of states of ground state $MoGe_{12}$ cluster and its orbital with their position in DOS



Though there is dominating contribution of Mo d-orbital in the $Ge_{12}Mo$ cluster, but close to the Fermi level hardly there is any DOS or any contribution from Mo d-orbital. This explains the presence of HOMO-LUMO gap in the cluster and less reactive nature of the cluster. This is also true for the ground state clusters for $n=10$ and 11 . From the DOS picture, it is clear that for $n=10, 11, 12$ and 13 ground state clusters the HOMO-LUMO gap is comparable. The DOS of the anionic $Ge_{11}Mo$, which is an 18-electron cluster, show the presence of considerable fraction of DOS on the Fermi level. Therefore, there is a possibility for anionic $Ge_{11}Mo$ cluster to form a ligand and at the higher charged states by combining with other species it can make a more stable species which is

an indication of possibility of making cluster assembled materials. To get an idea how the magnetic moment of the clusters are changing and reducing to zero from Ge-Mo dimer with the increase of the cluster size, we have studied the site projected magnetic moment of the small sized neutral and cationic clusters (up to n=3) following the work reported by Hou et al.[5]. The Ge-Ge dimer is in triplet state with ferromagnetic coupling between the germanium atoms with total magnetic moment of $2\mu_B$. On the other hand, in Mo-Mo dimer, though the individual moment of the Mo atoms are very high, but the interaction between them is antiferromagnetic and hence the magnetic moment of Mo-dimer is reduces to zero. Detailed results of the variation of magnetic moments are given in fig. 3SIA. The ground states of neutral and cationic Ge-Mo dimers in quintet and quartet spin states with the magnetic moment of the clusters are 4μ and 3μ respectively. The interaction between the Ge-Mo in the ground state is antiferromagnetic with a bond length of 2.50\AA . In the cationic cluster the bond length reduces to 2.67\AA with the presence of antiferromagnetic interactions between Ge and Mo. The same dimer, when it is in triplet and septet spin states, the magnetic interactions changes from antiferromagnetic to ferromagnetic, and the bond length changes from 2.34\AA to 2.73\AA respectively. Following the electronic configuration of 10 (4 from Ge and 6 from Mo) valance electrons (Triplet: $\sigma s^2 \sigma s^2 \pi p^2 \pi p^2 \sigma s^1 \pi p^1$; Quintet: $\sigma s^2 \sigma s^2 \pi p^2 \pi p^1 \sigma s^1 \pi p^1 \pi p^1$; Septet: $\sigma s^2 \sigma s^2 \pi p^1 \pi p^1 \sigma s^1 \pi p^1 \pi p^1 \pi p^1$) and corresponding orbitals (fig. 3SID (Appendix A), it can be seen that while shifting from triplet to quintet state, a beta electron from πp^2 state shifted to $\alpha\text{-}\pi p^1$ state, which is at much dipper position compare to the $\alpha\text{-HOMO}$ orbital. In the whole rearrangement of the orbitals due to this spin flip, the $\alpha\text{-HOMO}$ orbital of the triplet state move to $\alpha\text{-HOMO}$ orbital of quintet spin state with a small difference in energy of 0.08eV with the same antiferromagnetic interaction between the two atomic spins. It is also important to mention that in quintet state, the local spin of Mo increases, whereas the same in Ge decreases compare to the spins in triplet state. Due to the transition from quintet to septet, the πp^1 ($\beta\text{-HOMO}$) shifted to $\alpha\text{-HOMO}$ of energy difference of 1.10eV compare to the $\beta\text{-HOMO}$ in quintet state. The magnetic interaction also changes from antiferromagnetic to ferromagnetic. In triplet and septet states, the optimized energies of the clusters are 0.25eV and 0.57eV respectively more compare to the quintet ground state. Hence the dimer Ge-Mo is found more stable in quintet spin state. Addition of one germanium atom to the Ge-Mo dimer, the ground state found is in triplet spin state. In MoGe_2 ground state cluster in triplet spin state the interactions between the Mo and the two-germanium atoms are antiferromagnetic with the spin magnetic moments $3.34\mu_B$, $-0.67\mu_B$ and $-0.67\mu_B$ respectively and with different bond lengths fig.3SIA (Appendix A). Due to the antiferromagnetic bonding between the Mo and two Ge atoms, the magnetic moment reduces to $2\mu_B$ in MoGe_2 ground state cluster. The two-germanium atoms are connected by π -bonding as shown in the filled $\alpha\text{-HOMO}$ orbital

(fig. 3SIB (Appendix A). The other two low energy clusters are in singlet spin states. From the electronic configuration of 14 (4 from each Ge atoms and 6 from Mo) valance electrons (Triplet: $(3a_1)^2 2(b_2)^2 4(a_1)^2 2(b_1)^2 5(a_1)^2 1(a_2)^2 3(b_2)^1 6(a_1)^1$; Quintet: $(3a_1)^2 2(b_2)^2 4(a_1)^2 2(b_1)^2 5(a_1)^2 1(a_2)^1 3(b_2)^1 6(a_1)^1 3(b_1)^1$) and corresponding orbitals shown in fig. 1SID (Appendix A) in Ge_2Mo it can be seen that the β -HOMO electron from $1(a_2)^2$ in triplet state transferred to α -HOMO in quintet spin state of Ge_2Mo cluster which is at +0.93eV higher compare to triplet α -HOMO level. During this transition the overall ground state energy change is +0.56 eV. Therefore, addition of one Ge atom with the Ge-Mo dimer in quintet state reduces the magnetic moment and as a result the MoGe_2 cluster in triplet spin state is the ground state. It is also interesting to study the charge or the orbitals distributions in β -HOMO triplet and α -HOMO quintet of MoGe_2 cluster. The orbital distributions indicating the presence of electron distributions along the bond between the Ge-Mo dimers and hence the bonding nature is strong and therefore the spin magnetic moment of Mo reduces to $3.34\mu_B$. In the same state, the hardly there is any orbital distributions along Ge-Ge bond. When it switches in the septet state, the bonding between Ge-Mo has increased and reduced in Ge-Ge. Therefore the spin of Mo has increased. The magnetic moment vanishes in MoGe_3 ground state cluster completely with no non-zero onsite spin values of the atoms. With reference to the work reported by Khanna et al. [40], when a 3d transition atom makes bond with Si cluster in a Si_nTM , there always exists a strong hybridization between the 3d of the TM with 3s3p of Si atoms. The present investigation as discussed above following the same as reported by Khanna et. al [40] and is one of the strongest evidence of the quenching of spin magnetic moment of Mo atom. The strong hybridization between $4d^5$ of Mo with the $4s^2 4p^2$ of Ge atom, the magnetic moment of Mo quenched with no left over part to hold its spin moment in MoGe_3 ground state cluster. In this contest it is also worth to mention the work of Janssens et al. [41] on the quenching of magnetic moment of Mn in Ag_{10} cage where they suggested that the valance electrons of silver atoms in the cage can be considered as forming a spin-compensating electron cloud surrounding the magnetic impurity which is conceptually very much similar to Kondo effect in larger system and may be applied in our system also.

To get the idea about the kinetic stability of the clusters in chemical reactions the HOMO-LUMO gap (ΔE), ionization potential (IP), electron affinity (EA), chemical potential (μ), chemical hardness (η) are calculated. In general with the increase of HOMO-LUMO gap the reactivity of the cluster decreases. Variation of HOMO-LUMO gaps of neutral and cationic MoGe_n clusters is plotted and is shown in the fig. 4SI. The variation of HOMO-LUMO gap is oscillatory. Overall there is a large variation in HOMO-LUMO gap in the whole size range between 1.5 to 3.30eV with a local maxima at $n=12$ and at $n=13$ in neutral and cationic clusters respectively. This is again an

indication of enhance stability of 18-electron clusters. The large HOMO-LUMO gap (2.25eV) of MoGe₁₂ could make this cluster as a possible candidate as luminescent material in the blue region. In the neutral state the sizes n=8, 10, 12, 14, 18 are magic in nature, means a higher relative stability. Variation of HOMO-LUMO gap in different clusters around the Fermi level can be useful as device applications. The variation of ionization energy shown in fig. 4a with a sharp peak at n=12 with a value of 7.16eV as like other parameters supports the higher stability of MoGe₁₂ cluster. According to the electron shell model, whenever a new shell starts filling for the first time, its IP drops sharply. De Heer [42] has reported that in Li_n series, L₂₀ cluster is a shell field configuration and there is a sharp drop in IP when the cluster grows from L₂₀ to L₂₁. This is one of the most important evidence to support MoGe₁₂ as an 18-electron cluster. There is a local peak in the IP graph at n=12, followed by a sharp drop in IP at n=13. The drop in IP could be the strongest indication of the assumption of nearly free-electron gas inside the MoGe₁₂ cage cluster. Following the other parameters, one may demand that the MoGe₁₄ cluster is following the 20-electron counting rule. But we did not accept it, because the IP at n=14 does not show local maxima. From the above discussion, it is clear that the neutral hexagonal D_{6h} structure of MoGe₁₂ with a large fragmentation energy, averaged atomic binding energy and IP is suitable as the new building block of self assembled cluster materials. This is reflecting that the stability of the pure germanium cluster is obviously strengthened when the Mo atom is enclosed in its Ge_n frames. Hence it can be expected that the enhanced stability of MoGe₁₂ makes a contribution toward the initial model to develop a new type of Mo doped germanium superatom as well as Mo-Ge based cluster assembled materials. Further, to verify the chemical stability of Ge_nMo clusters, chemical potential (μ) and chemical hardness (η) of the ground state isomers are calculated. In practice chemical potential and chemical hardness can be expressed in terms of electron affinity (EA) and ionization potential (IP). In terms of total energy consideration if E_n is the energy of the n electron system, then energy of the system containing n+Δn electrons where Δn<<n can be expressed as:

$$E_{n+\Delta n} = E_n + \left. \frac{dE}{dx} \right|_{x=n} \Delta n + \left. \frac{1}{2} \frac{d^2E}{dx^2} \right|_{x=n} (\Delta n)^2 + \text{Neglected higher order terms}$$

Then, μ and η can be defined as:

$$\mu = \left. \frac{dE}{dx} \right|_{x=n} \quad \text{and} \quad \eta = \left. \frac{1}{2} \frac{d^2E}{dx^2} \right|_{x=n} = \left. \frac{1}{2} \frac{d\mu}{dx} \right|_{x=n}$$

Since, $IP = E_{n-1} - E_n$ and $EA = E_n - E_{n+1}$.

By setting $\Delta n = 1$, μ and η are related to IP and EA via the following relations:

$$\mu = -\frac{IP + EA}{2} \text{ and } \eta = \frac{IP - EA}{2} \quad (3.5)$$

Now for consider two interacting systems with μ_i and η_i (i=1,2) where some amount of electronic charge (Δq) transfers from one to other. The quantity Δq and the resultant energy change (ΔE) due to the charge transfer can be determined in the following way:

If $E_{n+\Delta q}$ is the energy of the system after charge transfer then it can be expressed for the two different systems 1 and 2 in the following way:

$$E_{1n_1+\Delta q} = E_{1n_1} + \mu_1(\Delta q) + \eta_1(\Delta q)^2$$

$$\text{and } E_{2n_2-\Delta q} = E_{2n_2} - \mu_2(\Delta q) + \eta_2(\Delta q)^2$$

Corresponding chemical potential becomes,

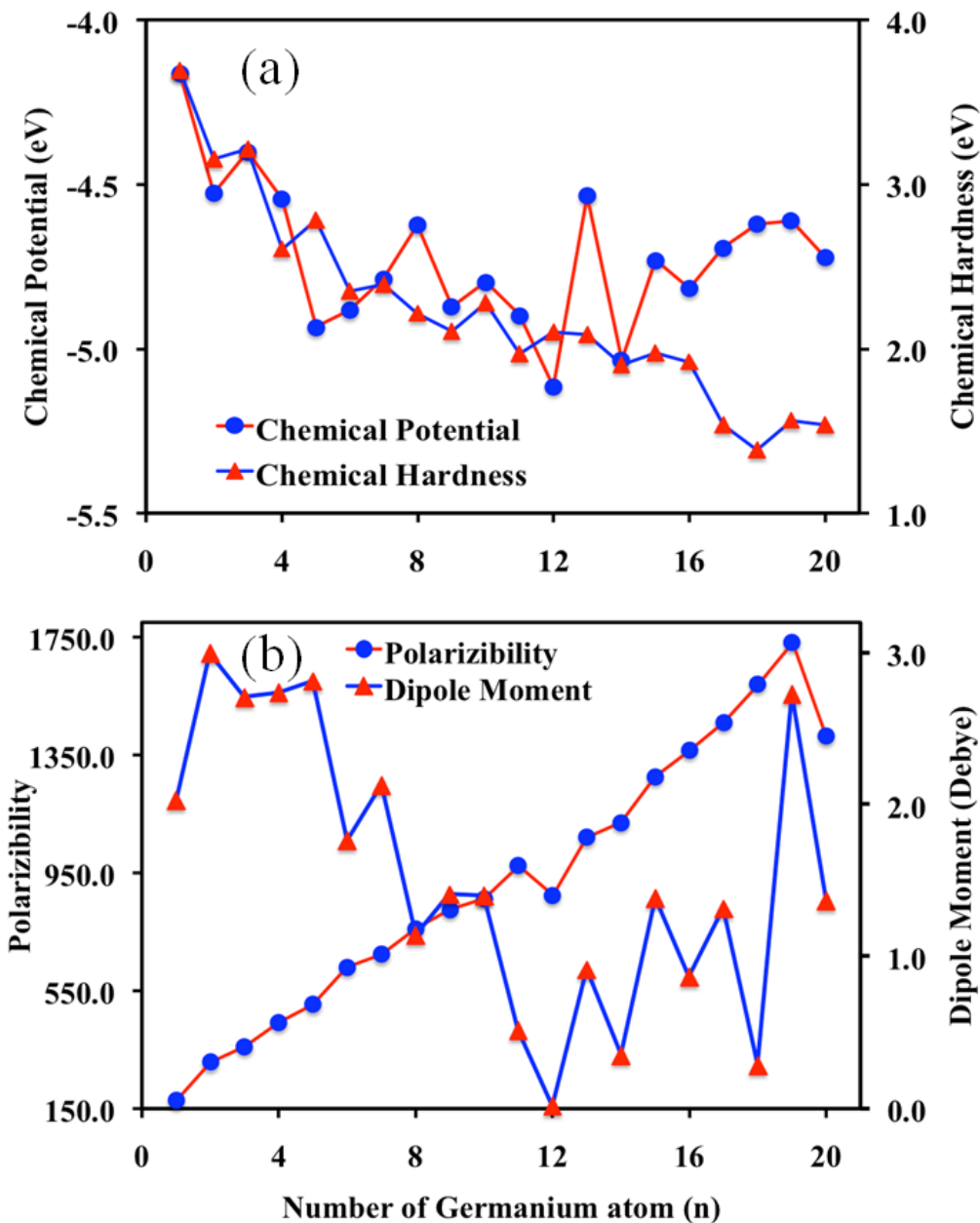
$$\mu'_1 = \left. \frac{dE_{1x+\Delta q}}{dx} \right|_{x=n_1} = \mu_1 + 2\eta_1\Delta q \text{ and } \mu'_2 = \left. \frac{dE_{2x-\Delta q}}{dx} \right|_{x=n_2} = \mu_2 - 2\eta_2\Delta q \text{ to first order in } \Delta M \text{ after the charge}$$

transfer. In chemical equilibrium, $\mu'_1 = \mu'_2$ which gives the following expressions:

$$\Delta q = \frac{\mu_2 - \mu_1}{2(\eta_1 + \eta_2)} \text{ and } \Delta E = \frac{(\mu_2 - \mu_1)^2}{2(\eta_1 + \eta_2)} \quad (3.6)$$

In the expression, energy gains by the total system (1 and 2) due to exclusive alignment of chemical potential of the two systems at the same value. From the above expressions that for easier charge transfer from one system to other it is necessary to have a large difference in μ together with low η_1 and η_2 . Therefore, Δq and ΔE can be taken as the measuring factors to get the idea about the reaction affinity between two systems. Since they are function of the chemical potential and chemical hardness related to the system,

Fig.3.5 Variation of (a) chemical potential and chemical hardness and (b) polarizability and electrostatic dipole moment of $MoGe_n$ clusters with the cluster size



so it is important to calculate these parameters of a system to know about its chemical stabilities in a particular environment. Keeping these in mind, chemical potential (μ) and chemical hardness (η) for Mo doped Ge_n clusters is calculated. Dip at $n=12$ in chemical potential plot (Fig. 3.6(a)) is actually indicating stable chemical species, hence low affinity of the system to take part in chemical reaction in a particular environment. Again at $n=12$, the presence of a local peak in chemical hardness plot is also supporting the result of low chemical affection $MoGe_{12}$ cluster. The ratio of these two parameters in positive sense shows a peak and hence indicating the low chemical affinity. Since

n=12 is an 18-electron cluster, it is clear that this cluster also show low affinity in chemical reaction and is in stability agreement with the other parameters.

3.3.2 Polarizability

It is known that the static polarizability is a measure of the distortion of the electronic density and sensitive to the delocalization of valance electrons [43]. Hence it is the measure of asymmetry in three-dimensional structures and orbital distributions. It gives the information about the response of the system under the effect of an external electrostatic electric field. The average static polarizability is defined as:

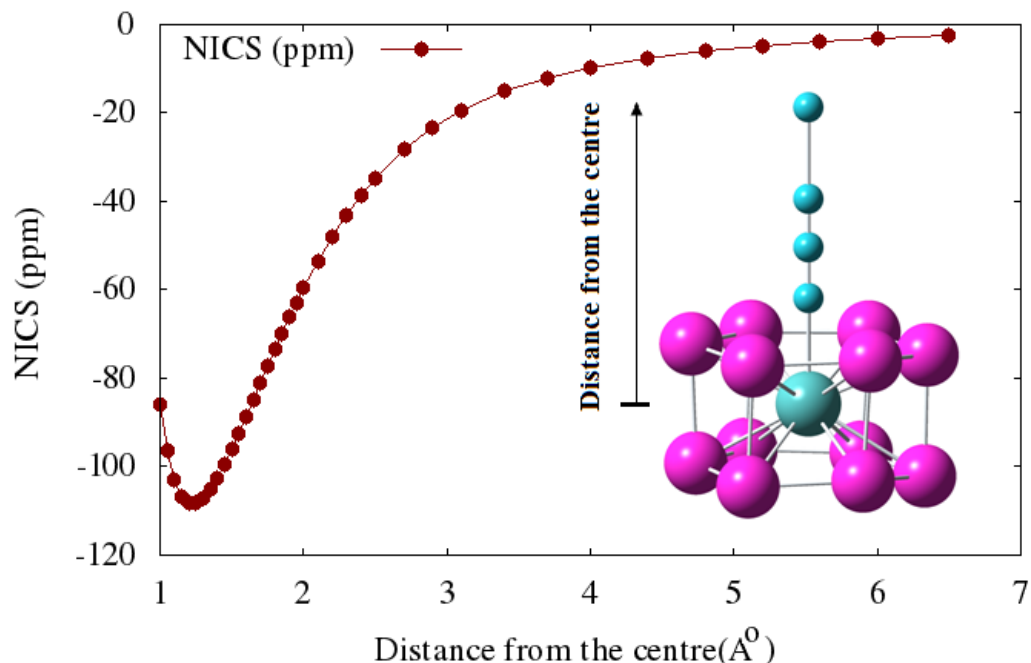
$$\langle \alpha \rangle = \frac{1}{3} (\alpha_{XX} + \alpha_{YY} + \alpha_{ZZ}) \quad (3.7)$$

in terms of principle axis, which is a function of basis set, used in the optimization of the clusters [44, 45]. In the current work, the variation of polarizability and the electrostatic dipole moment of the clusters are shown in fig. 3.6(b). Variation of the exact polarizability with the size of the cluster is shown in fig. 3SIG. As is exhibited in fig. 3.6(b), one can find that the polarizability of the cluster increase as a function of the cluster size 'n' which is nearly linear with local dip at n=12. At this size the electrostatic dipole moment is also minimum. This trend of variation of polarizability with the cluster size for MoGe_n clusters is similar to the water clusters reported by Ghanty and Ghosh [45].

3.3.3 Nucleus Independent Chemical Shift (NICS)

The most widely employed method to analyze the aromaticity of different species is the NICS index descriptor proposed by Schleyer et al. [46]. NICS index is defined as the negative value of the absolute shielding computed at a ring center or at some other point of the system which can describe the system nicely, as example, the symmetry point like the center of a hexagon. The rings with more negative NICS values are considered as more aromatic species. On the other hand, zero (or close to zero) and positive NICS values are indicative of non-aromatic and anti-aromatic species. NICS is usually computed at ring centers or at a distance on both side of the ring center. NICS obtained at 1Å above the molecular plane [47] is usually considered to better reflect the p-electron effects than NICS (0).

Fig. 3.6 – NICS plot of MoGe₁₂ cluster



Since we are interested to study the aromaticity of the overall ground state isomer MoGe₁₂, which is hexagonal prism like structure with Mo, doped at the center, we have measured NICS values at the position of Mo and then along the symmetry axis perpendicular to the hexagonal plane surface. The NICS calculations have been performed based on the magnetic shielding using GIAO-B3LYP level of theory by placing a ghost atom at certain points along the symmetry axis. Variation of NICS value with the distance from the center of the system is shown in fig.3.7. Nature of the variation of NICS indicates the aromatic behavior of the cluster with a maximum negative value of -96.033 ppm at the center of the hexagonal surface and with a distance 1.5Å from the center of the cluster. Aromaticity of hexagonal structures (like benzene) is an important conformation of its stability. Therefore, in the present calculations the NICS behavior of MoGe₁₂ also supports the stability of the cluste

3.4 Conclusions

In summary, a report on the study of geometry and electronic properties of neutral and cationic Mo-doped Gen (n =1-20) clusters within the framework of density functional theory is presented. Identification of the stable species, and variation of chemical properties with the size MoGe_n clusters will help to understand the science of Ge-Mo based clusters and superatoms that can be future building blocks for cluster-assembled designer materials and could open up a new field in electronic industry. The present work is the preliminary step in this direction and will

be followed by more detailed studies on these systems in near future. On the basis of the results, the following conclusions have been drawn.

1. The growth pattern of Ge_nMo clusters can be grouped mainly into two categories. In the smaller size range i.e. before encapsulation of Mo atom, Mo or Ge atoms are directly added to the Ge_n or Ge_{n-1}Mo respectively to form Ge_nMo clusters. At the early part in this region the binding energy of the clusters increase in a much faster rate than the bigger clusters. After encapsulation of Mo atom by the Ge_n cluster for $n > 9$, the size of the Ge_nMo clusters tend to increase by absorbing Ge atoms one by one on its surface keeping Mo atom inside the cage.

2. It is favorable to attach a Mo-atom to germanium clusters at all sizes, as the EE turns out to be positive in every case. Clusters containing more than nine germanium atoms are able to absorb Mo atom endohedrally in a germanium cage both in pure and cationic states. In all Mo-doped clusters beyond $n > 2$, the spin magnetic moment on the Mo atom is quenched in expenses of stability. As measured by the BE, EE, HOMO-LUMO gap, FE, stability and other parameters both for neutral and cationic clusters, it is found that those are having 18 valence electrons show enhanced stability which is in agreement with shell model predictions. This also shows up in the IP values of the Ge_nMo clusters, as there is a sharp drop in IP when cluster size changes from $n=12$ to 13. Validity of nearly free-electron shell model is similar to that of transition metal doped silicon clusters. Although the signature of stability is not so sharp in the HOMO-LUMO gaps of these clusters, there is still a local maximum at $n=12$ for the neutral clusters, indicating enhanced stability of an 18-electron cluster, whereas, and this signature is very much clear in cationic MoGe_{13} cluster. Variation in HOMO-LUMO gap in different sized clusters could be useful for devise applications. The large HOMO-LUMO gap (2.25 eV) of MoGe_{12} could make this cluster as a possible candidate as luminescent material in the blue region.

3. Major contribution of the charge from the d-orbital of Mo in hybridization and its dominating contribution in DOS indicate that the d-orbitals of Mo atoms are mainly responsible in the hybridization and stability of the cluster. Presence of the dominating contribution of Mo d-orbital close to the Fermi level in DOS is also significant for ligand formation and a strong indication of possibility to make stable cluster assembled materials.

4. Computations and detailed orbital analysis of the clusters confirmed the rapid quenching of the magnetic moment of Mo in Ge_n host cluster while increasing the size from $n=1$ to 3. Beyond $n=2$, all hybrid clusters are in singlet state with zero magnetic moment. Following the overall shape of the delocalized molecular orbitals of MoGe_{12} (fig.3.5) cage like clusters, the valance electrons of Ge_{12} cage can be considered as forming a spin compensating electron

cloud surrounding the magnetic element Mo as like a screening electron cloud surrounding Mo which is similar to the magnetic element doped bulk materials. Therefore, the system may be interpreted as very similar to that of a finite-size Kondo system.

5. Variation of calculated NICS values with the distance from the center of the cluster clearly indicates that the cluster is aromatic in nature and the aromaticity of the cluster is one of the main reasons for its stability.

3.5 References

- [1] Sattler K, Cluster assembled materials, CRC Press, **1996**; 232.
- [2] Kumar V, Kawazoe Y, Applied Physics Letters, **2001**; 5: 80.
- [3] Gopakumar G, Wang X, Lin L, Haeck JD, Lievens P, Nguyen MT, J Phys Chem C, **2009**; 113: 10858.
- [4] Gopakumar G, Lievens P, Nguyen MT, The J Phys Chem A, **2007**; 111: 4353.
- [5] Hou XJ, Gopakumar G, Lievens P, Nguyen MT, J Phys Chem A, **2007**; 111: 13544.
- [6] Ngan VT, HaeckJD, Le HT, Gopakumar G, Lievens P, Nguyen MT, J Phys Chem A, **2009**; 113 : 9080.
- [7] Bandyopadhyay D, Journal of Applied Physics, **2008**; 104: 084308.
- [8] Bandyopadhyay D, Molecular Simulation, **2009**; 35: 381.
- [9] Bandyopadhyay D, Journal of molecular modeling, **2012**, 18, 737.
- [10] D. Bandyopadhyay D Sen P, J Phys Chemi A, **2010**; 114: 1835.
- [11] D. Bandyopadhyay, M. Kumar, Chemical Physics, **2008**; 353: 170.
- [12] Beck SM, Journal of Chemical Physics, **1987**, 87, 4233.
- [13] Beck SM, J Chem Phys, **1989**; 90: 6306.
- [14] Atobe J, Koyasu K, Furuseand S, Nakajima A , Phys Chem Chem Phys, **2012**; 14: 9403
- [15] Hiura H, Miyazaki T, Kanayama T, Phys Rev Lett, **2001**; 86: 1733
- [16] Wang J, Han JG, Chem Phys, **2007**; 342: 253.
- [17] Guo,LJ, Zhao GF, Gu Y Z, Liu X, Zeng Z , Phys Rev B, **2008**; **77**: 195417
- [18] Reveles JU, Khanna SN, Phy Rev B, **2005**, 72, 16513
- [19] Khanna E, Witmer Witmer, **Z. Phys**, 1928; 51,:859
- [20] Koyasu,K, Akutsu M, Mitsui M, Nakajima A, J Amer Chem Soc, **2005**; 127: 4998
- [21] Lee C, Yang W, Parr RG, Phys Rev B, **1988**; 37: 785
- [22] Frisch MJ, Trucks GW, Schlegel HB, Scuseria GE, Robb MA, Cheesemen JR, Zakrzewski VG, Montgomery jr JA, Stratmenn RE, Burant JC, Dapprich S, Millam JM, Daniels AD, Kudin KN, Strain MC, Farkas O, Tomasi J, Barone V, Cossi M, Cammi R, Mennucci B, Pomelli C, Adamo C, Clifford S, Ochtrski J, Petersson GA, Ayala PY, Cui Q, Morokuma K, Malick DK, Rabuck AD, Raghavachari K, Foresman JB, Cioslowki J, Ortiz JV, Baboul AG, Stefanov BB, Liu B, Liashenko A, Piskorz P, Komaromi I, AL-Laham MA, Peng CY, Nanayakkara Challacombe M, Gill PMW, Johnson B, Chem W, Wong MW, Andress JL, Gonzalez C, Head-Gordon M, Replogle ES, Pople J A, Gaussian 03, revision E 01 Gaussian, Wallingford, 2004

- [23] Hay PJ, Wadt WR, J Chem Phys, **1985**; 82: 270.
- [24] Hay PJ, Wadt WR, J Chem Phys, **1985**; 82: 284
- [25] Glass CW, Oganov GAR, Hansen N, Compu Phys Commu, **2006**; 175: 713.
- [26] Kresse G, Furthmüller, Phys Rev B, **1996**; 54: 11169 .
- [27] Kresse G, Joubert D, Phys Rev B, **1999**; 59: 1758.
- [28] Northrup E, Cohen ML, Chem Phys Lett, **1983**; 102: 440.
- [29] Abteu TA, Darbold DA, Phys Rev B, **2007**; 75: 145201.
- [30] Wang J, Han JG, J Phys Chem A, **2006**; 110: 12670.
- [31] Wang J, Han JG, J Phys Chem A, **2008**; 112: 3224.
- [32] Lombardi JR, Davis B, Chemical Review, **2002**; 102: 2431.
- [33] Kohn W, Sham L, J Phys Rev, **1965**; 140: 1133.
- [34] Tai TB, Nguyen MT, J Chem Theo Commun, **2011**; 7: 1119
- [35] Dhaka K, Trivedi R, Bandyopadhyay D, J Mol Model, **2013**; 19: 1437.
- [36] Kumar M, Bhattacharya N, Bandyopadhyay D, J Mol Model, **2012**; 18: 405.
- [37] Bandyopadhyay D, Kaur P, Sen P, J Phys Chem A, **2010**; 114: 12986.
- [38] Bandyopadhyay D, J Mol Model, **2012**; 18: 3887.
- [39] Li Y, Tam NM, Claes P, Woodham AP, Lyon JT, Ngan VT, Nguyen MT, Lievens P, Fielicke A, Janssens E, J Phys Chem A, **2014**; 118: 8198.
- [40] Khanna SN, Rao BK, Jena P, Phys Rev Lett, **2002**; 89: 016803.
- [41] Janssens E, Neukermans S, Nguyen HMT, Nguyen MT, Lievens P, Phys Rev Lett, **2005**; 94: 113405
- [42] Heer WA, Rev Mod Physics, **1993**; 65: 611
- [43] Zhao YR, Kuang XY, Kuang, BB, Fang Y, Wang SJ, J Phys Chem A, **2011**; 115: 569
- [44] Ghanty TK, Ghosh SKJ, Chemical Physics, **2003**; 118: 8547.
- [45] Ghanty TK, Ghosh SKJ, Phys Chem, **1996**; 100: 17429.
- [46] Schleyer P, van R, Maerker C, Dransfeld A, Jiao H, Hommes NJRE, J Am Chem Soc, **1996**; 118: 6317
- [47] Kuznetsov AE, Boldyrev AI, Chem Phys Lett, **2004**; 388: 452.

CHAPTER 4

ROLE OF NICS AND SHELL CLOSING MODEL IN THE STABILITY OF NEUTRAL AND CATIONIC NbGe_n (n=7-16) CLUSTERS: A DENSITY FUNCTIONAL STUDY

4.1 Introduction

Modeling of computational materials based on non-metals are very rapidly growing field in nanoscience and nanotechnology. Among these, the field dealing with the clusters containing either with IV (Si, Ge) [1-6] or II-VI (ZnS, CdSe) [7-9] groups are important for their potential applications in semiconductor industries. Clusters are the ensembles of bound atoms intermediate in the size ranging between a molecule and the bulk contains few to few hundreds of atoms. Depending upon the composition and sizes, some clusters show enhanced stability compare to their immediate neighbors and are known as magic clusters. Several reasons are responsible for the enhanced stability of the neutral and charged clusters. Among different possibilities of stabilizing hybrid semiconductor nanoclusters, encapsulation of a transition metal (TM) in a pure semiconductor cage is one of the most effective methods. The transition metal atoms absorb the unsaturated bonds present in the semiconductor clusters and make it stable. It is worth mentioning here that the one-electron levels in spherically confined free electron gas distributed according to Hund's rule, and forming a sequence of electronic shell $1S^2$, $1P^6$, $1D^{10}$, $2S^2$, $1F^{14}$, $2P^6$, $1G^{18}$, $2D^{10}$ to give a closed shell electronic shell structure. This kind of clusters with shell closing number of electrons attains enhanced stability. Following this, many insights of the stability of the transition metal-doped Si and Ge clusters were reported on the basis of closed shell 18- or 20-electron counting rules [3-11]. In addition to the closed shell model, the aromatic behavior of the clusters is also one of the most important parameter to enhance in the stability of the clusters [11]. When the nuclear independent chemical shift (NICS), measured by magnetic shielding current, is negative, the cluster shows enhanced stability. Also the higher stability of the clusters could be due to the high point group structural symmetry, chemical inertness and comparatively higher HOMO-LUMO gap. Depending on the doped transition metal atom, even a single doped atom may significantly affect the stability of a semiconductor clusters and show magic behavior which is found by the anion photoelectron spectroscopy [12]. Recently, Kumar et al. [13] studied the divalent-metal (M) atom doped X_nM ($X = \text{Si, Ge, and Sn, } n = 8-12, 14$) clusters and showed that the nine and ten atom capped prism structures as well as 12 and 14 atom clusters can transform into magic clusters with higher symmetry and large HOMO-LUMO gap. One of the most interesting study on 4d transition metal doped Mg_n clusters ($TcMg_n$) were reported by Xian et al. [14] where they found that $TcMg_8$ cluster has enhanced stability and

high magnetic moment. Here the valence electronic configuration follows a sequence $1S^2, 2P^6, 1D^{10}$ which is according to a closed shell model. Chouhan et al. [15] reported a stable magnetic $FeCa_8$ cluster where 24 valance electrons are distributed following a closed shell sequence where last four electrons occupy the majority $2D_{xy}, 2D_x^2, 2D_y^2$, and $2D_{xz}$ and $2D_{yz}$ levels while the unfilled $2D_z^2$ level is separated by a large energy due to atomic deformation and exchange splitting. In the present work we report a density functional investigation to explain the enhanced stability of neutral $NbGe_{12}$ and cationic $NbGe_{16}$ clusters. One of our main goals is to seek stable individual units that can serve as the elementary building blocks for electronic and optical devices.

4.2 Computational Method

In the present work all calculations are performed within the framework of linear combination of atomic orbital's density functional theory (DFT). The exchange–correlation potential contributions were incorporated into the calculation using the spin-polarized generalized gradient approximation (GGA) proposed by Lee, Yang and Parr, popularly known as B3LYP [16]. The standard LanL2DZdp and LanL2DZ basis sets associated with effective core potential (ECP) are used for germanium and molybdenum to express molecular-orbitals (MOs) of all atoms as linear combinations of atom-centered basis functions. LanL2DZdp is a double- ζ , 18-valence electron basis set with a LANL effective core potential (ECP) and with polarization function [17-18]. All geometries are optimized under no external symmetry constrictions. Here we used some selective size as ($n = 7-18$) for optimization. Initially we took several guess geometries configuration at different spin states in a particular size. In order to check the reliability of the applied methodologies, we done calculation on Ge-Ge dimer having bond length 2.44\AA having triplet ground state, which is within the range of the values reported theoretically as well as experimentally studied by Nagendran et al. [19]. The optimized electronic structure was obtained by solving the Kohn-Sham equation self-consistently [20] following the optimization criteria of Gaussian' 03 [21]. All the geometries are constructed on the basis of previous reported work [1-5, 11, 22-25] and from intuitions. For each stationary point of clusters, we have calculated the frequency of harmonic vibration. If any imaginary frequency is found, a relaxation along that vibrational mode is carried out until the true local minimum is obtained.

4.3 Results and discussions

As pointed out earlier, that the electronic shell model can be used efficiently to understand the stability and to predict the electronic properties of the clusters [26-29]. To identify a stable cluster in a particular composition, it is necessary to study the variations of different thermodynamic and chemical parameters, such as, binding energy (BE), fragmentation energy (FE) stability, HOMO-LUMO gap, ionization potential, and electron affinity etc. with

the variation of cluster size during the growth process. In the present investigation, we have studied NbGe_n (n=7-18) clusters both in cationic and neutral states. A number of isomers have been calculated in each size. The most stable ground state isomer along with few lowest energy isomers in each size are shown in fig.4.1. The ground state structure of NbGe₇ is a distorted cube with C_s symmetry, where Nb atom locates at the vertex site. The six Ge atoms out of eight in NbGe₈ ground state structure, forms two rectangles with a common arm where the rectangular surfaces are capped by the rest of the two Ge atoms. The Nb atom caps the open surface forms by the two rectangles. So Nb atom is completely exposed. Starting from n=9, the Nb atom absorbs endohedrally in Ge_n cages. The ground state of NbGe₉ is a simple modification of ground state NbGe₈. The additional Ge atom is now replaced the capped Nb and the Nb atom is completely endohedrally doped by the Ge₉ cage. This is the 1st structure where Nb atom is doped endohedrally. Adding of a Ge atom with the capped rectangular Ge surface now make it pentagonal capped surface and gives the ground state NbGe₁₀. After addition of one more Ge atom, NbGe₁₀ ground state cluster converted to a structure where Nb atom sandwiched between two pentagonal surfaces where one of the surfaces is capped by a Ge atom with C_s symmetry. The immediate higher NbGe₁₂ ground state is a hexagonal prism structure where the endohedrally doped Nb atom makes bonds with all Ge atoms in the cage. The other low energy isomers are distorted icosahedral and fullerene kinds. The geometry of ground state isomer NbGe₁₃ can be understood after capping three germanium atoms at different surfaces of NbGe₁₀ ground state isomer. Ground state NbGe₁₄ is well known structure and is a combination of six pentagons and three rhombuses. The geometry of NbGe₁₅ is a modification of the ground state NbGe₁₀ structure where five additional germanium atoms are added in the form of two Ge-Ge dimers and one germanium atom at different places. NbGe₁₆ ground state is again fullerene kind of structure and is a combination of ten pentagons and two rhombi. The structure can be understood by adding a Ge-Ge dimer at the top of NbGe₁₄ ground state. By adding one Ge atom with the one of the rhombus in NbGe₁₆ and then after optimization one can get NbGe₁₇ ground state structure. NbGe₁₈ is a flying disk like structure where The central part is pentagonal prism kind. Most of these geometries we have reported in our earlier works obtained by global optimization methods in different systems [11]

4.3.1 Electronic structures and stabilities

To check the validity of the methodology used in the present study, first we apply our calculations on Ge-Ge, Ge-Nb and Nb-Nb dimers. The summery of the calculated bond length and harmonic vibration frequencies together with experimental data are summarized in table 4.1. The Ge-Ge dimer has a ground state with bond length of 2.43 Å, which is in excellent agreement with reported theoretical and experimental calculation [30-32]

Fig.4.1 Optimized ground state structures of $NbGe_n$ ($n=7-18$) clusters with point group symmetry. Blue balls are Ge and pink balls are Nb atoms.

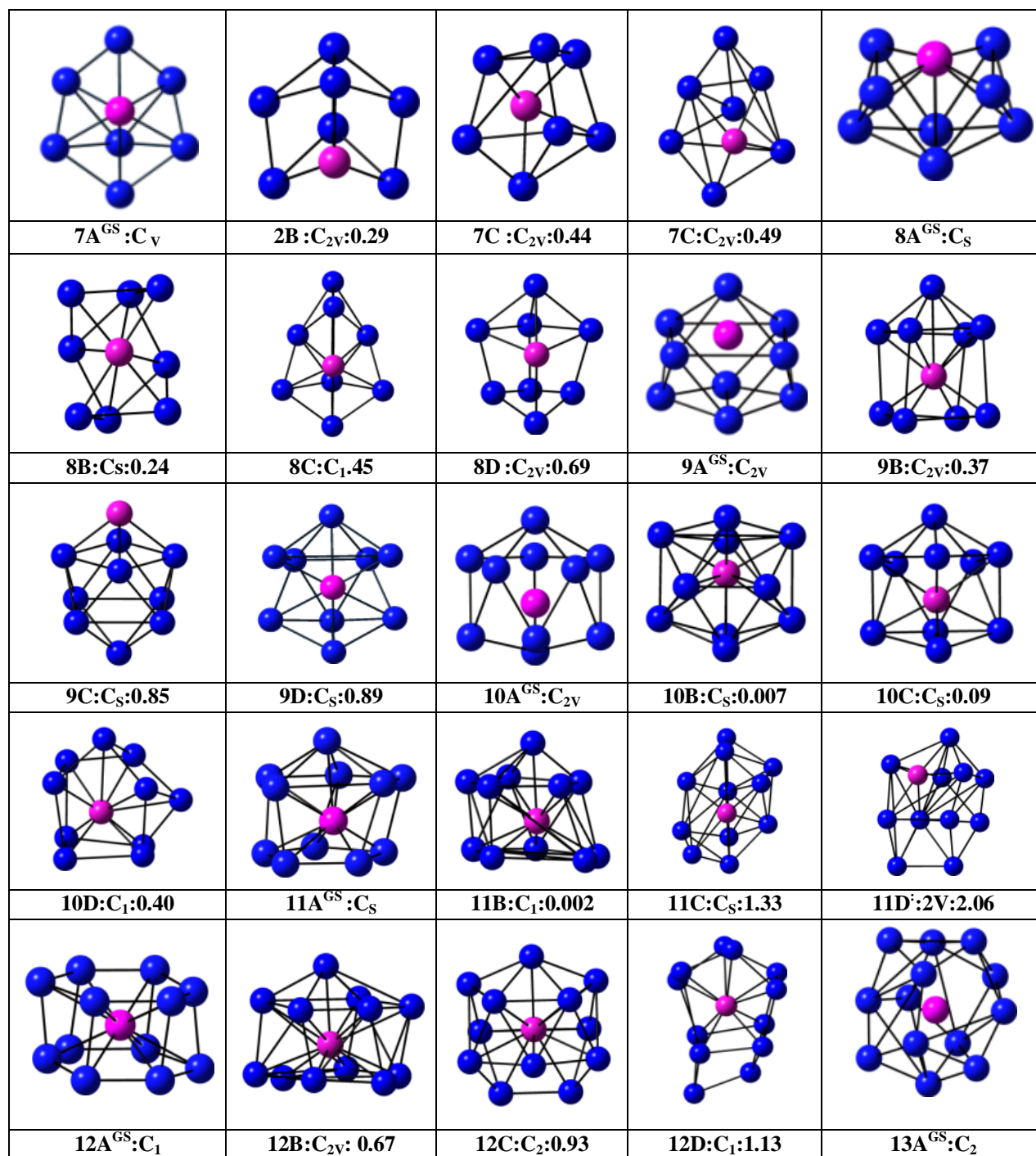
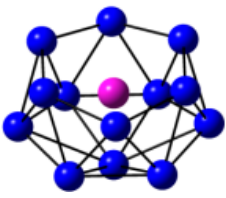
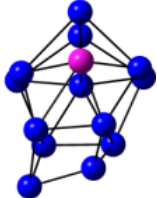
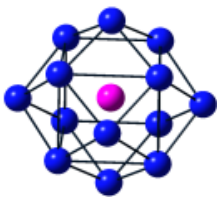
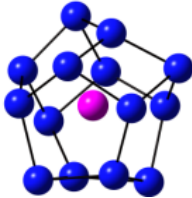
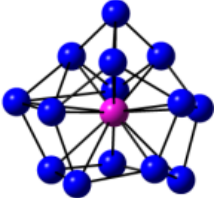
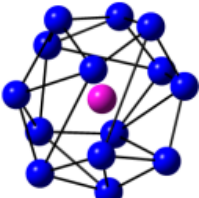
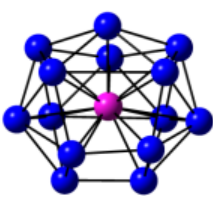
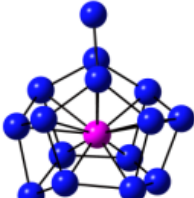
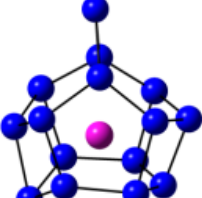
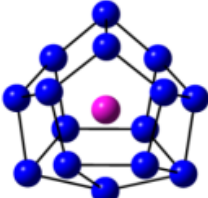
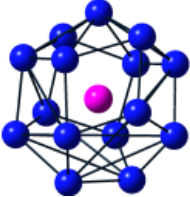
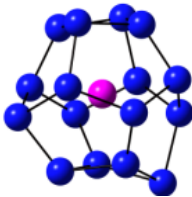
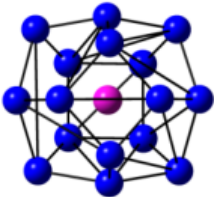
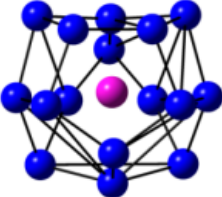
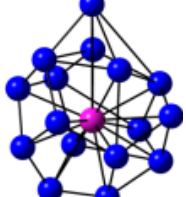
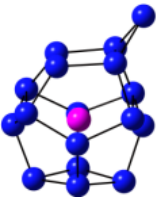
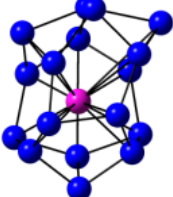
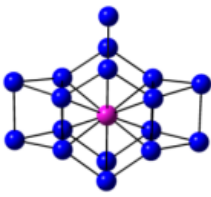
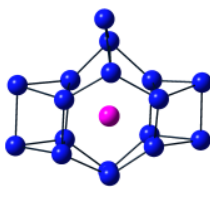
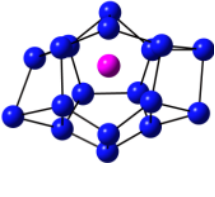
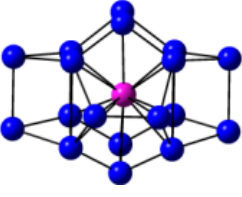
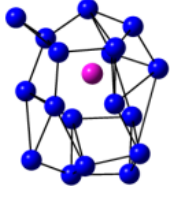
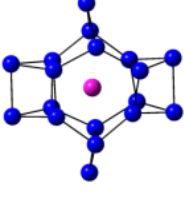


Fig.4.1 continue

				
13B:C ₁ :0.27	13C:C ₂ :0.84	13D:C ₁ :1.07	14A ^{GS} :C _s	14B:C _s :0.0002
				
14C:C ₁ :0.07	14D:C ₁ :0.20	15A ^{GS} :C ₂	15B:C ₁ :0.004	15C:C _s :0.19
				
15D:C ₁ :0.34	16A ^{GS} :C ₁	16B:C _s :0.30	16C:C ₁ :0.57	16D:C ₁ :0.92
				
17A ^{GS} :C ₁	17B:C:1.31	17C:C ₂ :2.67	17A:C ₁ :2.69	18A ^{GS} :C ₁
				
18B:C ₁ :0.37	18C:C ₁ :0.58	18D:C ₁ :3.22		

For Nb₂ dimer the theoretical and experimental bond length and vibrational frequencies are 2.08Å, 472 cm⁻¹ [33] and 2.08Å, 424.9 cm⁻¹ [34] respectively and are in good agreement with our theoretical observation. Therefore, the method B3LYP and basis set scheme, which we used in our calculation, is reliable and accurate enough to describe the stability and electronic structures of the present system.

Table 4.1 Bond length and lowest frequencies of Ge-Ge and Nb-Nb dimmers

Dimer	Bond length (Å)	Lowest frequency (cm ⁻¹)
Ge-Ge	2.44 ^a , 2.44 ^b , 2.36-2.42 [30,31], 2.46 [32]	250.63 ^a , 261 ^b , 258 [30]
Nb-Nb	2.13 ^a , 2.08 [33], 2.08* [34]	472.17 ^a , 424.9*[34], 472 [33]

^aB3LYP/LANL2DZdp ECP, ^bB3LYP/aug-cc-pvdz, *Experimental

It is important to obtain the relative stability of different clusters in a particular composition to identify the most stable size in the series so that it can be used as the building block in cluster assembled materials to design electronic devices for particular purpose. To explore the relative stability of the clusters with the increase of the cluster size during the growth process, we have calculated different thermodynamic and chemical parameters, such as, average binding energy per atom (BE), embedding energy (EE), fragmentation energy and the 2nd order change in energy, as mentioned in our previous report [1-5, 11]. These parameters are defined as:

$$BE = -(E_{NbGe_n} - E_{Nb} - nE_{Ge}) / n + 1 \quad (4.1)$$

$$FE = E_{Ge_{n-1}Nb} + E_{Ge} - E_{NbGe_n} \quad (4.2)$$

$$\Delta_2(n) = E_{NbGe_{n+1}} + E_{NbGe_{n-1}} - 2E_{NbGe_n} \quad (4.3)$$

$$VIP = E_{NbGe_n^+} - E_{NbGe_n} \quad (4.4)$$

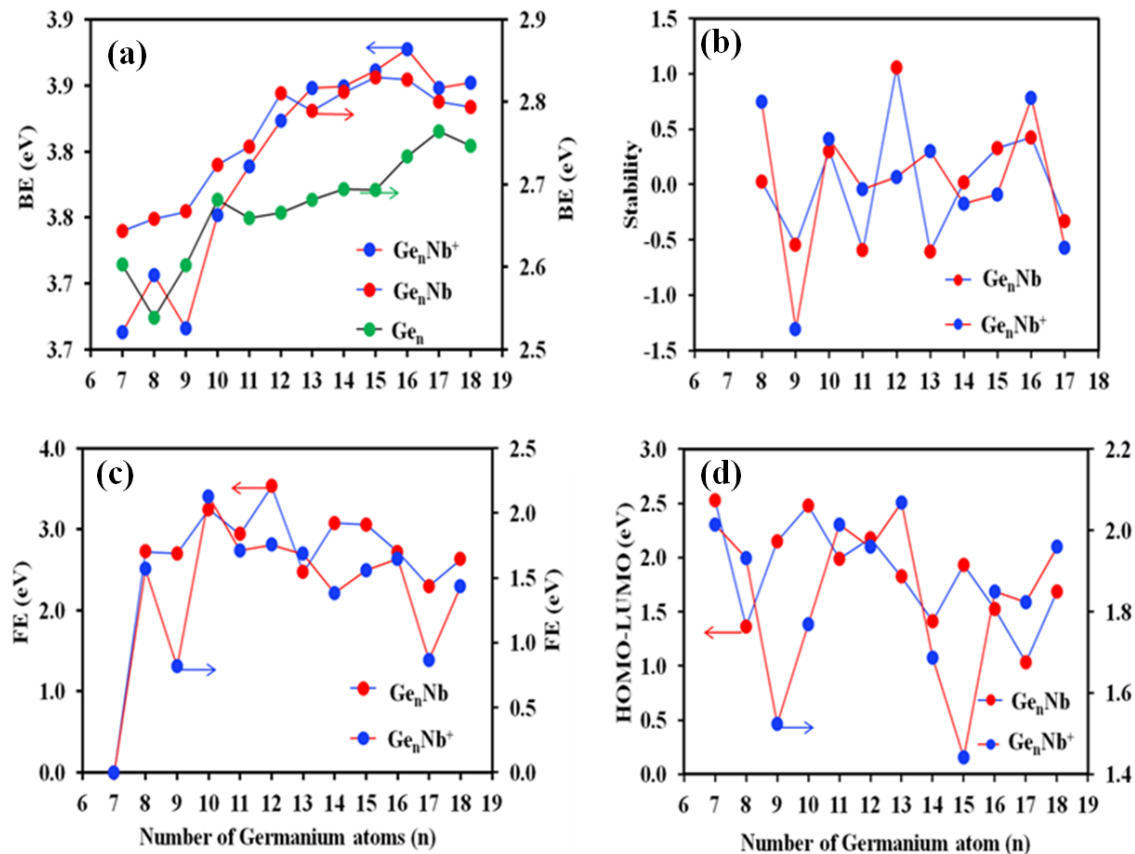
$$VEA = E_{NbGe_n^-} - E_{NbGe_n} \quad (4.5)$$

where, E_{Nb} , E_{Ge} , E_{NbGe_n} represent the total energies of Nb, Ge and NbGe_n respectively. Again for pure Ge_n cluster E_{Nb} in the above-mentioned equation is taken, as zero and n+1 will be replaced by n. To check the addition of Nb to Ge_n cage is favorable or not, we have calculated EE of each cluster during the growth. By the above definition of EE, if it is positive, then the addition of Nb to Ge_n cluster is favorable. To understand the relative stability of the clusters, we have studied the 2nd order change in energy using the above expression. By definition, [11] VIP is the

energy difference between the cationic and neutral clusters and both are at the same equilibrium geometry of the neutral cluster. Whereas, VEA is defining the energy difference between the neutral and its anionic clusters and both are at the same equilibrium geometry of the anionic cluster. With reference to the variation of binding energy (Fig. 4.2a) one can see that the binding energy increases with the size of clusters. The increase rate of BE for $n=7-12$ is relatively higher both in neutral and cationic NbGe_n clusters compare to the pure Ge_n clusters. This indicates that the doping of Nb atom increases the BE and helps to improve the stability of the clusters. Visible local peaks at $n=12$ for neutral and $n=16$ in cationic clusters indicate the enhanced stability of these clusters. With reference to the Fig.4.2b, a number of ups and downs are there in the variation of the 2nd order change in energy or stability parameter. The nature supports the magic nature of the neutral NbGe_{12} and cationic NbGe_{16} clusters. The stability variations show that the magic clusters NbGe_{12} and NbGe_{16}^+ gain energy during their formation from its immediate lower sizes and loose energy while growing to its next immediate bigger sizes. To further check the relative stability we calculate the fragmentation energy of different sized clusters. The variation of fragmentation energies with the size of clusters has shown in fig.4. 2c. the larger the fragmentation energies are, the more difficult the dissociation of clusters and thus the more stable. The sharp rise in FE from $n = 11$ to 12 and sharp drop in the next step from $n = 12$ to 13 during the growth process indicate that NbGe_{12} cluster is stable compared to its neighboring sizes. The same is true for cationic cluster at $n = 16$. This is again indication of higher stability of neutral and cationic clusters respectively.

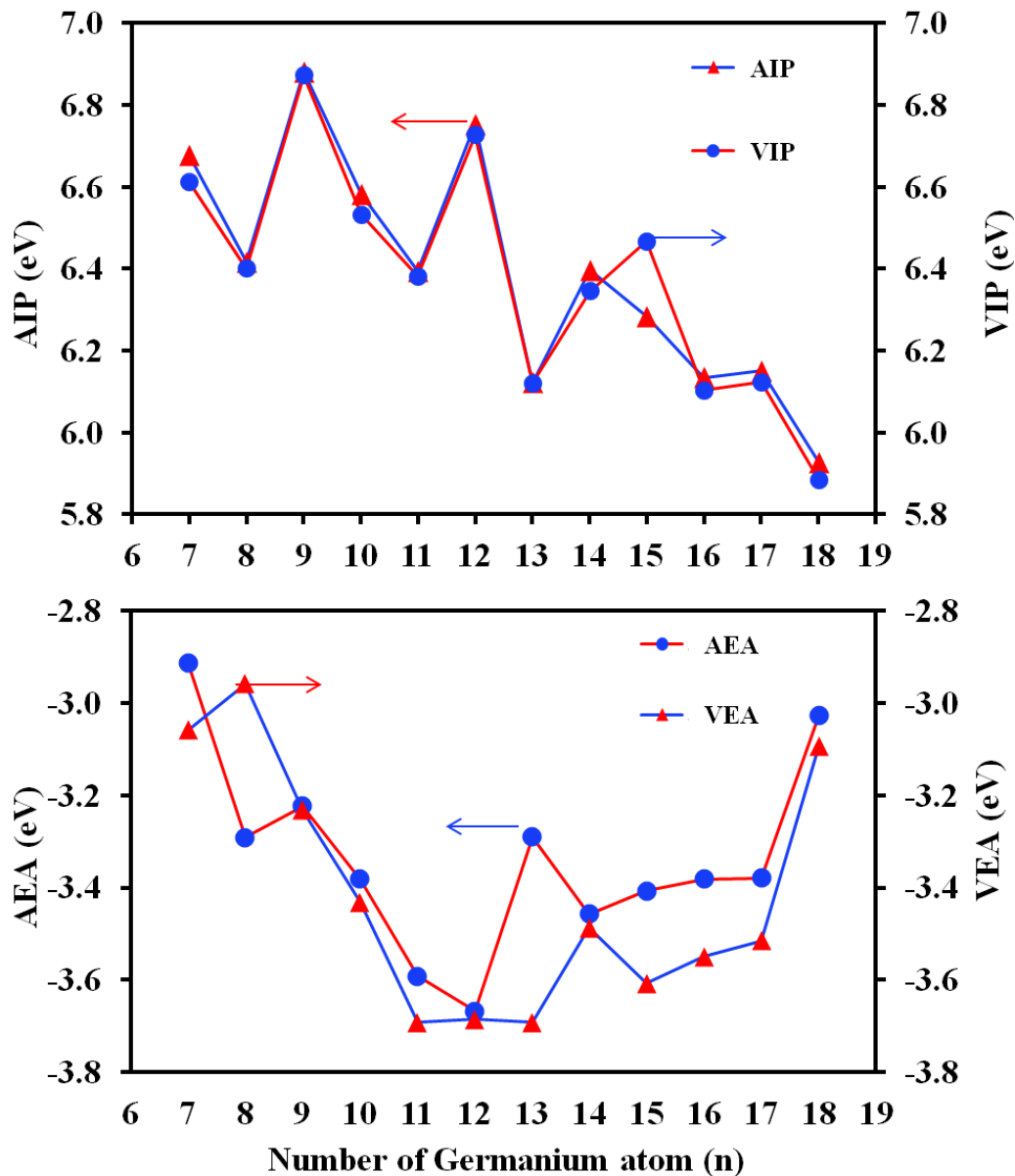
From the behavior of the thermodynamic parameters one can conclude that NbGe_{12} and NbGe_{16}^+ clusters have enhanced stability. To further check the chemical stability of the clusters, we have studied HOMO-LUMO gap, AIP, VIP, AEA, VEA with the variation of the cluster size during growth process. Variations of HOMO-LUMO gap in neutral and cationic clusters are shown in fig. 4.2d. Relative maxima at $n=12$ (2.17 eV) in neutral and $n=16$ (2.18 eV) in cationic clusters supports the enhanced stability of these clusters as like thermodynamic parameters. The HOMO-LUMO gap is responsible for the chemical inertness of these clusters. In summary, from the variation of the thermodynamic parameters and HOMO-LUMO gap, it is found that NbGe_{12} and NbGe_{16}^+ clusters have enhanced stability.

Fig. 4.2 Variation of (a) Binding energy, (b) stability, (c) fragmentation energy and (d) HOMO-LUMO gap and of $NbGe_n^+$ and $NbGe_n$ with the number of germanium atom.



Variation of chemical parameters with the cluster size is shown in fig. 4.3. Ionization of a molecule or a cluster often changes its geometry on ionization. Therefore, we have calculated both AIP and VIP values in the present study. Calculated results are shown in Fig. 4.3. Both IPs are almost same at all sizes (with a sharp peak at $n=12$) indicating that the cluster geometries are remains same after ionization. The analysis indicates that both VIP and AIP increase sharply for $n=11$ to 12 , however, there is a decreasing trend in VEA. The variation of VEA does not show any clear indication of stability in the range of $n=11$ to 13 . Both IPs and AEA the trends support the enhanced stability of neutral $NbGe_{12}$ cluster in the series. Further, to understand the cause of the stability of $NbGe_{12}$ and $NbGe_{16}^+$, we have calculated NICS and electronic distributions in the orbitals for all clusters as discussed in the following section.

Fig. 4.3 Variation of Vertical ionization potential (VIP), Adiabatic ionization potential (AIP) and Vertical electron affinity (VEA), Adiabatic electron affinity (AEA) with number of germanium atom.

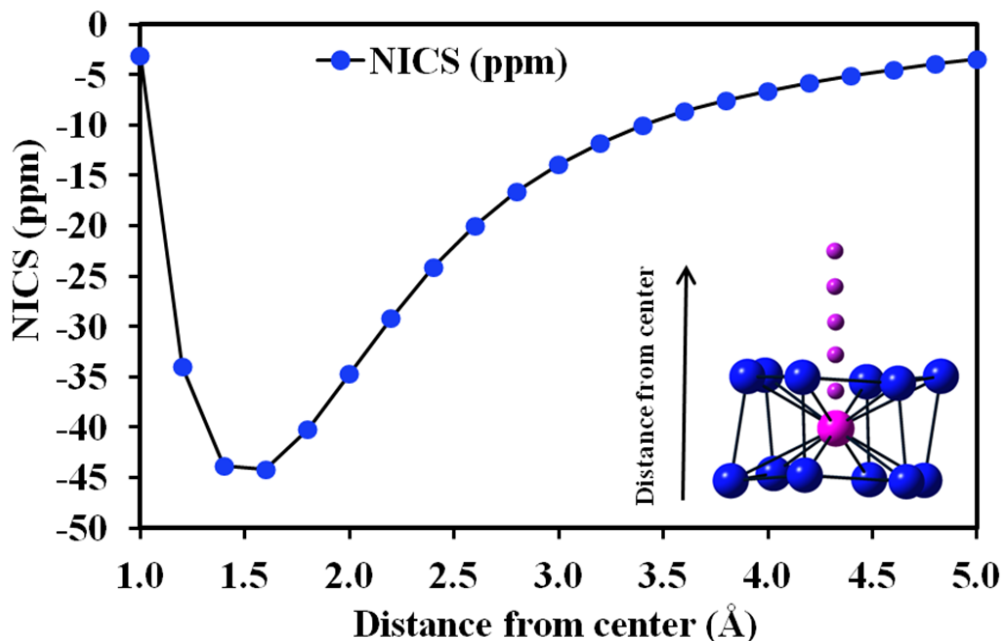


4.3.2 NICS and Orbitals of neutral NbGe₁₂ and cationic NbGe₁₆

In chemistry and in cluster science, the aromaticity is a key concept [35] to understand the stability. The aromatic behavior of a cluster is the measure nucleus independent chemical shift (NICS) index and is defined as the negative value of the magnetic shielding, computed at the ring center (as like benzene ring) or at some other selected point. Chen and Coworkers [36] reported the NICS approach as aromaticity criteria based on magnetic properties, which have been applied to characterize the metallic clusters with aromatic and antiaromatic nature. The rings with more

negative values are considered as more aromatic species and hence with enhanced stability nature. However, positive and zero NICS values indicate anti-aromatic and non-aromatic species. Using the GIAO-B3LYP/Lan12dz method with effective core potential, we have calculated NICS values. The variation of NICS values of NbGe₁₂ cluster is shown in fig. 4.4.

Fig.4.4 NICS plot of NbGe₁₂ cluster

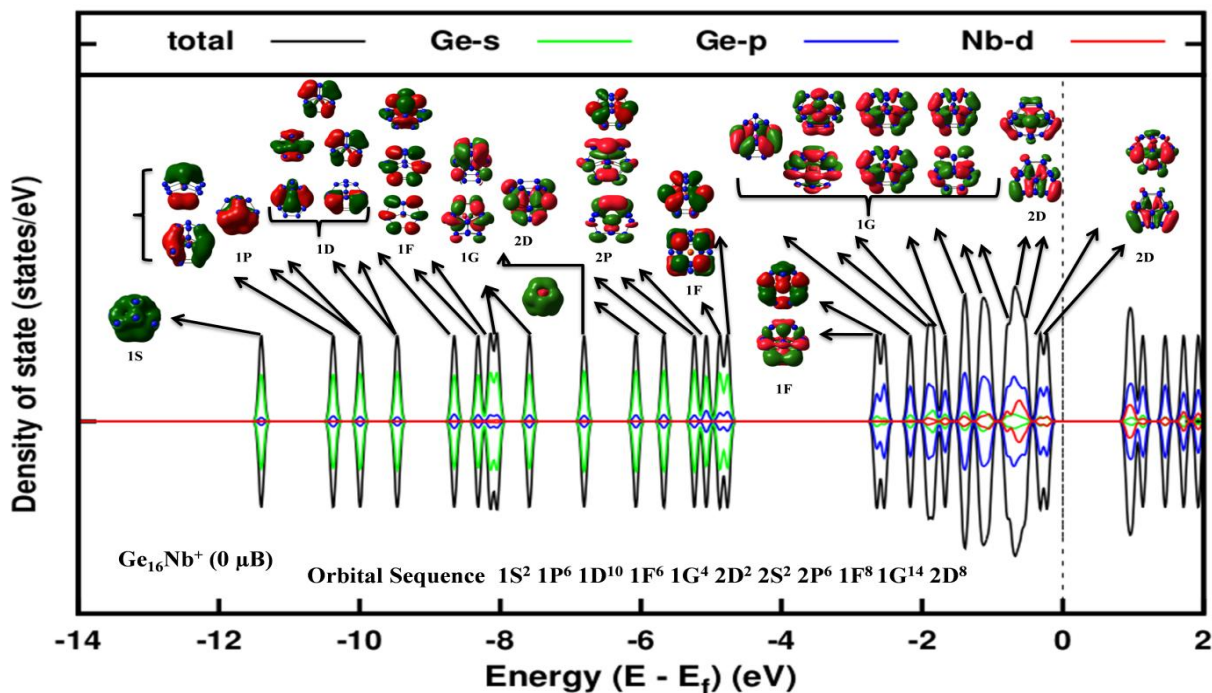


Calculated NICS values close to the outer surface are relatively smaller than the NICS values inside the cage. Calculated NICS variation with the distance from the central Nb atom shows a maximum value of -44.89 ppm at a distance 1.20Å above from the center of the cluster. Aromaticity in hexagonal structure like benzene is an important conformation of stability of NbGe₁₂ cluster. With reference to our previous work [11] on MoGe₁₂, the variation of NICS supports the aromatic nature and hence enhanced stability of neutral NbGe₁₂ cluster. However, in the cationic series, there is no such evidence that could explain the stability of the cationic clusters.

A number reports are there to explain the enhanced stability of the clusters using the closed shell model. It has already been reported that in FeMg₈ cluster, partially filled sub-shells can enhance chemical stability [37] with a closed core of 1S², 1P⁶, 1D¹⁰, 2S² superatomic shells followed by a crystal field split 2D⁴ valence state resulting a magnetic moment of 4.0 μ_B. Similarly Xinxing Zhang et al.[38] reported that VN₈, a magnetic superatom, with a filled d sub-shell and a magnetic moment of 5μ_B with 1S² 1P⁶ 1D⁵ electronic distributions. Vijay et al.[13] studied doping of different divalent M atoms and report the finding of Mn doped Ge and Sn clusters with 5 μ_B magnetic moment in accordance with the Hund's rule in clusters. Khanna and Jena [39] proposed that the stable clusters could

be treated as superatoms that form a 3rd dimension to the periodic table. Further we have calculate the density of states (DOS) and projected density of states (PDOS) of the stable n=12 and 16 clusters in neutral and cationic states in fig. 4.5. From the PDOS, it is clearly seen that most of the contribution in DOS is from Nb d- orbital and from p-orbitals of all Ge atoms. Therefore, Nb d-orbital is mainly taking part in hybridization to make the cluster stable. Again, the HOMO-LUMO gap is more in the cationic states compare to the neutral clusters. We have assigned few single electron orbitals of cationic NbGe₁₆ in DOS and the complete sequence of the orbitals is written in the fig. 4.5. It is important to mention that calculated HOMO-LUMO gap from DOS using VASP and the same using Gaussian may not be same. In the present case also we found that the HOMO-LUMO calculated is also not same. But comparing the gap between the neutral and the same sized cationic clusters, the later one always found stable. Due to finite broadening during the calculation of DOS, closely spaced orbitals are taken as one in DOS and on the basis of it we have assign the orbitals as shown. We found that cationic NbGe₁₆ cluster follow the orbital sequence 1S²1P⁶1D¹⁰1F⁶1G⁴2D²2S²2P⁶1F⁸1G¹⁴2D⁸ (fig. 4.5) and adjust total 68 electrons as like closed shell model. Due to crystal field splitting, some of the lower orbitals appear at the higher energy levels as shown in the sequence. With

Fig. 4.5 Density of states of cationic NbGe₁₆ cluster and its orbital with their position in PDOS



references to the reported work as discussed, this is the strongest evidence of the stability of cationic NbGe₁₆ cluster and at the same time it can be taken as a superatom with very high embedding energy 10.58 eV, IP (10.25 eV) and HOMO-LUMO gap of 1.85 eV.

4.3.3 IR and Raman spectrum

To understand the dynamical stability of the ground state clusters and their vibrational properties IR and Raman spectra of the optimized geometries are calculated. Absence of any imaginary frequency in the spectrum represents the real nature of the clusters. The dominant peaks shown in the IR and Raman spectra are due to the vibration of the atoms in the cage. There is nearly no movement of the doped atom in this region. The vibration of the doped atom contributes very low intensity in the relatively low frequency regions. Careful observation shows the presence of mainly three to four dominating modes in IR and Raman spectra for all clusters. A lower number of vibrational modes in IR are basically the indication of the vibration of the bonds (stretching) present in the structure nearly at the same frequency or within a very narrow frequency range. This is because of the strong structural symmetry of these clusters. Raman frequency in general indicates the bending mode in the clusters. The dominating higher mode frequency with very high intensity is the breathing mode [40] of the cage cluster atoms, while the IR intensities have three or four peaks in neutral and cationic cluster corresponding to the motion of Nb atom in different direction. In the breathing mode all Ge atoms vibrate in the same phase whereas the doped atom remains static. The frequency region, which is less than 200 cm⁻¹ is mainly due to the vibration of the germanium atoms and the doped atom as well. This frequency shifted towards the low frequency region except for n=12 structure. The infrared spectrum and Raman activity of NbGe_n (n = 10, 14 and 15) has several peaks (fig. 4SIC Appendix B) due to its low symmetry. Also for n = 14 and 15 the dominant peaks in the infrared spectrum shifting towards lower frequencies suggesting that the Ge-Nb bonds become relatively weak as the size of the cluster grows. The low frequency region is mainly due to the vibration of the caged atom. Closer observation of the dominating mode frequencies both in IR and Raman spectrum, it is found that the infrared spectrum of NbGe₁₂ has dominant peak at around 251 cm⁻¹ due to additional strength in bonding because of NICS behavior.. The high frequency region indicates the higher bond energy between the elements. Comparing this with the binding energy graph, it can be said that the increase in bond energies helps to increase the binding energy per atom in the clusters. So IR and Raman activities show distinct spectra for these clusters and it reflects the effect of structural change and bonding nature. Detailed frequency analysis is shown in table 4.2. This also helpful to identify the ground state isomers in experiments as reported by Atobe et al. [12]

Table 4.2 Dominant Raman and Infrared (IR) frequencies, IR intensity and Raman activity for NbGe_n (n = 10-15) Clusters, where dominant peak shown in bold.

NbGe ₁₀			NbGe ₁₁			NbGe ₁₂		
ω (cm ⁻¹)	Raman	IR	ω (cm ⁻¹)	Raman	IR	ω (cm ⁻¹)	Raman	IR
95.22	0.91	0.00	113.51	1.18	0.02	127.36	0.02	3.03
107.67	3.34	0.09	114.43	4.95	0.24	133.03	0.00	5.91
107.83	2.68	0.10	119.62	3.35	0.81	146.31	10.45	0.00
108.19	4.52	0.09	125.94	2.1	1.90	160.65	17.75	0.00
132.50	2.77	0.00	128.87	3.38	1029	161.36	0.04	0.11
132.89	1.96	0.00	138.88	3.77	0.01	162.83	12.65	0.00
133.11	4.58	0.00	145.45	1.86	0.05	167.33	0.00	0.35
136.66	0.10	0.00	145.80	2.45	0.19	172.02	13.49	0.00
140.49	6.31	0.10	156.45	7.09	0.61	174.15	0.03	0.45
140.64	6.25	0.10	161.38	3.02	0.50	190.05	59.44	0
156.21	6.16	0.16	167.07	8.72	0.37	190.94	0.00	0.53
175.95	5.42	0.12	173.10	15.12	0.63	200.54	4.77	0
176.21	5.47	0.13	181.00	56.02	0.61	206.61	3.70	0.00
183.56	94.47	0.24	188.12	6.63	0.49	209.07	0.00	1.35
188.14	17.51	2.98	192.10	0.96	0.14	218.69	0.04	0.00
268.52	2.70	22.12	252.96	0.23	21.30	246.17	0.00	22.52
268.93	2.77	22.21	262.76	1.45	20.85	251.83	0.00	17.41
322.72	7.71	17.76	280.70	1.84	14.23	253.54	0.00	13.88

NbGe ₁₃			NbGe ₁₄			NbGe ₁₅		
ω (cm ⁻¹)	Raman	IR	ω (cm ⁻¹)	Raman	IR	ω (cm ⁻¹)	Raman	IR
136.06	3.77	0.27	166.12	33.48	0.66	141.03	2.59	0.70
139.98	4.8	0.37	175.67	1.37	0.10	148.34	0.22	0.89
153.02	1.05	0.64	179.23	0.64	4.54	159.95	66.32	1.69
160.08	5.79	0.16	180.68	4.13	3.30	166.27	1.43	0.24
163.18	4.39	0.13	183.81	2.41	0.43	16856	5.44	6.83
168.16	17.76	0.93	187.97	3.25	0.16	175.86	2.09	2.42
169.50	9.88	0.36	190.27	0.63	0.04	185.62	4.40	0.01
177.05	18.03	0.82	191.65	1.98	1.30	188.97	4.67	1.97
178.86	6.49	0.97	198.80	0.03	0.70	190.5	0.31	0.09
182.14	4.85	0.33	200.96	1.07	0.00	196.13	3.02	4.73
186.13	6.95	1.33	210.76	1.11	0.44	201.53	2.56	0.26
196.86	1.19	0.94	224.33	2.60	0.01	202.41	5.96	0.70
203.44	13.06	0.78	225.25	0.36	9.45	207.21	0.24	0.88
205.94	8.53	0.07	226.48	23.26	0.06	208.16	2.77	5.61
228.51	0.42	9.65	233.72	2.25	0.42	217.15	1.36	9.63
230.60	1.58	7.09	236.62	0.91	8.57	221.86	1.26	8.67
244.57	0.55	12.21	236.70	2.06	0.97	224.13	0.57	2.17
253.03	0.79	15.50	244.76	0.77	11.96	228.72	2.50	3.13

4.4 Conclusions

In summary we have done theoretically study of the electronic properties, vibrational properties and superatomic behavior of Nb doped germanium clusters at different sizes in neutral and cationic states. Different physical and chemical parameters of the clusters show that neutral NbGe₁₂ and cationic NbGe₁₆ are the most stable species in the whole range of study. In addition, neutral NbGe₁₀ and NbGe₁₆; and cationic NbGe₁₃ also show enhanced stability. Therefore, to identify the most stable behavior, we have further studied NICS and closed shell model in both neutral and cationic state of these clusters. We found that the NICS behavior of the ground state NbGe₁₂ cluster supports the aromatic nature of this cluster, whereas, cationic NbGe₁₆ follow the closed shell superatomic model. The large HOMO-LUMO gap of 1.85eV makes this cluster suitable for optoelectronic devices and chemical stable. Further, the absence of any imaginary frequencies in these clusters shows that there is no presence of imaginary bonds in the clusters and clusters can be physically acce

4.5 References

- [1] Bandyopadhyay D, Sen P, *J Phys Chem A*, **2010**; 114: 1835-1842.
- [2] Bandyopadhyay D, *J Appl Phys*, **2008**; 104: 084308-084317.
- [3] Bandyopadhyay D, *Molecular Simulation*, **2009**; 35: 381-394.
- [4] Bandyopadhyay D, *Nanotechnology*, **2009**; 20: 275202.
- [5] Brack M, *Rev Mod Phys*, **1993**; 65: 677-732
- [6] Kapila N, Garg I, Jindal, V K and Sharma H, *J Magnetism & Mag Material*, **2012**; 324: 2885-2893.
- [7] Murray CB, Norris DJ and Bawendi MG, *J Am Chem Soc*, **1993**; 115: 8706-8715.
- [8] Colvin V, Schlamp MC, and Alivisatos AP, *Nature*, **1994**; 370: 354-357.
- [9] Klimov VI, Mikhailovsky AA, Xu S, Hollingsworth JA, Leatherdale CA, Eisler HJ and Bawendi MG, *Science*, **2010**; 290: 314-317.
- [10] Dhaka K, Trivedi R and Bandyopadhyay D, *J Mol Model*, **2012**; 19: 1473-1488.
- [11] Trivedi R, Dhaka K and Bandyopadhyay D, *RSC Advance*, **2014**; 4: 64825- 64834.
- [12] Atobe J, Koyasu K, Furusea S and Nakajima A, *Phys Chem Chem Phys*, **2012**; 14: 9403-9410.
- [13] Kumar V and Kawazoe Y, *Appl Phys Lett*, **2003**; 83: 2677-2679.
- [14] Ge GX, Han Y, Wan JG, Zhao JJ and Wang GH, *J Chem Phys*, **2013**; 139: 174309-174317.
- [15] Chouhan V, Medel VM, Reveles JU, Khanna SN and Sen P, *Chem Phys Lett*, **2012**; 528: 39-43.
- [16] Lee C, Yang W and Parr RG, *Phys Rev B*, 1998; **37**: 785-789.
- [17] Hay PJ and Wadt WR, *J Chem Phys*, **1985**; 82: 270-283.
- [18] Hay PJ and Wadt WR, *J Chem Phys*, **1985**; 82: 284-298.
- [19] Nagendran S, Sen SS, Roesky HW, Koley D, Grubmüller H, Pal A and Herbst- Irmer R, **2008**; 27: 5459- 5463.
- [20] Khon W and Sham LJ, *Phys Rev A*, **1965**; 140: 1133-1138.
- [21] Frisch, M. J., Trucks, G. W., Schlegel, H. B., Scuseria, G. E., Robb, M. A., Cheesemen, J. R., Zakrzewski, V.G., Montgomery, J. R. JA, Stratmann, R. E., Burant, J. C., Dapprich, S., Millam, J. M., Daniels, A. D., Kudin, K. N., Strain, M. C., Farkas, O., Tomasi, J., Barone, V., Cossi, M., Cammi, R., Mennucci, B., Pomelli, C., Adamo, C., Clifford, S., Ochterski, J., Petersson, G. A., Ayala, P. Y., Cui, Q., Morokuma, K., Malick, D. K., Rabuck, A. D., Raghavachari, K., Foresman, J. B., Cioslowski, J., Ortiz, J. V., Baboul, A. G., Stefanov, B. B., Liu, B., Liashenko, A., Piskorz, P., Komaromi, I., Al-Laham, M. A., Peng, C. Y., Nanayakkara, A., Challacombe, M., Gill,

P. M. W. , Johnson, B., Chem, W., Wong, M. W., Andress, J. L.,Gonzalez, C., Head-Gordon, M., Replogle, E. S. , Pople, J. A., Gaussian 03,revision E 01 Gaussian, Wallingford. (2004).

[22] Zhao RN, Ren ZY, Guo P, Bai JT, Zhang CH and Han JG, *J Phys Chem A*, **2006**; 110: 4071-4079.

[23] Han JG and Hagelberg F, *J. Mol. Struc. THEOCHEM*, **2001**; 549: 165-180.

[24] Jaiswal S, Baber VP and Kuamr V, *Phys Rev B*, **2013**; 88: 085412.

[25] Kawamura H, Kumar V and Kawazoe Y, *Phys Rev B*, **2004**; 70: 245433.

[26] Knight WD, Clemenger K, de Heer WA, Saunders WA, Chou MY and Cohen ML, *Phys Rev Lett*, **1984**; 52: 2141-2143.

[27] Clemenger K, *Phys Rev B*, **1985**; 32:1359-1362.

[28] de Heer WA, *Rev Mod Phys*, 1993; 65: 611-676.

[29] Kumar V, *Computational and Theoretical Chemistry*, **2013**; 1021: 149-154.

[30] Northrup E and Cohen ML, *Chem Phys Lett*, **1983**; 102: 440-441.

[31] Abtew TA and Drabold DA, *Phys Rev B*, **2007**; 75: 045201-045209.

[32] Lombardi JR and Davis B, *Chem Rev*, **2002**; 102: 2431-2460.

[33] Goodwin L and Salahub DR, *Phys Rev A*, **1993**; 47: 774-777.

[34] Hales DA, Lian L and Armentrout PB, *Int J of mass spectrum Ion process*, **1990**; 102, 269-301.

[35] Dmitry Yu, Zubarev BB, Averkiev, Zhai HJ, Sheng WL and Boldyrev AI, *Phys Chem Chem Phys*, **2008**; 10: 257-267.

[36] Chen Z, Corminboeuf C, Heine T, Bohmann J and Schleyer PVR, *J Am Chem Soc*, 2003; **125**: 13930-13931.

[37] Medel VM, Reveles JU, Khanna SN, Chauhan V, Sen P, Castleman AW, *PNAS*, **2011**; 108: 10062-10066.

[38] Zhang M, Zhang J, Feng X, Zhang H, Zhao L, Luo Y and Cao W, *J Phys Chem*, **2013**; 117: 13025-13036.

[39] Khanna SN and Jena P, *Phys Rev B*, **1995**; 51: 13705.

[40] Kumar M, Bhattacharya N and bandyopadhyay D, *J Mol Model*, **2012**; 18: 405-418.

CHAPTER 5

HYDROGEN STORAGE IN SMALL SIZE Mg_nCo ($n = 1-10$) CLUSTERS: A DENSITY FUNCTIONAL INVESTIGATION

5.1 Introduction

In last few decades, study of the interaction between hydrogen with the materials has evolved immense interest in the research field of hydrogen storage. To solve the future energy problems, it is important to understand the science behind this interaction from theory and experimental knowledge. Theory and computation can be used not only to understand experimental results, but also to design low cost materials with improved hydrogen storage efficiency. It is well known that magnesium and magnesium alloys have potential as high hydrogen storage elements [1]. Moreover, these alloys are lightweights, cost effective and hence the most promising candidates for hydrogen storage. However, due to the physical nature of hydrogen, it is difficult to store it in a large quantity in small a volume. Therefore, modeling and experimental verification for the safe, reliable and cost effective hydrogen storage elements is one of the main challenges in this field. Along with Mg based alloys, many more metals and their alloys are capable of absorbing large amounts of hydrogen to form metal hydrides. So it is important to understand the interaction of hydrogen with the storage material matrix in the nano as well as bulk form. In general, at the initial stage, metal hydride formation is initiated by the chemisorption of H_2 on the metal surface. In the later stage, the adsorbed H atoms diffuse into the crystal lattice in case of bulk systems. Usually, small sized transition metal clusters improves the absorption process because of their higher surface to volume ratio. This makes more surfaces available for chemisorption of hydrogen compared to the bulk materials. The present study mainly focuses on understanding how the hydrogen molecule or atom adsorbs and dissociates with the nano Mg_nCo clusters within the size range of $n=1$ to 10. A number of experimental and theoretical research have been reported on hydrogen adsorption and dissociation processes. Experimental and theoretical investigation of chemisorptions of H_2 on small unsupported Pd_n clusters ($n<25$) were reported by Fayet [2]. In a stable rutile structure of Mg_nH_2 they minimized the total energy by optimizing the lattice parameters. Electronic simulation using first principle can offer great insight into the understanding of the influence of alloying elements on the hydride properties. An accurate model has been developed by Giusepponi and Celino [3] which studied the mechanism of action of the catalyst and how it interacts with the interface MgH_2 -Mg, through which H atoms diffuse, followed by molecular dynamics simulations at several temperature that provided a clear description of the desorption mechanism and an estimate of the desorption temperature. Song et al. [4] has investigated the influence of Al, Ti, Fe, Ni, Cu on stability of MgH_2 by means of

electronic structure and total energy calculations. Stier et al. [5] carried out various theoretical calculation based on density functional theory to study how binding energy and diffusivity of hydrogen change in magnesium hydride when other elements are added with it. Zaluski et al. [6] studied the effect of Pd addition to nanocrystalline hydrogen absorbing Mg_2Ni and $LaNi_5$ alloys. Substantial improvement have been found in the hydriding-dehydrating kinetics by adding small amount of catalyzing elements constituted either by (i) Metals (Ce, Ti, Nb, Fe, Co, and Ni) (ii) non metals (C and Si) (iii) transition metal oxide (iv) intermetallic compounds ($LaNi_5$, Mg_2Ni and $FeTi$) to Mg based hydrogen storage materials [7-11]. In the study of Zhang and Wu [12] different amount of $LiNH_2$ in the Li_3N - MgH_2 (1:1) system was added the hydrogen storage capacity was improved from 3.2 wt% to approximately 5.1 wt% at 250 °C by the addition of $LiNH_2$ from 0 to 2 mol. The microstructural evolution and hydrogen storage mechanisms during the hydrogenation/dehydrogenation process for the Li_3N - MgH_2 - $2LiNH_2$ sample were also discussed.

Among additives to improve hydrogen storage capacities metal can act through two different mechanism: (a) metals like Ni, Pd or Ti form hydrides, which can behave as "Hydrogen pumps"; (b) transition metal such as Fe, Co, and Cr, which favor the hydrogen molecule dissociation and phase transformation of Mg matrix to MgH_2 [13]. Recently, it is found that high-energy ball milling of magnesium hydride decreases the particle size and induces stresses and defects in the structures [14-15]. Mananghaya [16] reported the implementation and effectiveness of the ability of Nitrogen doped Carbon Nanotube (4ND-CN_xNT) decorated with Sc for Hydrogen storage under the spin-unrestricted Density Functional Theory. Detailed structural and electronic properties were reported starting from one up to five hydrogen molecules absorbed by the system. Bobet et al. [17] reported that the addition of Co or Fe during reactive ball milling of Mg significantly increases the quantity of formed MgH_2 , since the processing was able to induce reduction of Mg particle size and easy formation of hydride phase. Amica et al. [18] reported the hydrogen storage properties of $LiNH_2$ - LiH system with MH_2 added ($M = Mg, Ca, Ti$) and clarifies the chemical interactions occurring during hydrogen cycling. Detailed structural investigations reveal that during heating under hydrogen, MH_2 ($M = Mg, Ca$) reacts with $LiNH_2$ to form $Li_2Mg(NH)_2$ and $2CaNH$ - $Ca(NH_2)_2$ solid solution and at the same time release of hydrogen. They found a new reversible pathway for hydrogen storage in the Li - Ca - N - H system after dehydrogenation of the $LiNH_2$ - LiH when added with CaH_2 by XRPD and FTIR with notable improvement in the dehydrogenation temperature. To understand the storage mechanism and to model hydrogen storage elements, a number of theoretical studies based on density functional studies have been reported [19-22]. Henry and Yarovsky [23] have studied the dissociative chemisorptions of molecular hydrogen on charged and neutral aluminum clusters $Al_{12}X$ ($X = Mg, Al, Si$) using DFT. Retuerto et al. [24] studied the ternary metal hydride Mg_2FeH_6 prepared by high-

pressure and high-temperature reaction from the simple hydrides and then characterized by neutron powder diffraction to understand the crystallographic details and hydrogen occupancy. Wang et al. [25] investigated the H₂ molecule dissociation on the doped icosahedral Al₁₂X (X = B, Al, C, Si, P, Mg, Ca) clusters by means of DFT. Varano and Henery [26] investigated the hydrogen adsorption on magnesium doped aluminum clusters using DFT method. Ren et al. [27] studied thermally stable Zr-MOF and Cr-MOF nanofiber composites as hydrogen storage media. They found that with the 20 wt.% loading of MOF nanocrystals, the composites were able to achieve over 50% of the H₂ uptake capacity of individual MOF nanocrystals. Lu and Wan [28] studied hydrogen molecules adsorption and storage in Sc coated Si@Al₁₂ cluster using DFT. Kumar and Tarakeshwar [29] have studied the geometric and electronic structures of capable transition metal (Sc, Ti, Zr) clusters useful for hydrogen storage. Biliškov et al. [30] reported the study of SmNi_{5-x}Al_x (x=0.25,0.5,0.75,1,1.5,2,2.5) alloys prepared by arc melting and then characterized by X-ray powder diffraction to understand the crystal structures followed by pressure-composition desorption isotherms to understand the hydrogen absorption ability and thermodynamic quantities of the systems which has been checked by their DFT based. Their combined experimental and computational approach provided a detailed insight into the mechanistic details of hydrogen storage in the systems. Sheng [31] investigated the adsorption and dissociation of H₂ on Zr clusters using density functional theory (DFT). Yu and Lam [32] have studied the electronic and structural properties of Mg_nH₂ clusters using DFT. Recently, Hasan et al. [33] presented the results of our DFT-based investigations on the effects of the substitution of magnesium with cobalt and nickel in the bulk magnesium hydride; and the hydrogen adsorption and desorption on the MgH₂ (001) surface by studying the energetic aspects of these interactions. The results also showed the merit of the cobalt and nickel dopants in the magnesium hydride destabilization, which facilitates the hydrogen release. Huaiyu et al. [34] synthesized the nanostructure Mg₂CoH₅ and Mg₂Co from Mg and Co nanoparticles by hydrogen plasma-metal reaction method, and they found that the nanometer scale effect plays an important role in synthesis. Recently, Fanjie and Yanfei [35] reported the electronic, structural and magnetic properties of Mg_nX cluster (X= Fe, Co, Ni) and found X atom is endohedrally localized in Mg_nX clusters and Mg₄X cluster is stable in whole series. Keeping the development in the theoretical studies of hydrogen storage elements, in the present report we proposed a simple model to find out how transition metal Co plays an important role in the hydrogen dissociation process on Mg clusters and the reaction with H₂ using density functional theory based calculations. The present theoretical study gives a number of useful understandings of hydrogen storage in Mg_nCo nanoclusters.

5.2 Computational Methodology

In the present work, the geometry optimizations of all the structures and the corresponding hydrogen reaction have been studied at the B3LYP [36] level with Gaussian' 03 [37] program package using density functional theory. To find the lowest energy structure of Mg_nCo clusters, we designed as many initial configurations as possible based on our previous reports [38, 39]. To avoid trapping in the local minima of the potential energy surface, all the geometries with unconstrained symmetry and various possible spin multiplicity were considered. The position of all atoms in the structure are relaxed to get the final structure with the minimum total energy with no imaginary frequency values and hence conforming their existence at the minima on the potential energy surface. An all electron basis set 6-311G** is used for H atom and LANL2DZ with effective core potential (ECP) is used for both Mg and Co atom. This scheme is good compromise between accuracy and computational effort. The quadratic synchronous transit (QST) method [40] is used in determining the transition state geometries. For reaction pathways, minima are connected to each transition state by tracing the intrinsic reaction coordinate. To confirm the validity of the present methodology, first we applied it to the Mg-Mg, Co-Co and H-H dimers and the calculated results are presented in table 5.1. Comparing these results with the experimentally and theoretically reported values, we confirm that our computational methods are in good agreement with the reported values. The structure of the hydride Mg_nCoH_2 and H_2Mg_nCo clusters were also optimized to study the favorability of hydride formation at the Co site or Mg site.

5.3 Results and Discussion

An important parameter of hydrogen storage system is the surface adsorption and dissociation of hydrogen with the storage matrix. The transition metal element Co in the present study works in three ways. At the beginning it favors the hydrogen molecule absorption in Mg matrix to make a low valence complex Mg_nH_2 . At the end the Co helps to remove these hydrogen atoms from the metal complex by starting up an exothermic hydrogen reaction known as hydrogen dissociation.

Table 5.1 Bond length and Lowest frequency of different dimers

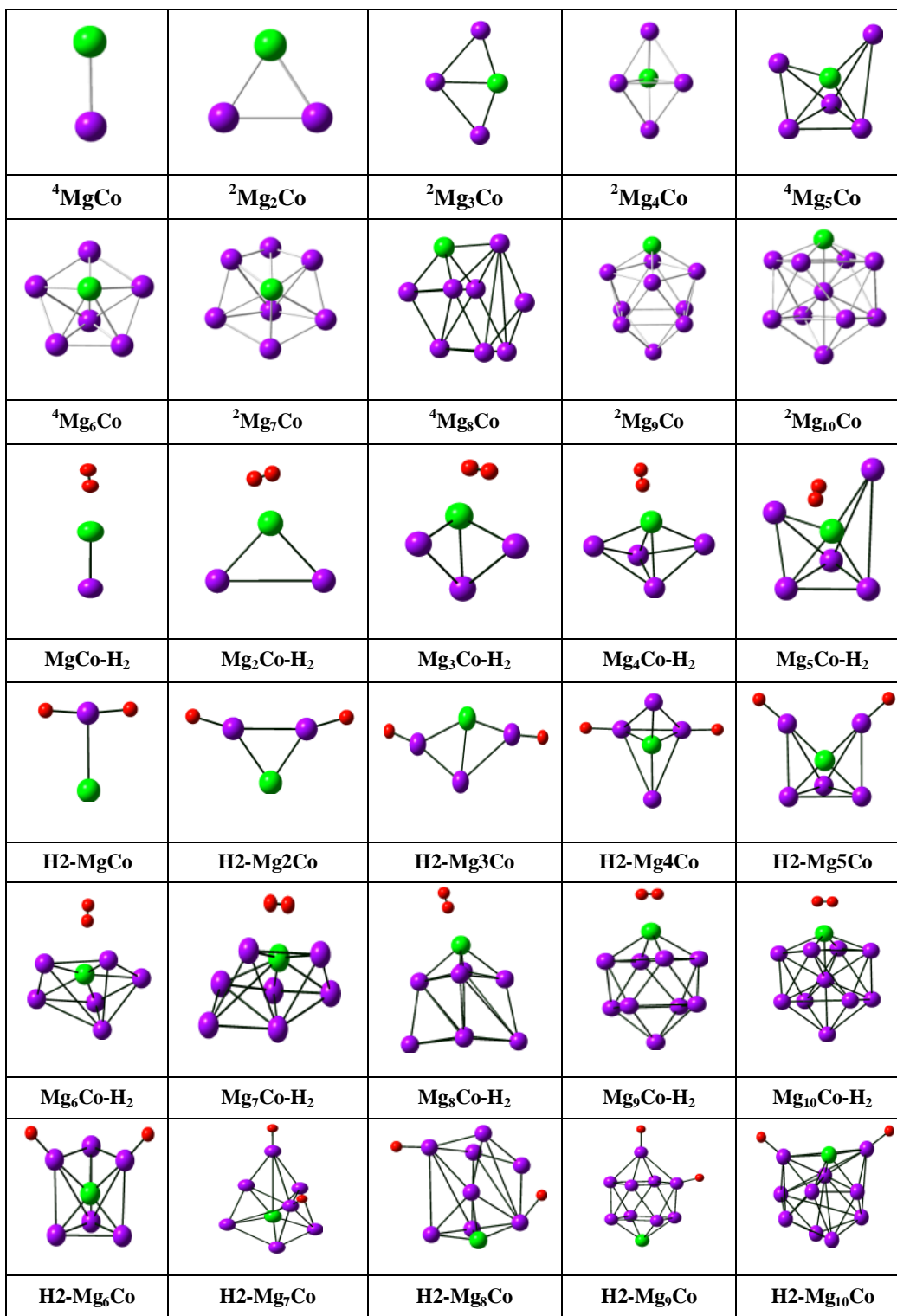
Dimer	Bond length (Å)	Lowest frequency (cm^{-1})
Mg_2	3.96, 3.89 [41]	43.28, 51.12 [44]
Co_2	2.32, 2.31 [42]	245.21, 297 [45]
H_2	0.743, 0.741 [43]	5112.4, 4401 [46]

†Experimental

Following the growth pattern of the Mg_nCo clusters within the size range $n=1$ to 10, it can be found that the Co atom always adsorbs on the surface of magnesium cluster. There is always a chance of absorbing the Co atom endohedrally for $n=10$ magnesium cluster, but it has no use at present, because in that case the Co atom would not be available for hydrogen absorption. The ground state clusters in each size with the addition of hydrogen and with different parameters are shown in the fig. 5.1. To check the thermodynamic and to study the electronic properties of different clusters we have studied the variation of average binding energies (BE) and 2nd order change in energy (Δ_2) with the cluster size and discussed in the following section.

The ground state spin multiplicity of Mg_nCo isomers is either in doublet or in quartet spins state. The Mg-Co dimer is in quartet ground state with the bond length of 2.52 Å and having C_1 point group symmetry. The ground state structure of Mg_2Co is a triangle with quartet state C_1 point group symmetry. Ground state of Mg_3Co is a rhombus with doublet electronic state and C_1 point group symmetry. The Co capped bent rhombus in the 2A_1 electronic state with C_{2v} point group symmetry is found as the ground state in $n=4$ size. The other three optimized low energy isomers are in the form of rhombus with a tail, which are not presented here. Three low energy optimized isomers are found in the Mg_6Co series. These structures can be obtained by adding a Co atom to Mg_6 or by replacing a Co atom from Mg_7 structure. The Co capped pentagonal bi-pyramidal in the 4A_1 electronic state with C_v point group symmetry is found as the ground state structure. The minimum energy structure within the size range $n= 4, 6$ and 9 are all much known structure in most of the transition Metal doped clusters. The predicted ground state spin multiplicity for Mg_nCo is found to be a doublet and quartet for $n= 4$ and 6 respectively. Four low energy isomers are found in Mg_4Co . Out of these, the ground state structure is Co capped bent rhombus in the 2A_1 electronic state with C_{2v} point group symmetry. The other three are planar rhombus with a tail are not presented here. Three low energy optimized isomers found in the Mg_6Co series. These structures can be obtained by adding a Co atom to Mg_6 or by replacing a Co atom from Mg_7 structure. The Co capped pentagonal bi-pyramidal in the 4A_1 electronic state with C_v point group symmetry is found as the ground state structure. A number of isomers are obtained in the sizes with $n>6$. The ground state isomers are shown in fig. 5.1. To get the idea of the stability of the pure Mg_n , Mg_nCo and H_2Mg_nCo clusters, we define average binding energy per atom and second order energy difference in the present study following our previous reports [38, 39] for neutral clusters as follows:

Fig.5.1 Optimized ground state isomers of Mg_nCo , Mg_nCo-H_2 and H_2-Mg_nCo clusters ($n=1-10$). Dark purple balls are Mg atom, green balls are Co atom and small red balls are H atoms. Superscript indicates the multiplicity of the clusters.



$$BE(Mg_nCo) = [nE(Mg) + E(Co) - E(Mg_nCo)]n + 1 \quad (5.1)$$

$$BE(H_2 - Mg_nCo) = [nE(Mg) + E(Co) + 2E(H_2) - E(H_2 - Mg_nCo)]n + 3 \quad (5.2)$$

$$\Delta_2(Mg_nCo) = E(Mg_{n+1}Co) + E(Mg_{n-1}Co) - 2E(Mg_nCo) \quad (5.3)$$

$$\Delta_2(H_2 - Mg_nCo) = E(H_2 - Mg_{n+1}Co) + E(H_2 - Mg_{n-1}Co) - 2E(H_2 - Mg_nCo) \quad (5.4)$$

Where, 'E' represents the optimized energies of the clusters or the energy of a single atom in a particular system. All calculated parameters of the clusters are tabulated in table 5.2. Following the above definitions of binding energy, it means the average gain in energy per atom during the formation of cluster from individual atoms. Whereas, the 2nd order change in energy means the difference of the energy of a cluster surrounding to its neighbor. The fig. 5.2 represents the variation of binding energy and second order change in energy of both the clusters with the number of Mg atoms. Following the binding energy graph, there is a local maxima at n=4, 6 and 9 in Mg_nCo. The behavior of BE in Mg_nCo is in agreement with the recent report [35]. Variation of binding energy after addition of hydrogen with Co in Mg_nCo decays exponentially. This means that the hydrogen atoms attached with the cluster loosely. The average binding energy of Mg_nCo changes from 0.35eV to 0.4eV within the range of the present study. This is in other words the binding energy of these clusters are almost stable and this is an indication of thermodynamic stability. The same clusters when absorbs hydrogen, the binding energy sharply drops from 4.78 eV to 1.02 eV when the size varies from n =1 to10. Combining the two variations it can be found that in relatively stable Mg_nCo clusters (n=4 to 10) the average binding energy per atom varies between 2 to 1eV (fig.5.2) after joining hydrogen with Co atom, which is lesser compare to the Mg_nCo. This means after releasing hydrogen the cluster will regain their stability, which is an indication to use it as a suitable candidate for hydrogen storage. Comparing the bond lengths of Mg-Mg in Mg_n clusters shown in table 5.2 (a) with the same in Mg_nCo clusters, one can see that the Mg-Mg bond length of Mg_nCo is always higher than that in Mg_n for the same value of n. This is due to the fact that the electronegativity of a Co atom is higher than that of Mg and hence the interactions of Mg-Co bonds are stronger than that of Mg-Mg bonds.

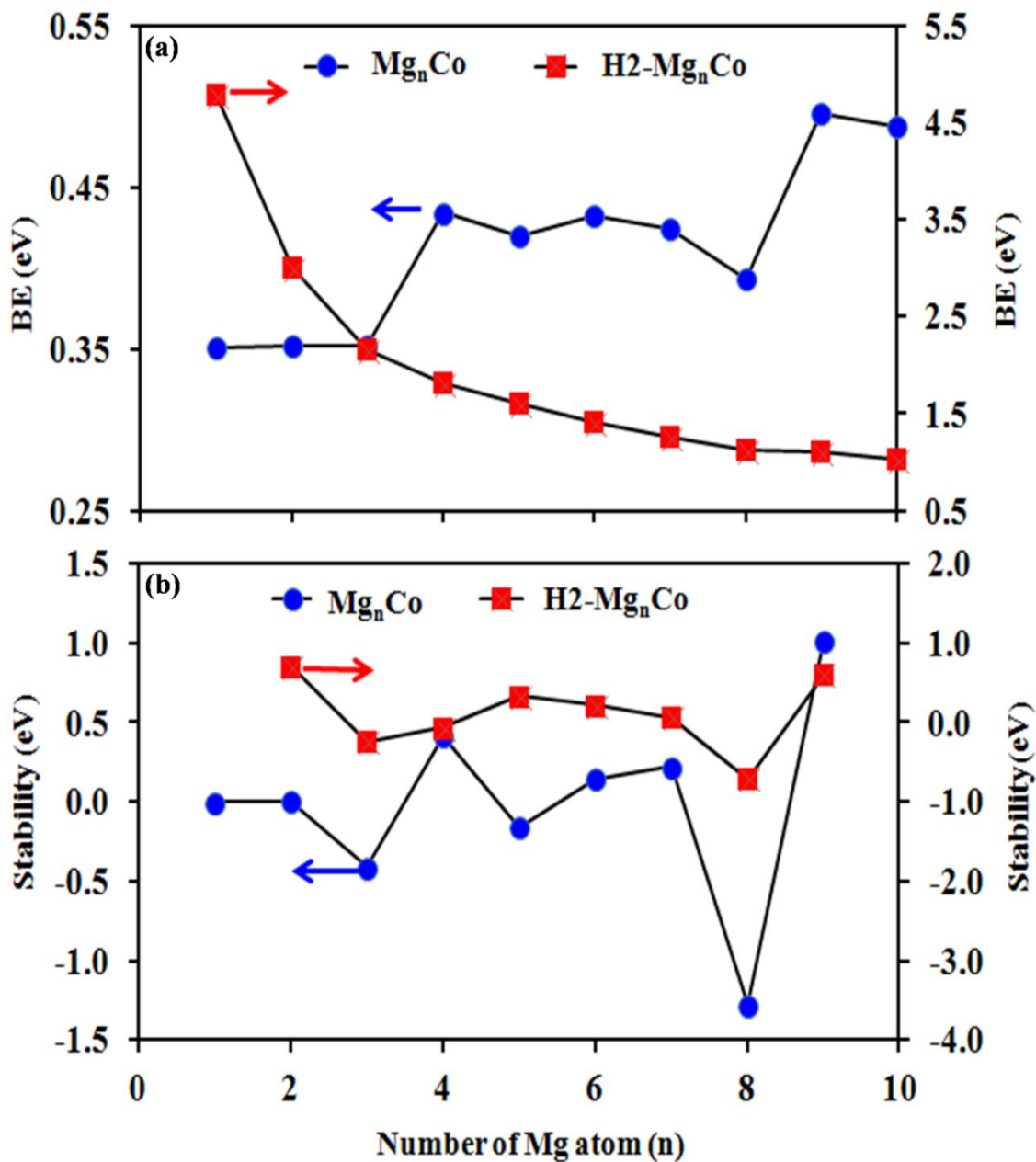
Table 5.2 (a) Bond length (Å) of Mg_n, Mg_nCo, Mg_nCo-H₂ and H₂-Mg_nCo cluster

n	Mg _n		Mg _n Co		Mg _n Co-H ₂		H ₂ -Mg _n Co	
	Mg-Mg	Mg-Mg	Mg-Co	Co-H	Mg-Co	Mg-H	Mg-Co	
1			2.58	5.62	2.52	1.72	3.02	
2	3.96	3.09	2.75	1.50	2.54	1.92	2.69	
3	3.45	3.25	2.65	2.16	2.64	1.72	2.53	
4	3.13	3.11	2.70	3.41	2.63	1.80	2.70	
5	3.24	3.26	2.53	1.66	2.65	1.73	2.44	
6	3.16	3.11	2.68	4.69	2.68	1.73	2.38	
7	3.82	3.13	2.70	1.96	2.76	1.72	2.52	
8	3.91	3.15	2.70	1.91	2.64	1.73	2.48	
9	3.19	3.01	2.70	2.02	2.70	1.73	2.66	
10	3.89	2.57	2.60	1.81	2.57	1.72	2.80	

Table 5.2(b) Binding energy (BE), Fragmentation energy (FE) and HOMO-LUMO (eV) gap in Mg_nCo, Mg_nCo-H₂ and H₂-Mg_nCo cluster

n	Mg _n Co			Mg _n Co-H ₂			H ₂ -Mg _n Co		
	BE (eV)	FE (eV)	Gap (eV)	BE (eV)	FE (eV)	Gap (eV)	BE (eV)	FE (eV)	Gap (eV)
1	0.35	0	2.80	5.50	0	4.54	4.75	0	2.85
2	0.35	0.35	2.91	2.98	0.46	2.17	2.99	1.20	2.25
3	0.35	0.35	2.06	2.10	0.35	2.77	2.16	0.50	2.25
4	0.43	0.76	2.23	1.74	0.64	2.12	1.80	0.73	2.23
5	0.42	0.34	2.09	1.45	0.31	2.14	1.60	0.80	1.95
6	0.43	0.50	2.14	1.30	0.54	1.65	1.41	0.47	2.17
7	0.42	0.36	1.87	1.15	0.27	1.60	1.25	0.26	1.57
8	0.39	0.14	1.00	1.06	0.44	1.82	1.12	0.20	1.49
9	0.49	1.41	1.63	1.08	1.24	1.65	1.09	0.90	1.63
10	0.48	0.40	2.09	0.90	-0.77	1.46	1.02	0.30	1.93

Fig. 5.2 Variation of Binding energy (a) and stability (b) of CoMg_n and $\text{H2-Mg}_n\text{Co}$ clusters with the number of magnesium atom



To explore the relative stability of Mg_nCo clusters with the increase of the cluster size within the range of $n = 1$ to 10, we have studied the stability or the second order difference energy (Δ_2). Following the definition of stability as mentioned, large positive value of Δ_2 is the indication of enhanced stability as they correspond to a gain in energy during growth process from the immediate lower size and lower gain in energy to the next bigger size. Variation of stabilities of Mg_nCo and $\text{H2-Mg}_n\text{Co}$ clusters with the variation of 'n' is shown in fig. 5.2. There are a number of maxima in the stability variation of Mg_nCo . The picture is different in $\text{H2-Mg}_n\text{Co}$. Here in the middle region this

variation is comparatively less with a local maxima at $n=5$ in the hydrogenated Mg_nCo . Following the variation of stability parameter, we found that the clusters at $n=4$ and 6 are behaving in the same manner as binding energy parameter. Though there is no sharp peak in stability parameter of Mg_nCo , but there is an increasing trend. Since our size limit is $n=10$, therefore, we cannot make any comment for the cluster at $n=9$ on its stability. Therefore, we will focus our study on the clusters with $n=4$ and 6 in Mg_nCo clusters and $n=5$ for hydrogenated Mg_nCo clusters.

To study the chemical stability of the clusters, the vertical ionization potential (VIP), vertical electron affinity (VEA), chemical potential (μ), chemical hardness (η) of each cluster. We have calculated above parameters following our previous reports [47-51]. Variation of VIP is basically defining the energy difference between the cationic and neutral clusters both are at the same equilibrium geometry of the neutral cluster. Whereas, VEA is defining the energy difference between the neutral and its anionic clusters both at the equilibrium geometry of the anionic cluster. By the definition

$$VEA(Mg_nCo) = E(Mg_nCo) - E(Mg_nCo^-) \quad (5.5)$$

$$VIP(H_2 - Mg_nCo) = E(H_2 - Mg_nCo^+) - E(H_2 - Mg_nCo) \quad (5.6)$$

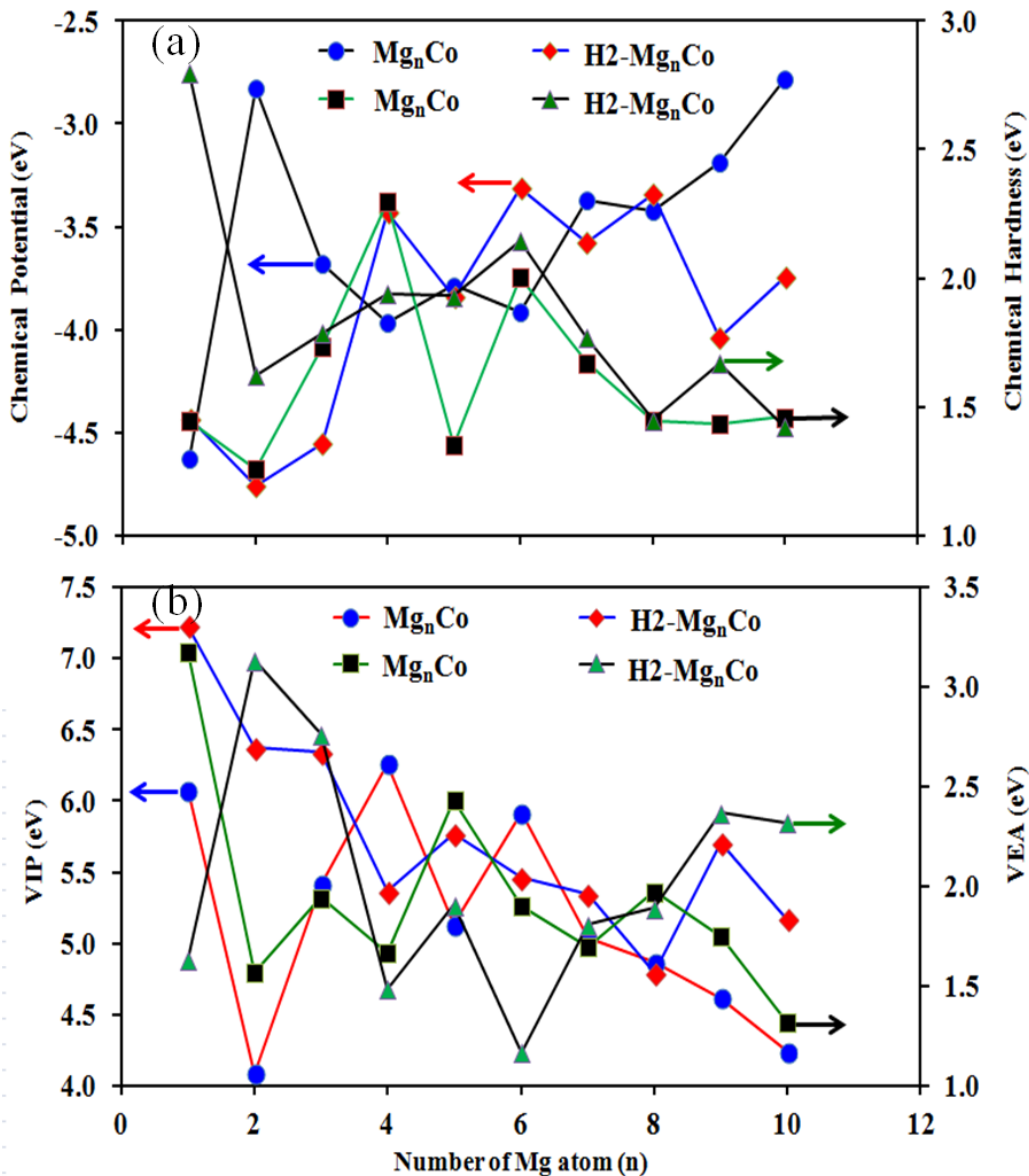
In the above expressions, when hydrogen attached with Mg as atomic form, we have used the formula of the cluster as H_2Mg_nCo , whereas, when it has been attached with the Co, we have used Mg_nCoH_2 . We have used this convention throughout presentation. Variation of VIP and VEA with the cluster size for different clusters is shown in table 5.3. This can be seen clearly from the VIP variation that there is a rise of VIP at $n = 4$ and 6 for Mg_nCo clusters and drop at the same sizes for H_2-Mg_nCo clusters. The values of VEA also support the variation of VIP. Following these results and the data for H_2-Mg_nCo presented in table 5.3, it is a clear indication of easy release of hydrogen from stable H_2-Mg_5Co clusters. The variation of chemical potential and chemical hardness; VIP and VEA are shown in Fig. 5.3. For Mg_nCo cluster there are local peaks at $n = 4$ and 6 for chemical hardness and minima for chemical potential. Again for H_2-Mg_nCo series there are local peaks at $n = 5$ and 7 for chemical hardness and minima for chemical potential. As mentioned above the values of VIP indicating local peak at $n = 4$ and 6 for Mg_nCo cluster and at $n = 5$ and 7 for H_2-Mg_nCo clusters. Following the stability nature of H_2-Mg_nCo , $n=5$ is more stable than $n=7$.

Table 5.3 VIP and VEA values of CoMg_n and H₂-Mg_nCo cluster

n	VIP		VEA	
	Mg _n Co (eV)	H ₂ -Mg _n Co (eV)	Mg _n Co (eV)	H ₂ -Mg _n Co (eV)
1	6.07	7.22	3.17	1.63
2	4.08	6.34	1.56	2.76
3	5.41	6.04	1.94	2.83
4	6.26	5.36	1.66	1.48
5	5.13	5.77	2.43	1.90
6	5.91	5.45	1.90	1.16
7	5.03	5.34	1.69	1.8
8	4.86	4.79	1.97	1.89
9	4.61	5.7	1.75	2.36
10	4.24	5.16	1.31	2.32

Therefore, it is logical to consider H₂-Mg₅Co as only suitable candidate in hydrogen adsorption and dissociation process. The values of VEA showing local minima at n = 4 and 6 for Mg_nCo cluster is indication of higher stability. These behaviors again support our results and also support that H₂-Mg₅Co cluster is the best candidate for hydrogen dissociation.

Fig. 5.3 Variation of chemical potential and chemical hardness (a), vertical ionization potential (VIP) and vertical electron affinity (VEA)(b) of different clusters with number of magnesium atom



5.3.2 Physisorption and Chemisorptions energy

Accumulation of atoms or molecules from their vapor phase over a solid surface, commonly known as adsorption, occurs due to attractive force acting between the atoms (or molecules) and the solid surfaces. Due to van-der Waals forces acting between the solid surfaces and the nearby atoms or molecules, when the atoms or molecules adsorb on the solid surface is known as physisorption. On the other hand, when this adsorption occurs due to the formations of bonds between the atoms or molecules with the solid surfaces, is known as chemisorption. The chemisorption may affect the electronic structure of the solid surfaces as due to the perturbation effect. The

most stable adsorption modes obtained in the present study is shown in fig.5.1. Adsorption energy, the H-H bond length, the Co-H bond length and the HOMO-LUMO gap are summarized in table 5.4.

Table 5.4 Adsorption energy, the H-H bond length, the Co-H bond length and the HOMO-LUMO gap

Cluster	ΔE_{ad} (eV)	D_{H-H} (eV)	D_{Co-H} (eV)	Gap (eV)
MgCoH ₂	0.56	0.74	5.62	2.85
Mg ₂ CoH ₂	0.67	0.74	4.38	2.25
Mg ₃ CoH ₂	0.68	0.74	5.49	2.25
Mg ₄ CoH ₂	0.56	0.74	3.41	2.23
Mg ₅ CoH ₂	0.52	0.87	1.66	1.95
Mg ₆ CoH ₂	0.63	0.74	4.69	2.17
Mg ₇ CoH ₂	0.46	0.77	1.96	1.57
Mg ₈ CoH ₂	0.6	0.77	1.91	1.49
Mg ₉ CoH ₂	0.59	0.76	2.02	1.63
Mg ₁₀ CoH ₂	0.55	0.78	1.81	1.93

The adsorption energy [52] is evaluated using the following equation

$$\Delta E_{ad} = E(Mg_nCo) + E(H_2) - E(Mg_nCo - H_2) \quad (5.7)$$

where, $E(Mg_nCo)$, $E(H_2)$ and $E(Mg_nCo - H_2)$ are the optimized energies of Mg_nCo , H_2 molecule and Mg_nCoH_2 clusters.

Table 5.5 Location of H, Multiplicity, H-H Bond length (Å), HOMO-LUMO gap and Chemisorption energy

Cluster	location	M (μ_B)	D_{H-H}	Gap (eV)	ΔE_{CE} (eV)
H2-MgCo	t (Mg), t (Mg)	4	3.42	4.54	0.154
H2-Mg ₂ Co	n, b (Mg, Mg)	2	2.51	2.17	0.694
H2-Mg ₃ Co	n, t (Mg, Mg)	2	8.64	2.77	0.847
H2-Mg ₄ Co	o, t (Mg, Mg)	2	3.53	2.12	0.819
H2-Mg ₅ Co	n, t (Mg, Mg)	2	5.98	2.14	1.273
H2-Mg ₆ Co	o, t (Mg, Mg)	2	5.18	1.65	1.325
H2-Mg ₇ Co	o, t (Mg, Mg)	2	5.99	1.6	1.145
H2-Mg ₈ Co	o, t (Mg, Mg)	2	8.04	1.82	1.053
H2-Mg ₉ Co	t, n (Mg, Mg)	2	8.13	1.65	0.699
H2-Mg ₁₀ Co	o, t (Mg, Mg)	2	7.98	1.46	1.743

We found that the most favored adsorption site for most clusters is on the Co top site (fig.5.1) as reported by other groups on transition metal doped Mg_n systems [7,8,11]. With reference to the fig. 5.1, hydrogen atoms absorbed with Mg atoms in Mg_nCo cluster via chemisorption process. In general chemisorptions energies [52] is used to describe the reactivity of H_2 on the Mg_nCo clusters. It can be defined as:

$$\Delta E_{CE} = E(Mg_nCo) + E(H_2) - E(H_2 - Mg_nCo) \quad (5.8)$$

Where E_{Mg_nCo} , E_{H_2} and $E_{H_2-Mg_nCo}$ are the calculated optimized energies of the Mg_nCo , H_2 molecule and H_2-Mg_nCo clusters respectively. As per the thermodynamic data, VIP, VEA, and the data presented in table 5.4, we can choose H_2-Mg_5Co cluster as the most stable as well as most reactive for hydrogen dissociation.

5.3.3 H_2 Dissociation mechanisms

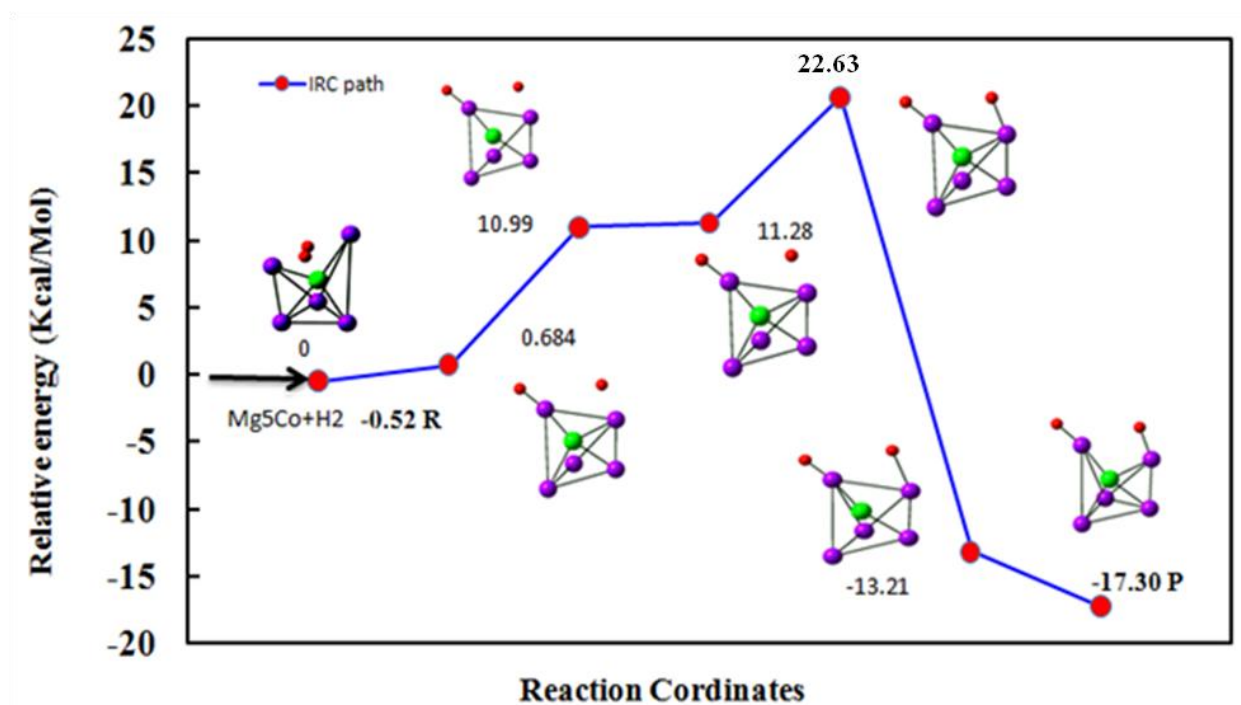
Again to examine the H_2 dissociative process; we define the physisorption and chemisorptions with the H_2 molecule as the reactant and product. In physical adsorption, the forces of attraction between the molecule of the adsorbate and the adsorbent are of the weak Van der Waals type. Since the forces of attraction are weak, the process of physisorption can be easily reversed. In chemical adsorption, the forces of attraction between the adsorbate and the adsorbent are very strong. The molecules of adsorbate form chemical bonds with the molecule of the adsorbent present in the surface. The computed reaction energy is directly calculated by the total energy difference between the reactant and product. This is the minimum amount of energy needed before a reaction can start. Negative reactant energy means the process is exothermic otherwise it is endothermic. The activation barrier (kcal/mol) is calculated by the total energy difference between the reactant and the transition state.

H_2 dissociation on all Mg_nCo clusters is exothermic (-3.7 to -27.19 Kcal/mol) showing in table 5.6. The computed reaction energy (ΔE_o), activation barrier (eV) for the transition from the physisorbed Mg_nCo-H_2 cluster to the related chemisorbed form is shown in table 5.6. Among the Mg_nCo clusters the Mg_5Co cluster shows lower activation barrier and the largest reaction energy and largest chemisorption energy. So it is showing significant chemical reactivity and can break the H-H bond endothermically when interacting with a H_2 molecule. Again this supports the results obtained from the calculated optimized potential energy (kcal/mol) surfaces for Mg_5Co-H_2 for the dissociative chemisorptions reactions shown in fig.5.6.

Table 5.6 Reaction energy (ΔE_0) including zero point energy, Activation barrier, and Frequency (cm^{-1})

Cluster	Reaction Energy(kcal/mol)	Activation Barrier (kcal/mol)	ω (cm^{-1})
MgCo	-16.49	27.82	-743.65
Mg ₂ Co	-0.42	7.55	-466.04
Mg ₃ Co	-3.70	17.17	-39.55
Mg ₄ Co	-5.92	13.93	-329.69
Mg ₅ Co	-17.26	20.63	-180.49
Mg ₆ Co	-15.85	23.80	-21.97
Mg ₇ Co	-15.62	11.00	-36.35
Mg ₈ Co	-10.22	12.38	-153.54
Mg ₉ Co	-22.46	15.57	-252.46
Mg ₁₀ Co	-27.19	14.48	-38.60

Fig. 5.4 Potential energy surface of H₂-Mg₅Co clusters.



After optimization, the H-H bond lengths are 2.53 Å, which is 1.79 Å more than the H-H bond length of the isolated H₂ molecule (0.743Å). This is a clear indication of relaxation of hydrogen on the cluster surface where it can be easily removable. The calculation of reaction path is important to verify the transition state as calculated before. If we know the transition state, we can calculate IRC path starts from TS and give the information about the potential

energy surface. It steps toward reactant and then towards products. These results illustrate the chemical behavior of molecular hydrogen dissociation into hydrogen atoms on clusters. The calculated difference between energy of product of reaction path and reactant ($\text{Mg}_5\text{Co} + \text{H}_2$) energy is 22.63 Kcal/mol, which is nearly equal to our calculated value from the IRC path (20.63 Kcal/mol). These results exhibit the dissociation process of hydrogen atom on Mg_nCo clusters.

5.4 Conclusions

Present study reports the use of Mg_nCo as an effective hydrogen storage element in the form of nanoclusters. From the growth pattern of Mg_nCo ($n=1-10$) clusters it is found that Mg_4Co and Mg_6Co both are stable in the series where Co prefers to take peripheral position. From the chemisorptions and physisorptions energies and VIP and VEA parameters, we found Mg_5Co only can be used as effective hydrogen storage and dissociate element. After addition of H_2 , $\text{H}_2\text{-Mg}_5\text{Co}$ is appears as efficient hydrogen catalyst. Together with these two, $\text{H}_2\text{-Mg}_5\text{Co}$ shows highest reaction energy in IRC path and we found the same activation barrier during the chemical process as we calculated in our simulation. The complete study shows that in the Mg_nCo ($n=1-10$) series, Mg_5Co can be selected as an efficient hydrogen storage element.

5.5 References

- [1] Novakovic N, Garbovic Novakovic J, Matovic I, Manasijevic M, Radisavijevic I, Mamula BR, Ivanovic N, Int J Hydrogen Energy, **2010**; 35: 598-606.
- [2] Fayet P, Kaldor A, Cox DM, J Chem Phys, **1990**; 92: 254-261.
- [3] Giusepponi S, Celino M, Int J Hydrogen Energy, **2015**; 40: 9326-9334.
- [4] Song Y, Guo ZZ, Yang R, Phys Rev B, **2004**; 69: 094205-094215.
- [5] Stier W, Gabriel Camargo L, Oskarsson F, Jonsson H, Am, Chem. Soc., Div. Fuel Chem, **2005**; 50:15.
- [6] Zaluski L, Zaluska A, Strom Olsen JO, Schulz R, J Alloy Comp, **1995**; 217: 295-300.
- [7] Zaluski L, Zaluska A, Strom Olsen JO, Schulz R, J Alloy Comp, **1999**; 288: 217-225.
- [8] Oelerich W, Klassen T, Bormann R, J Alloy Comp, **2001**; 315: 237-242.
- [9] Zaluski L, Zaluska A, Strom Olsen JO, Appl Phys A, **2001**; 72: 157-165.
- [10] Ming Au, Mat Sci Engineering B **2005**; 117: 37
- [11] Liang G, Huot J, Boily S, Naste AV Schulz R, J Alloy Comp, **2000**; 297: 261-265.
- [12] Zhang B, Wu Y, Int J Hydrogen Energy, **2015**; 40: 9298-9305.
- [13] Huot J, Linag G, Schulz R, Appl Phys A, **2001**; 72:187-195.
- [14] Zaluski L, Zaluska A, Strom Olsen JO, Schulz R, J Alloy Comp, **1997**; 70: 253-254.
- [15] Hout J, Liang G, Boily S, Neste AV, Schulz R, J Alloy Comp, **1999**; 495: 293-295.
- [16] Mananghaya M, Int J Hydrogen Energy, **2015**; 40: 9352-9358.
- [17] Bobet JL, Akiba E, Nakamura Y, Darriet B, Int J Hydrogen Energy, **2000**; 25: 987-996.
- [18] Amica G, Arneodo Larochette P, Gennari FC, Int J Hydrogen Energy, **2015**; 40: 9335-9346.
- [19] Banerjee S, Pillai CGS, Majumdar C, Int J Hydrogen Energy, **2010**; 35: 2344-2350.
- [20] Li S, Jena P, Ahuja R, Phys Rev B **2006**; 74: 132106
- [21] Suleyman Er, Tiwari D, Gills A, Brocks G, Phys Rev B, **2009**; 79: 024105.
- [22] Nonose S, Sone Y, Onodera K, Sudo S, Kaya K, Chem Phys Lett, **1989**; 164: 427-432.
- [23] Henry DJ, Yarovsky I, J Phys Chem A, **2009**; 113: 2565-2571.
- [24] Retuerto M, Alonso JA, Martínez R, Jiménez-Villacorta F, Sánchez-Benítez J, Fernández- Díaz MT, Garcia-Ramos CA, Ruskov T, Int J Hydrogen Energy **2015**; 40: 9306-9313
- [25] Wang L, Zhao J, Zhou Z, Zhang SB, Chen Z, J Comp Chem, **2009**; 30: 2509-2514.
- [26] Varano A, Henry DJ, J Phys Chem A, **2010**; 114: 3602 -3608.

- [27] Ren J, Musyoka NM, Annamalai P, Langmi HW, North BC, Mathe M, *Int J Hydrogen Energy*, **2015**; 40: 9382-9387.
- [28] Lu QL, Wan JG, *J Chem Phys*, **2010**; 132: 224308.
- [29] Kumar TJD, Tarakeshwar P, *Phys Rev B*, **2009**; 79: 205415.
- [30] Biliškov N, Miletić GI, Drasner A, Prezelj K, *Int J Hydrogen Energy*, **2015**; 40: 8548-8561.
- [31] Xue-feng S, Gao-feng Zhao Li-li Z, *J Phys Chem C*, **2008**; 112: 17828-17834.
- [32] Yu R, Lam PK, *Phys Rev B*, **1988**; 37: 8730-8737.
- [33] AlMatrouk HS, Chihaiia V, *Int J Hydrogen Energy*, **2015**; 40: 5319-5325.
- [34] Huaiyu S, Tong L, Yuntao W, Hairuo X, Xingguo L, *J Solid State Chem*, **2004**; 177: 3626-3632.
- [35] Fanjie K, Yanfei H, *J Mol Model*, **2012**; 20: 2087-2093.
- [36] Lee C, Yang W, Parr RG, *Phys Rev B*, **1998**; 37:785.
- [37] Frisch MJ, Trucks GW, Schlegel HB, Scuseria GE, Robb MA, Cheesemen JR, Zakrzewski VG, Montgomery jr JA, Stratmann RE, Burant JC, Dapprich S, Millam JM, Daniels AD, Kudin KN, Strain MC, Farkas O, Tomasi J, Barone V, Cossi M, Cammi R, Mennucci B, Pomelli C, Adamo C, Clifford S, Ochtrski J, Petersson GA, Ayala PY, Cui Q, Morokuma K, Malick DK, Rabuck AD, Raghavachari K, Foresman JB, Cioslowki J, Ortiz JV, Baboul AG, Stefanov BB, Liu B, Liashenko A, Piskorz P, Komaromi I, AL-Laham MA, Peng CY, Nanayakkara A, Challacombe M, Gill PMW, Johnson B, Chen W, Wong MW, Andress JL, Gonzalez C, Head-Gordon M, Replogle ES, Pople J A, **2004**; Gaussian 03, revision E 01 Gaussian, Wallingford
- [38] Dhaka K, Trivedi R, Bandyopadhyay D, *J Mol Model*, **2012**; 19: 1473-1488.
- [39] Trivedi R, Dhaka K, Bandyopadhyay D, *RSC Adv*, **2014**; 4: 64825-64834.
- [40] Peng C, Ayala PY, Schlegel HB, Frisch MJ, *J Comp Chem* **1996**; 17: 49-56.
- [41] Ouyang Y, Wang P, Xiang P, Chen H, Du Y, *Comp Theo Chem*, **2012**; 984: 68-75.
- [42] Kant A, Strauss B, *J Chem Phys*, **1964**; 41: 3806-3808.
- [43] Fukai Y, Berlin, Springer- Verleg, **1993**.
- [44] Balfour WJ, Douglas AE, *Can J Phys*, **1970**; 48: 901-914.
- [45] Lombardi JR, Davis B, *Chem Rev*, **2002**; 102: 2431-2460.
- [46] Kumar M, Bhattacharya N and Bandyopadhyay D., *J Mol Model*, **2012**; 18: 405-418.
- [47] Bandyopadhyay D, Kaur P and Sen P, *J Phys Chem A*, **2010**; 114: 12986-12991.
- [48] Bandyopadhyay D, *J Mol. Model*, **2012**; 18: 3887-3902.

- [49] Bandyopadhyay D, J Appl Phys, **2008**; 104: 084308-084308-7.
- [50] Bandyopadhyay D, J Mol. Model, **2012**, 18: 737-749.
- [51] Bandyopadhyay D, Sen P, J Phys Chem A, **2010**; 114: 1835-1842.
- [52] Guo L, J Phys Chem, **2013**; 117: 3458-3466.

CHAPTER 6

STUDY OF ADSORPTION AND DISSOCIATION PATH WAY OF H₂ MOLECULE ON Mg_nRh (n = 1-10) CLUSTERS: A FIRST PRINCIPLE INVESTIGATION

6.1 Introduction

At present huge consumption of fossil fuels are causing serious air pollution and is the source of greenhouse gases. Moreover, the stored renewable fossil fuels are limited in the Earth. Therefore, searching for a plentiful, renewable and particularly clean, alternative energy resource is vital for the mankind. Hydrogen is being considered as a gifted alternative fuel source because of its efficiency, abundance and environmental friendliness [1-2]. Hydrogen is a promising clean energy carrier and has been attracting much interest to the scientific communities, governments and industries [3]. One of the primary technical challenges is to search for the economic, effective and safe hydrogen storage medium. The storage of hydrogen in solid-state materials offers an alternative way in this direction. The use of magnesium based systems is considered as one of the promising hydrogen storage material due to its lightweight, low cost and having high hydrogen storage capacity [4]. But the challenging problem in using magnesium as hydrogen storage materials is due its high thermal stability and slow kinetics of hydrogen adsorption and dissociation reaction processes [5-6]. A number of theoretical and experimental works have been done to improve the efficiency of Mg metal to meet the stringent criteria for hydrogen storage [7-12]. One of these attempts is to drop transition metal atom into magnesium clusters, which can greatly reduce the activation barrier for dissociation process of hydrogen [13-15]. Metal hydrides are natural hydrogen storage materials and are make relatively strong bonds between hydrogen and the host. So hydrogen adsorption on hydride metal surface and nanoclusters is a widely studied subject that gives us an opportunity to gain a basic knowledge in the hydrogen storage science. Experimentally, the chemisorptions process on H₂ on Pd_n clusters and Pd clusters deposited on a thin film of alumina [16-17] have been investigated in order to understand the reaction mechanism of Pd_n with hydrogen during addition and dissociation reaction processes. Later, Amica et al. [18] reported the hydrogen storage mechanism of LiNH₂-LiH system with MH₂ added (M = Mg, Ca, Ti) and clarifies the chemical interactions occurring during hydrogen cycling. Detailed structural investigations reveal that due to heating, MH₂ (M = Mg, Ca) metal hydrides reacts with LiNH₂ to form Li₂Mg-(NH)₂ and 2CaNH-Ca-(NH)₂ solid solution and at the same time release of hydrogen. They found a new reversible pathway for hydrogen storage in the Li-Ca-N-H system after dehydrogenation of the LiNH₂-LiH when added with CaH₂ by XRPD and FTIR with distinguished development in

the dehydrogenation temperature. Retuerto et al. [19] studied the tri-atomic metal hydride clusters, Mg_2FeH_6 , prepared by high-pressure and high-temperature reaction from the hydrides and then characterized by neutron powder diffraction to understand the crystallographic details and hydrogen occupancy. Gutfleish et al. [20] have recently studied Mg alloyed with Ni and Pd. They found that the product of ternary alloy can be used as an excellent hydrogen adsorption and dissociation element with high kinetic and cyclic stability. In addition, many researchers [21-24] experimentally investigated the catalytic effects of transition metals elements, Co, Cu, Mn, Y, Ti, and Cr on the hydrogen storage properties of Mg based metal hydrides. They found again that adding a small amount of transition metal could improve the hydrogen storage properties. At the same time, many theoretical investigations related to hydrogen storage, many groups have been studying hydrogen adsorption and dissociation processes. Varano and Henry [25] used density functional theory (DFT) method to investigate the hydrogen adsorption on magnesium-doped aluminum clusters. Liu et al. [26] studied the hydrogen molecules adsorption and storage in Sc coated $SiAl_{12}$ cluster using DFT. It has been found that by doping the transition metal atom can grow weaker the Mg-H bond and reduce the stability of the hydride. Liang et al. [27] and Schulz et al. [28] found that V and Ti are better catalysts than Ni for hydrogen adsorption and desorption when they form Mg- H_2 metal composites. In this direction Song et al. [29] and Shang et al. [30] found that the stability of MgH_2 -Ti is higher than MgH_2 -Ti. Recently, Estevania et al. [31] used DFT to study hydrogen desorption energy in pure Nb or Zr doped system containing vacancy like defects and an MgH_2 defect free surface. Nb and Zr modify the surface geometry and make weaker the Mg-H bonds, hence, easing the H desorption process. First principle calculation based on DFT carried out by Larsson et al. [32] to show that Ti, V, Fe and Ni significantly lowered the hydrogen desorption energies in MgH_2 nanoclusters. A computational study carried out by Liang [33] using DFT showed that substitution of two Mg atoms in MgH_2 by a Li or Al may improve its hydrogen storage capability by lowering the reaction energies as well as activation barrier. It is well known that Pd, Rh and Ni have very high affinity towards hydrogen absorption and form metal hydrides. These elements are very useful in hydrogen storage technology as catalysts due to their high hydrogen solubility, diffusivity and corrosion resistance [34-38]. Therefore, overall view is that due to doping of transition metal elements improves the hydrogen storage and dissociation properties of materials. It is still very interesting to know about the transition metal atoms that could be efficient for hydrogen storage. Our previous theoretical work [39] on small sized Mg_nCo clusters found that Co plays an important role in the hydrogen dissociation process on magnesium clusters. Research on Mg is aiming to reduce the high temperature required for the dissociation of its hydride phase and to accelerate the H_2 adsorption kinetics. In the present work we have

studied the hydrogen adsorption and dissociation process of Mg_nRh nanoclusters within the size range $n=1-10$. Our results show the effectiveness of Rh transition metal to improve the hydrogen adsorption energy and the hydrogen storage capacity. It is also qualify as good catalysts for accelerating the kinetics of hydrogen adsorption.

6.2 Computational methodology

We perform first principle density functional theory calculation using Becke, three-parameter, Lee- Yang-Parr (B3LYP) functional [40]. The exchange correlation contribution is included in the calculation by using the generalized gradient approximation proposed by Perdew-Burke-Ernzerhof [41]. The geometry optimizations are carried out starting from several initial geometries reported in our previous work [39, 42-44] without imposing any symmetry constraints. With increasing size of cluster, the number of isomers in a particular size increases. So it is a challenging job to find out ground state geometry in a particular size. Tai and Nguyen [45] adopted a stochastic method that covers a good number of isomeric structures and enhance the chance of searching the ground state geometry. The standard Lanl2dz [46, 47] basis set with effective core potentials are used for Mg and Rh atoms, while, 6-311G (d) [48] basis set is used for hydrogen molecule. After establishing the ground state geometries of pure Mg_nRh clusters, we find out the most preferred sites for hydrogen substitution. The QST [49] method has been employed to find out the transition state and intrinsic reaction coordinate (IRC) path to relate the activation energy barrier and then compared with calculated results for the dissociation of hydrogen molecules attached with the Mg_nRh clusters. For reaction pathways, minima are connected to each transition state by tracing the IRC path. All computations are performed using Gaussian' 03 program package [50]. The number of imaginary frequency of all the optimized geometry of Mg_nRh clusters are zero, thereby conforming stable ground state structures. In order to establish the accuracy of the present method we have performed few test calculation on Mg-Mg, Mg-Rh, Rh-Rh and H-H dimers, and is summarized in table 6.1. The results show an excellent agreement between the present calculations with the experimental and theoretical studies.

6.3 Results and discussions

As discussed in the last section, a number of starting geometries for Mg_nRh clusters are considered in the optimization process. The lowest energy isomers of Mg_nRh , Mg_nRh-H_2 and H_2-Mg_nRh clusters are shown in fig. 6.1. It shows a clear growth pattern of Mg_nRh clusters from Mg-Rh dimer within the range of $n=1-10$. We found that the theoretical ground state of Mg-Rh dimer with $C_{\infty v}$ point group symmetry hold a doublet state. The next higher

sized isomer is also a doublet. Three optimized isomers are found at Mg_2Rh composition. The triangular isomer in C_{2v} point group symmetry is the ground state. The structure of others two are linear as shown in fig. 6.1. With the increasing size of clusters, out of three isomers in Mg_3Rh clusters the isomer with triplet bend rhombus with C_{2v} point group symmetry is the lowest energy structure, which is similar to the previous theoretical report [51, 52]. Similarly, three isomers are optimized with composition Mg_4Rh , where, the isomer with the C_s point group symmetry and distorted pyramidal structure is the theoretically ground state. The edge capped trigonal bi-pyramidal isomer found as ground state geometry with C_{2v} point group symmetry among the isomers with Mg_5Rh composition. Pentagonal structure with C_s point group symmetry is the lowest energy structure in Mg_6Rh cluster. Similarly bi-capped pentagonal structure with D_{5h} symmetry group is the ground state structure at the Mg_7Rh clusters. For Mg_8Rh , the most stable structure is a capped square prism with C_s point group symmetry in doublet state. The lowest energy isomers Mg_9Rh and Mg_{10}Rh are in doublet spin state with C_1 point group symmetry. Following our previous report [39] we did not take the endohedrally position of the Rh atom, because, in that case it will be not available for reaction with hydrogen. By the adsorption and dissociate capabilities of magnesium transition metal alloy clusters, we explore the possibility of hydrogen adsorption and dissociation process on Mg_nRh clusters via examining the reaction energy, activation barrier and chemisorptions energy.

Table 6.1 Bond lengths (\AA) and frequencies (cm^{-1}) of different dimer

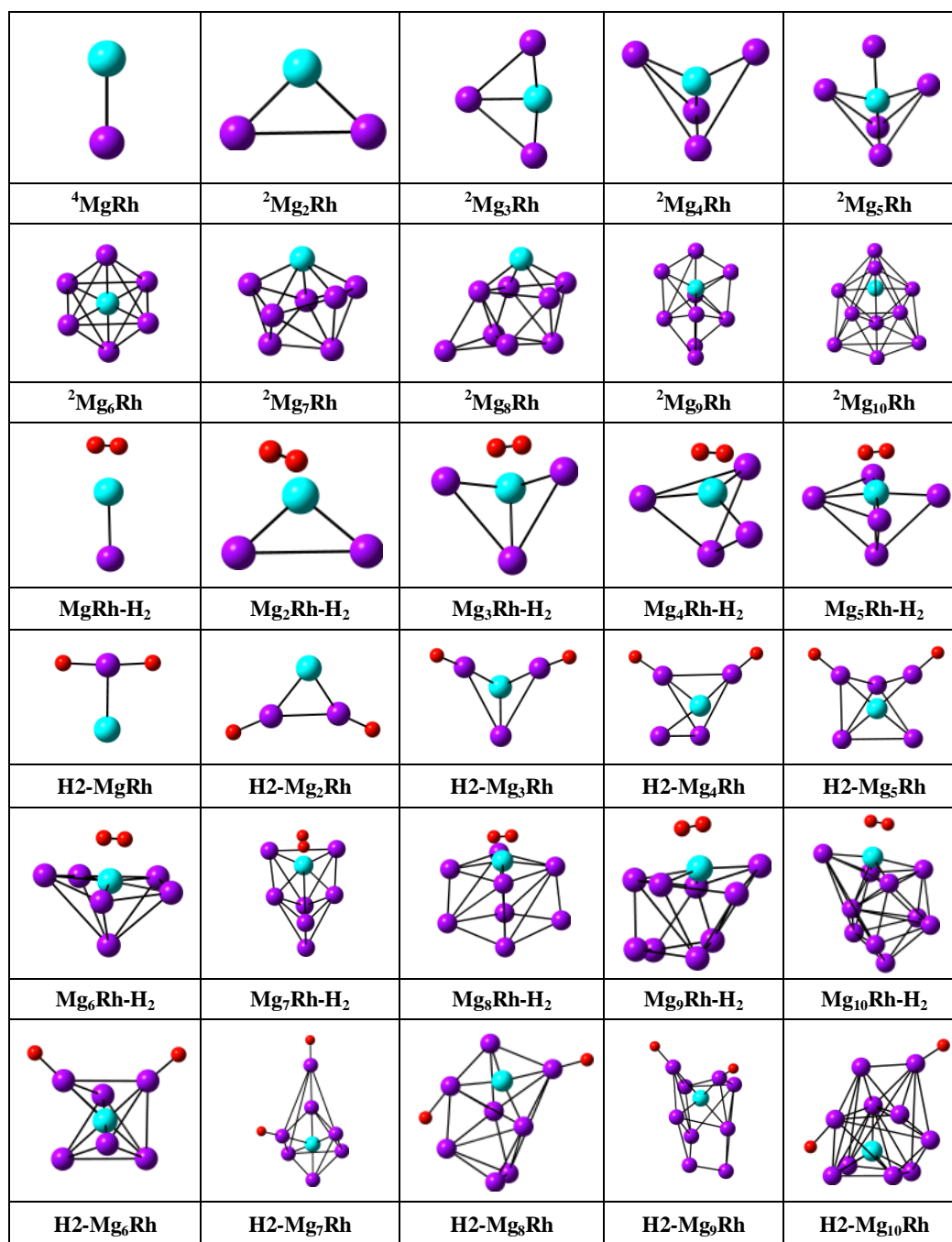
Dimer	Bond length (\AA)	Lowest frequency (cm^{-1})
Mg_2	3.96 [†] , 3.89, 3.88 [‡] [46,47]	43.28 [†] , 51.12 [‡] [51]
Rh_2	2.32 [†] , 2.31 [‡] , 2.28 [‡] [48,49]	245.21 [†] , 297 [‡] [48]
H_2	0.743 [†] , 0.741 [‡] , 0.743 [‡] [50,57]	5112.4 [†] , 4401 [‡] [50]

[†] Present [‡] Reported

6.3.1 Energetic and Stability

It is important to understand the relative stability of different sized Mg_nRh and $\text{H}_2\text{-Mg}_n\text{Rh}$ ($n = 1-10$) clusters in the series during growth process. To get this idea we have studied the variation of different thermodynamic and chemical parameters of the clusters, such as, average binding energy (BE), 2nd order change in energy (Δ_2), adiabatic chemical affinity (ADE) etc. with the cluster size.

Fig. 6.1 Optimized ground state isomers of $RhMg_n$, Mg_nRh-H_2 and H_2-Mg_nRh clusters ($n=1-10$). Dark purple balls are Mg atom, green balls are Rh atom and small red balls are H atoms. Superscript indicates the multiplicity of the clusters.



The relative stability of the clusters can be represented with the calculation of average binding energy and second order difference of the total energy of the clusters in the present study following our previous reports [39] for neutral clusters as follows:

$$BE(Mg_nRh) = [nE(Mg) + E(Rh) - E(Mg_nRh)]n + 1 \quad (6.1)$$

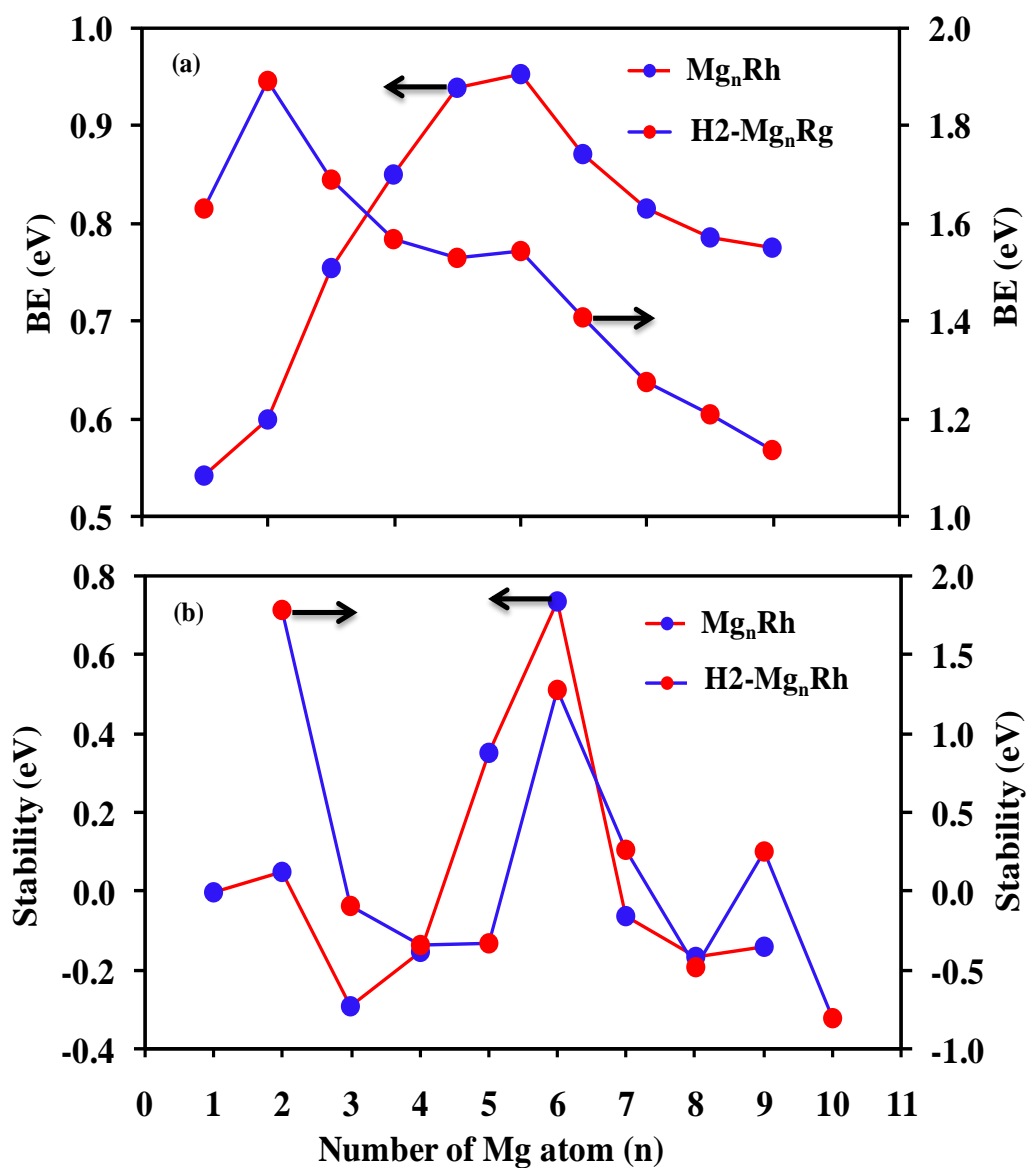
$$BE(H_2 - Mg_nRh) = [nE(Mg) + E(Rh) + 2E(H_2) - E(H_2 - Mg_nRh)]n + 3 \quad (6.2)$$

$$\Delta_2(Mg_nRh) = E(Mg_{n+1}Rh) + E(Mg_{n-1}Rh) - 2E(Mg_nRh) \quad (6.3)$$

$$\Delta_2(H_2 - Mg_nRh) = E(H_2 - Mg_{n+1}Rh) + E(H_2 - Mg_{n-1}Rh) - 2E(H_2 - Mg_nRh) \quad (6.4)$$

where, E represent the optimized energy of the clusters or the energy of a single atom in a particular system. We tabulated all the parameters in Table 6.2. In the above expression, when hydrogen attached with Mg in atomic form we used the formula of the cluster as H2-Mg_nRh, whereas, if hydrogen attached with the Rh as molecule, we used Mg_nRhH₂ throughout this report. The above definition of binding energy (BE) means the average gain in energy per atom during the formation of cluster from individual atom, while, the second order change in energy (Δ_2) indicates the difference of the energy of a cluster surrounding to its neighbor. fig. 6.2 (a) show the variation of the average atomic binding energy of the Mg_nRh or H2-Mg_nRh clusters with the increasing clusters size. It is clear that during the growth process of Mg_nRh, the BE increases with a maximum value of 0.95 eV and then decrease. The initial increase in the average binding energy is an indication of thermodynamic instability of the clusters. Furthermore, with the increasing the cluster size, the binding energy of H2-Mg_nRh clusters displays an asymptotic decrease, indicate these clusters attain stability more quickly at n = 6, which is similar to the trend obtained by Ling Guo [51]. fig. 6.2 (b) shows the variation of 2nd order change in energy of Mg_nRh and H2-Mg_nRh clusters. It is a sensitive quantity that reflects the stability of the clusters and also known as stability parameter. As shown in fig. 6.2, the local maxima of the Δ_2E of the Mg_nRh clusters appear at the n=6, which is in good agreement with the binding energy curve. The relatively higher stability is mainly associated with the geometry of the cluster. There is no clear local maxima of H2-Mg_nRh BE variation at n=9. However, the local maxima at n=9 in the stability parameter of H2-Mg₉Rh show additional stability at n=9.

Fig.6.2 Variation of Binding energy (a) and stability (b) of $RhMg_n$ and H_2-Mg_nRh clusters with the number of magnesium atom.



To get more insight into the stability of the cluster we calculated the vertical ionization potential (VIP) and vertical electron affinity (VEA). Vertical ionization potential is often used to investigate the chemical stability of small clusters. Larger value of VIP leads to less reactivity and higher stability. Vertical electron affinity is also means the evaluation of the relative stability of the cluster. It explains the amount of energy needed to add an electron to a neutral molecule. So to understand their behavior with the cluster size the vertical ionization potential is obtained as the energy difference between the cluster and its positive ion in the same neutral geometry. Similarly we have calculated the vertical electron affinity, which is the energy difference between the neutral and anionic cluster both at the equilibrium of the anionic cluster.

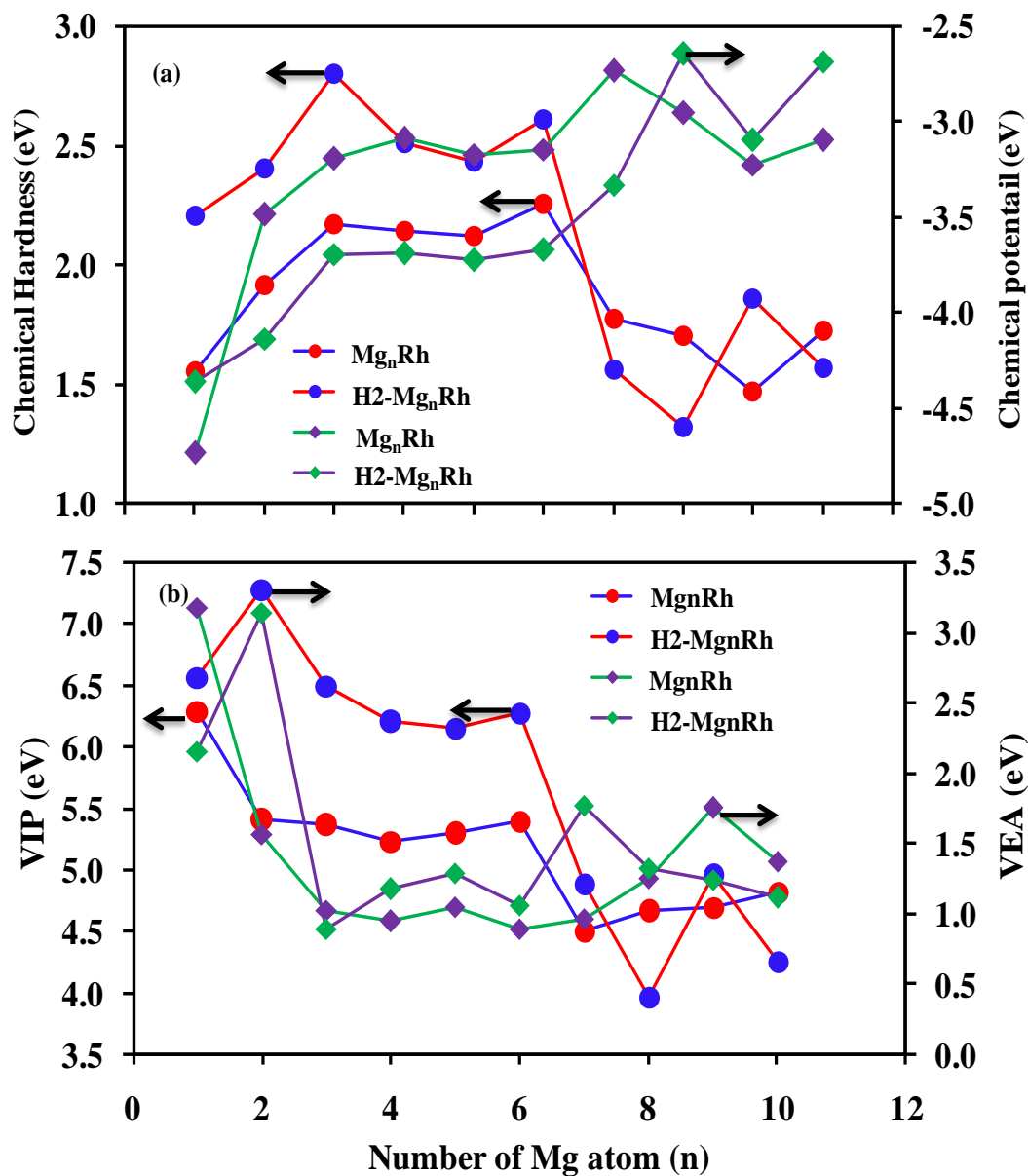
Table 6.2 (a) Bond lengths (Å) of Mg_n, RhMg_n, Mg_nRh-H₂ and H₂-Mg_nRh clusters

n	Mg _n		Mg _n Rh		Mg _n Rh-H ₂		H ₂ -Mg _n Rh	
	Mg-Mg	Mg-Mg	Mg-Rh	Rh-H	Mg-Rh	Mg-H	Mg-Rh	
1			2.58	5.62	2.52	1.72	3.02	
2	3.96	3.09	2.75	1.50	2.54	1.92	2.69	
3	3.45	3.25	2.65	2.16	2.64	1.72	2.53	
4	3.13	3.11	2.70	3.41	2.63	1.80	2.70	
5	3.24	3.26	2.53	1.66	2.65	1.73	2.44	
6	3.16	3.11	2.68	4.69	2.68	1.73	2.38	
7	3.82	3.13	2.70	1.96	2.76	1.72	2.52	
8	3.91	3.15	2.70	1.91	2.64	1.73	2.48	
9	3.19	3.01	2.70	2.02	2.70	1.73	2.66	
10	3.89	2.57	2.60	1.81	2.57	1.72	2.80	

Table 6.2 (b) Binding energy (BE), Fragmentation energy (FE) and HOMO-LUMO gap (eV) Mg_n, RhMg_n, Mg_nRh-H₂ and H₂-Mg_nRh clusters

n	Mg _n Rh			Mg _n Rh-H ₂			H ₂ -Mg _n Rh		
	BE (eV)	FE (eV)	Gap (eV)	BE (eV)	FE (eV)	Gap (eV)	BE (eV)	FE (eV)	Gap (eV)
1	0.54	0	2.72	6.26	0	2.96	1.63	0	2.47
2	0.59	0.71	2.04	3.64	1.01	2.47	1.33	2.67	2.13
3	0.75	1.22	1.95	2.78	1.06	1.98	1.68	0.88	2.39
4	0.85	1.23	1.98	2.36	1.12	1.38	1.56	0.96	2.31
5	0.93	1.38	1.27	2.06	0.86	2.12	1.53	1.30	2.53
6	0.95	1.03	1.57	1.73	0.04	1.87	1.54	1.62	1.76
7	0.87	0.30	1.44	1.59	0.77	1.27	1.40	0.34	1.74
8	0.81	0.36	1.30	1.06	0.73	1.44	1.27	0.07	1.30
9	0.78	0.52	1.22	1.36	0.39	1.30	1.21	0.55	1.44
10	0.77	0.66	1.25	1.25	0.29	1.46	1.02	0.29	1.93

Fig.6.3 Variation of chemical potential, chemical hardness (a) vertical ionization potential (VIP), vertical electron affinity (VEA) (b) of different clusters with number of magnesium atom.



By the definition:

$$VIP(Mg_nRh) = E(Mg_nRh^+) - E(Mg_nRh) \quad (6.5)$$

$$VEA(Mg_nRh) = E(Mg_nRh) - E(Mg_nRh^-) \quad (6.6)$$

$$VIP(H_2 - Mg_nRh) = E(H_2 - Mg_nRh^+) - E(H_2 - Mg_nRh) \quad (6.7)$$

$$VEA(H_2 - Mg_nRh) = E(H_2 - Mg_nRh) - E(H_2 - Mg_nRh^-) \quad (6.8)$$

fig. 6.3 indicates the variation of VIP and VEA with the cluster size. It can be seen clearly from the VIP variation (fig. 6.3a) that there is a sharp rise of VIP at $n = 6$ for Mg_nRh clusters and it drops at the same size for $H2-Mg_nRh$. Larger the value of VIP indicates higher stability of the clusters. In $H2-Mg_nRh$ cluster series it can be seen that there is a peak at $n=9$, which exhibits the stability of the $H2-Mg_9Rh$ cluster. Further, it is interesting to note that the VEA shows drop at the $n = 6$ for Mg_nRh cluster that supports the VIP results which is not recommended for hydrogen storage. For $H2-Mg_nRh$ cluster, the variation of VEA with the cluster size again shows a drop at the $n = 9$. Following these results and the data in the table 6.3, it is easy to predict that hydrogen adsorption and dissociation process will take place efficiently at the $H2-Mg_9Rh$ cluster.

Table 6.3 Vertical ionization potential (VIP) and Vertical electron affinity (VEA) of clusters

n	VIP (eV)		VEA (eV)	
	Mg_nRh	$H2-Mg_nRh$	Mg_nRh	$H2-Mg_nRh$
1	6.28	6.56	3.17	3.17
2	5.40	6.51	1.56	1.56
3	5.36	6.49	1.02	1.02
4	5.23	6.20	0.94	0.94
5	5.29	6.15	1.04	1.04
6	5.39	6.27	0.89	0.89
7	4.50	4.89	0.95	0.95
8	4.66	3.96	1.24	1.24
9	4.69	4.95	1.75	1.75
10	4.82	4.25	1.37	1.37

6.3.2 Physisorption and Chemisorptions

The transition metal, specially, Mg, have been used as a catalysts in hydrogen adsorption and dissociation reaction [53-56]. In fact, most of the metals in the periodic table, and their alloys or inter-metallic compound react with hydrogen to form metal hydrides. The bonding between hydrogen and the metal can be ranging from covalent to ionic, as well as multi centered bonds and metallic bonding. In fact some metal hydride can store hydrogen with a higher density than that of liquid hydrogen [58]. As we know that molecules interact with the surface with a force originating either from the physical Van der Waals interaction or from the chemical hybridization of their orbitals with those of the surface atoms of the substrate. Depending on the dominating contribution, we call the absorption as physisorption or chemisorptions. In physisorption gas molecule or atom can be adsorbed by the transition metals

retaining its gas phase electronic structure without forming any chemical bonds with the transition metals. In chemisorptions, there is strong perturbation of the gas molecular electronic structure due to the formation of chemical bond with the substrate element. Due to specificity, the nature of chemisorptions can greatly differ, depending on the chemical identity and the surface structure of the substrate element. Therefore, it is necessary to understand the behavior of hydrogenation in Mg_nRhH_2 and H_2-Mg_nRh clusters. The most effective adsorption sites of the cluster in the present study are shown in fig.6.1. Adsorption energy, the H-H bond length, the Rh-H bond length (D_{Rh-H}) and the HOMO-LUMO gap (Δ) are summarized in table 6.4.

Table 6.4 Adsorption energy, H-H bond length (Å), Rh-H bond length (Å) and HOMO-LUMO gap (eV) of physisorption system

Cluster	ΔE_{ad} (eV)	D_{H-H} (Å)	D_{Rh-H} (Å)	Δ (eV)
$MgRhH_2$	0.42	0.82	1.80	2.96
Mg_2RhH_2	0.44	0.94	1.68	2.47
Mg_3RhH_2	0.57	0.85	1.76	1.98
Mg_4RhH_2	0.46	0.86	1.75	1.38
Mg_5RhH_2	-0.05	0.86	1.78	2.12
Mg_6RhH_2	-1.04	0.86	1.78	1.87
Mg_7RhH_2	-0.57	0.85	1.78	1.27
Mg_8RhH_2	-0.20	0.85	1.78	1.44
Mg_9RhH_2	-0.33	0.88	1.73	1.30
$Mg_{10}RhH_2$	0.55	0.85	1.77	1.93

It is found for all clusters that hydrogen molecule interacts with the clusters via dissociative chemisorptions. The adsorption energy of hydrogen was calculated by the following equation:

$$\Delta E_{ad} = E(Mg_nRh) + E(H_2) - E(Mg_nRh - H_2) \quad (6.9)$$

where, ΔE_{ad} is the adsorption energy, $E(Mg_nRh-H_2)$ is the total energy of the system after interacting with hydrogen. For Rh doped Mg cluster, the binding energy of hydrogen energy is found higher when Rh remains at the surface of the cluster. This is because of direct Rh-H bond formation which is similar to Ti substituted Mg cluster [32]. It is also explained by the Rui Jin et al. [57] in his report that the adsorption tendency of H_2 molecule are of two types: (a) H_2 molecule prefers the low coordinative sites, because of low coordinative sites has unsaturated orbitals which can receive electron easily and (b) the adsorption sites are always keep symmetry to minimize the system energy, which means, the adsorbed structure prefer to occupy the symmetrical sites to keep the structural

stability. In our previous report [39] we found that when H₂ molecules interact with Mg_nCo clusters, the H-H bond length increase slightly. In our present work we found it as 2.71Å, which is 1.97Å more than H-H bond length which indicates the H-H bond length has relaxation after adsorption by Mg_nRh cluster as reported earlier [59]. The Rh-H bonds in the Mg_nRh-H₂ cluster ranges from 2.35 to 3.63Å, which is an important characteristic physical parameter in physical adsorption of hydrogen by Mg_nRh cluster. The vibrational frequency of H₂ on Mg_nRh clusters also obtained. The H-H symmetric stretching vibrational frequency in Mg_nRh-H₂ clusters is in the range from 1000-1554 cm⁻¹, while in the gaseous phase it is 4650 cm⁻¹. So the H-H vibrational frequency shifted towards low wave number after adsorption. The shift of vibrational frequency in adsorbed clusters is recognized to the increase of H-H bond length (D_{H-H}).

To understand the hydrogen chemisorptions mechanism on the small Mg_nRh clusters, we have carried out an extensive minimum energy structural search and the optimum energy structures are shown in fig. 6.1. The position of hydrogen chemisorptions absorption sites are defined as top (t), neighbor (n), opposite (o) and bridge (b).

Table 6.5 Location of H, Multiplicity, H-H bond length, HOMO-LUMO gap (eV) and Chemisorption energy (eV)

Cluster	Location	M (μ _B)	D _{H-H} (Å)	Δ (eV)	ΔE _{CE} (eV)
H2-MgRh	t (Mg), t (Mg)	2	2.87	2.47	0.95
H2-Mg ₂ Rh	n, b (Mg, Mg)	2	5.63	2.13	0.72
H2-Mg ₃ Rh	n, t (Mg, Mg)	2	5.86	2.39	0.66
H2-Mg ₄ Rh	o, t (Mg, Mg)	2	5.82	2.31	0.40
H2-Mg ₅ Rh	n, t (Mg, Mg)	2	6.03	2.53	0.31
H2-Mg ₆ Rh	o, t (Mg, Mg)	2	5.93	1.76	0.90
H2-Mg ₇ Rh	o, t (Mg, Mg)	2	8.25	1.74	0.95
H2-Mg ₈ Rh	o, t (Mg, Mg)	2	8.33	1.30	0.67
H2-Mg ₉ Rh	t, n (Mg, Mg)	2	5.53	1.44	0.69
H2-Mg ₁₀ Rh	o, t (Mg, Mg)	2	8.67	1.14	0.32

We have carried out an extensive minimum energy structural search and the optimum energy structures are shown in fig.6.1. The position of hydrogen chemisorptions absorption sites are defined as top (t), neighbor (n), opposite (o) and bridge (b). We have defined the chemisorptions energy following the equation:

$$\Delta E_{CE} = E(Mg_nRh) + E(H_2) - E(H_2 - Mg_nRh) \quad (6.10)$$

Where, $E(Mg_nRh)$, $E(H_2)$ and $E(H_2-Mg_nRh)$ are the calculated optimized energies of the Mg_nRh , H_2 molecule and H_2-Mg_nRh clusters respectively. Ground state search shows that the most stable H_2-Mg_nRh clusters always come from the lowest energy Mg_nRh clusters plus attached 2H atoms. So, when two individual hydrogen atoms are chemisorbed on Mg_nRh clusters, the equilibrium structure is found. In table 6.5, location of H atoms, spin multiplicity, H-H bond energy, HOMO-LUMO gap and chemisorptions energy of the clusters are shown. Present study show that the chemisorptions energy is maximum for the H_2-Mg_9Rh cluster, which indicates this cluster, has high activity as similar to Al_7Cr cluster reported earlier [51].

Table 6.6 Reaction energy ΔE_0 including zero point energy (kcal/mol), Activation barrier (kcal/mol) and frequency (cm^{-1})

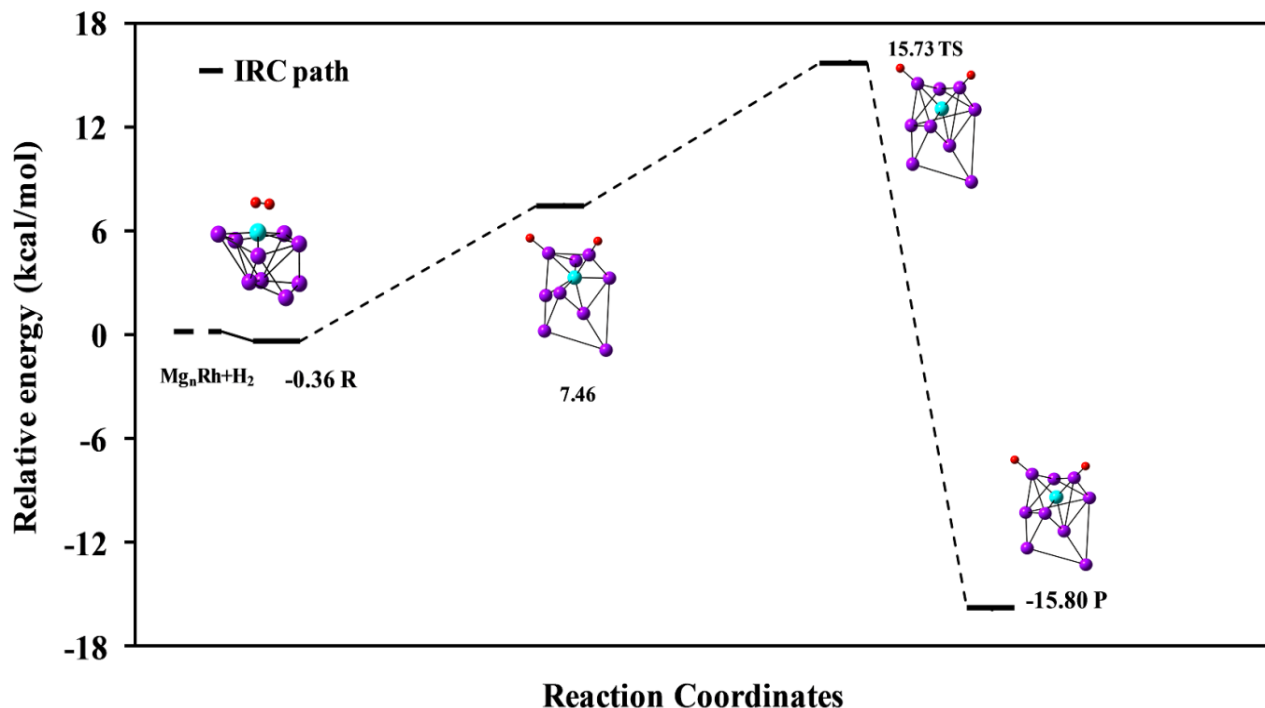
Cluster	Reaction energy (kcal/mol)	Activation barrier (kcal/mol)	ω (cm^{-1})
MgRh	-38.66	6.76	-1411
Mg ₂ Rh	-9.86	7.55	-1476
Mg ₃ Rh	-4.62	7.47	-1554
Mg ₄ Rh	-11.24	7.28	-1547
Mg ₅ Rh	-13.63	13.95	-1516
Mg ₆ Rh	-60.26	20.71	-1533
Mg ₇ Rh	-47.90	35.96	-1524
Mg ₈ Rh	-27.20	20.08	-1504
Mg ₉ Rh	-33.19	14.44	-1523
Mg ₁₀ Rh	-32.60	16.51	-1008

6.3.3 Activation pathway for hydrogen dissociation

To find out the dissociation mechanism of hydrogen on Mg_nRh clusters, we explore the minimum energy pathway as shown in fig. 6.4. This pathway over the potential energy surface is obtained through the intrinsic reaction coordinates analysis from forward and reverse direction of their transition state following our reported work [39]. To get actual pathway, we define the physisorbed and chemisorbed with the hydrogen molecule as the reactant and product respectively. Important parameter for dissociation of hydrogen on clusters, like, reaction energy (kcal/mol),

activation barrier (kcal/mol) and imaginary frequency of transition state of the transition state are summarized in table 6.6. Here the reaction energy (ΔE_0) calculated by the total energy difference between the reactant and product (exothermic means negative reaction energy whereas positive reaction energy indicate endothermic process). Similarly, activation barrier is calculated by the total energy difference between the reactant and the TS.

Fig. 6.4 Potential energy surface of H₂-Mg_nRh clusters.



Dissociation of H₂ on Mg_nRh clusters is exothermic as defined in the table 6.6. In the dissociation process, the H₂ molecule initially placed on the top site of Rh atom moves to the adjacent site of Mg_n clusters as shown in fig.6.1. The increasing bond length of H-H in transition state (TS) also indicate that it has been elongated like H₂ on (ZrO₂)_n [57] clusters. Among the Mg_nRh cluster, the Mg₉Rh cluster exhibits the lower activation barrier (14.44 kcal/mol) and the maximum value of reaction energy (33.19 kcal/mol), which are important criteria to demand a compound as effective hydrogen storage element. Chemisorptions energy of Mg₉Rh cluster is also shows large value. It is observed in the path way that hydrogen molecule breaks and combines with the Mg atom. The hydrogen dissociation path of Mg₉Rh cluster from reactant to product undergoes a transition state overcoming the energy barrier of 15.73 kcal/mol, which is the nearly equal to the calculated theoretical value. Hence, the IRC path connecting the reactant to product with right transition state. It shows significant results that Mg₉Rh cluster can be taken as a good candidate for hydrogen adsorption and dissociation process and a good catalysis.

Conclusions

To sum up, we have studied the adsorption and dissociation behavior of hydrogen molecule on Mg_nRh ($n=1-10$) clusters by DFT calculation. Mg_6Rh cluster is found as physically as well as chemically most stable species in the whole series. In the different optimized adsorption modes, H_2 molecule can be easily adsorbed on the top of the Rh atom. Due to this the increasing H-H bond length exhibit relaxation of hydrogen bonds when adsorbed on the cluster. The vibrational frequency of hydrogen in Mg_nRh-H_2 cluster also varies. In Mg_nRh-H_2 , H-H bond frequency is in the range from $1000-1554\text{ cm}^{-1}$, while in the gaseous phase it is 4650 cm^{-1} . So the H-H vibrational frequency shifted towards low wave number after adsorption. The shift towards low vibrational frequency in adsorbed clusters is recognized to the increase of H-H bond length. Following the calculated IRC path of H_2-Mg_9Rh cluster, it is found that H_2 molecule adsorbs at the Rh atom site in Mg_9Rh with low coordinate number and then moves to the Mg atom to form Mg-H bonds by overcoming the energy barrier of 15.73 kcal/mol . The maximum chemisorptions energy, low activation barrier and large value of reaction energy indicate that though Mg_6Rh is more stable compare to Mg_9Rh cluster, but, Mg_9Rh is the most qualified candidate for adsorption and dissociation of hydrogen; and hence can be used as an effective hydrogen storage element.

6.5 References

- [1] Shevlin SA, Guo ZX. *Chem Soc Rev*, **2009**; 38: 211-225.
- [2] Zuttel A, *Mater Today*, **2003**; 6: 24-33.
- [3] Coontz R, Hanson R, *Science*, **2004**; 305: 957.
- [4] Milanese C, Girella A, Bruni G, Berbenni V, Cofrancesco P, Marini A, *J Alloys Comp*, **2008**; 465: 396-405.
- [5] Zaluska A, Zaluski L, Strob-Olsen JO, *Appl Phys A Mater Sci Process*, **2001**; 72: 157-165.
- [6] Tsuda M, Dino WA, Nakanishi H, Kasai H, *J Phys Soc*, **2004**; 73: 2628-2630.
- [7] Varin RA, Czujko, T, Wronski, ZS, *Int J Hydrogen Energy*, **2009**; 34: 8603-8610
- [8] Tsuda M, Dino WA, Kasai H, Nakanishi H, Aikawa H, *Thin Solid Films*, **2006**; 509: 157-159.
- [9] Zaluski L, Zaluska A, Stron Olsen JO, Schulz R. *J Alloy Comp*, **1999**; 288: 217-225
- [10] Zhang B, Wu Y, *Int J Hydrogen Energy*, **2015**; 40: 9298-9305
- [11] Suleyman Er, Tiwari D, Gills A, Brocks G, *Phys Rev B*, **2009**; 79: 024105
- [12] Mananghaya M, *Int J Hydrogen Energy*, **2015**; 40: 9352-9358
- [13] Xue-feng S, Gao-feng Zhao Li-li Z, *J Phys Chem C*, **2008**; 112: 17828-17834
- [14] Kumar TJD, Tarakeshwar P, *Phys Rev B*, **2009**; 79: 205415.
- [15] Fanjie K, Yanfei H, *J Mol Model*, **2012**; 20: 2087-2093.
- [16] Fayet P, Kaldor A, Cox DM, *J Chem Phys*, **1990**; 92: 254-261.
- [17] Doyle AM, Shaikhutdinov SK, Jackson SD, Freund HJ, *Chem Int Ed*, **2003**; 42: 5240- 5243.
- [18] Amica G, Arneodo Larochette P, Gennari FC, *Int J Hydrogen Energy*, **2015**; 40: 9335-9346.
- [19] Retuerto M, Alonso JA, Martínez R, JiménezVillacorta F, Sánchez-Benítez J, Fernández Díaz MT, Garcia Ramos CA, Ruskov T, *Int J Hydrogen Energy*, **2015**; 40: 9306-9313.
- [20] Gutfliesh O, Dal Toe S, Herrich M, Handstien A, Pratt AJ, *Alloys Compd*, **2005**; 404: 413- 416.
- [21] Vyas D, Jain P, Khan J, Kulshrestha V, Jain A, Jian IP, *Int J Hydrogen energy*, **2012**; 37: 3755-3760.
- [22] Zhnag YH, Zhao C, Yang T, Shnag HW, Xu C, Zhao DL, *J Alloys Comp*, **2013**; 555: 131-137.
- [23] Zhang QA, Zhang LX, Wang QQ, *J Alloys Comp*, **2013**; 551: 376-381.
- [24] Vyas D, Jain P, Agarwal G, Jain A, Jian IP, *Int J Hydrogen energy*, **2012**; 37: 16013-16017.
- [25] Varano A, Henry DJ, *J Phys Chem A*, **2010**; 114: 3602 -3608.
- [26] Lu QL, Wan JG. *J Chem Phys*, **2010**; 132: 224308.
- [27] Liang G, Hout J, Boily S, Van Neste A, Schulz R. *J Alloy Compd*, **1999**; 292: 247-252.

- [28] Schulz R, Liang G, Hout J, Riso national laboratory, Roskilde, Denmark, **2001**; 141-153.
- [29] Song Y, Guo ZX, Yang R, Phys Rev B, **2004**; 69: 094205-094215.
- [30] Shang CX, Bououdina M, Song Y, Guo ZX, Int J Hydrogen energy, **2004**; 29: 73-80.
- [31] Esteania G, Valeria V, Carla RL, Alfredo J, David S, J Phy Chem C, **2014**;118:4231-4237.
- [32] Larsson P, Araujo CM, Larsson J, Jena P, Ahuja R, Proc Natt Acad Sci, **2008**; 105:8227-8231.
- [33] Liang J, J Alloys Comp, **2007**; 446: 72-79.
- [34] Wang XF, Andrews L, J Phys Chem, **2002**; 106: 3706-3713.
- [35] Bauer HJ, Wagner FE, Pol J Chem, **2004**; 78: 463-514.
- [36] Watson GE, Wells RPK, Willock DJ, Hutchings GJ, J Phys Chem B, **2001**; 105: 4889-4894.
- [37] Jung SC, Kang MH, Phys Rev B, **2005**; 72: 205419.
- [38] Dus R, Nowicka E, Nowakowski R, Appl Surf Sci, **2008**; 254: 4286-4291.
- [39] Trivedi R, Bandyopadhyay D, Int J Hydrogen energy, **2015**; 40: 12727-12735.
- [40] Lee C, Yang W, Parr RG, Phys Rev B, **1998**; 37:785.
- [41] Perdew JP, Burke K, Wang Y, Phys Rev B, **1996**; 54: 16533-16539.
- [42] Bandyopadhyay D, J Appl Phys, **2008**; 104: 084308-084315.
- [43] Bandyopadhyay D, J Mol Model, **2012**;18: 737-749.
- [44] Bandyopadhyay D, Sen P, J Phys Chem A, **2010**; 114: 1835-1842.
- [45] Tai TB, Nguyes MT, J Chem Theory Comput, **2011**; 7:1119.
- [46] Ouyang Y, Wang P, Xiang P, Chen H, Du Y, Comp Theo Chem, **2012**; 984: 68-75.
- [48] Fukai Y. Springer- Verleg **1993**.
- [49] Peng C, Ayala PY, Schlegel HB, Frisch MJ, J Comp Chem, **1996**; 17: 49-56.
- [50] Frisch MJ, Trucks GW, Schlegel HB, Scuseria GE, Robb MA, Cheesemen JR, Zakrzewski VG, Montgomery jr JA, Stratmenn RE, Burant JC, Dapprich S, Millam JM, Daniels AD, Kudin KN, Strain MC, Farkas O, Tomasi J, Barone V, Cossi M, Cammi R, Mennucci B, Pomelli C, Adamo C, Clifford S, Ochtrski J, Petersson GA, Ayala PY, Cui Q, Morokuma K, Malick DK, Rabuck AD, Raghavachari K, Foresman JB, Cioslowki J, Ortiz JV, Baboul AG, Stefanov BB, Liu B, Liashenko A, Piskorz P, Komaromi I, AL-Laham MA, Peng CY, Nanayakkara A, Challacombe M, Gill PMW, Johnson B, Chem W, Wong MW, Andress JL, Gonzalez C, Head-Gordon M, Replogle ES, Pople J A, Gaussian 03, revision E 01 Gaussian, Wallingford **2004**.
- [51] Guo L, J Phys Chem, **2013**; 117: 3458-3466.
- [52] Venkataramanan NS, Sahara R, Mizuseki H, Kawazoe Y, J Phys Chem A, **2010**; 114: 5049-5057.

- [53] Bobet JL, Akiba E, Nakamura Y, Darriet B, *Int J Hydrogen Energy*, **2000**; 25: 987-996.
- [54] Zeng K, Klassen T, Oelerich W, Bormann R, *Int J Hydrogen Energy*, **1999**; 24:989-1004.
- [55] Pozzo M, Alfe D, *Int J Hydrogen Energy*, **2009**; 34: 1922-30.
- [56] Zhang J, Huang YN, Mao C, Long CG, Shao YM, Fu JQ, *Acta Chim Sinica*, **2010**; 68: 2077-2085.
- [57] Jin R, Zhang S, Zhang Y, Huang S, Wang P, Tian H, *Int J Hydrogen Energy*, **2011**; 36: 9069-9078.
- [58] Hirscher M, Panella B, *Scripta Materialia*, **2007**; 56: 809-812.
- [59] Lyalin A, Taketsugu T, *Faraday Discuss* **2011**; 152: 185–201.

CHAPTER 7

SUMMARY AND FUTURE SCOPE

7.1 Summary

Germanium and silicon both are the most important elements in the semiconductor industries due to their scientific and technological applications. With the development of theoretical and experimental work, results suggest that structure of small clusters is quite different from bulk materials due to the surface effect (atoms at surfaces have fewer neighbors than atoms in the bulk) and quantum size effects. However, pure germanium and silicon cluster cannot be directly used for application since they are chemically reactive due to the presence of dangling bonds on the surface. Properly doping with metal atoms overcomes this deficiency. Metal doped cage like nanoclusters are evolves a lot of interest in potential applications in many fields. The system chosen in this present work is transition metal doped germanium nanoclusters because in the field of semiconductor materials, germanium is one of the most important alternatives to silicon due to its superior electron and hole mobilities. Therefore, metal doped cage like clusters are expected to become important materials for a new generation of electronic devices and optoelectronic applications.

As a preliminary step towards developing and understanding, the geometrical, electronic and magnetic properties, and related aromaticity of Mo doped germanium cluster using density functional theory. Identification of the stable species, and variation of physical and chemical properties with the size MoGe_n ($n=1-20$) clusters will help to understand the science of Ge-Mo based clusters and superatoms that can be used as future building blocks for cluster-assembled designer materials and this could open up a new field in electronic industry. The output can be summarized as follows:

[1] The growth pattern of Ge_nMo clusters can be grouped mainly into two categories. In the smaller size range i.e. before encapsulation of Mo atom, Mo and Ge atoms are directly added to the Ge_n and Ge_{n-1}Mo respectively to form Ge_nMo clusters. In the growth process, the binding energy of the clusters increases for small sized clusters with in the range $n \leq 5$ with a faster rate than the bigger clusters. After encapsulation of Mo atom by the Ge_n cluster OF $n > 9$, the size of the Ge_nMo clusters tend to increase by absorbing Ge atoms one by one on its surface keeping Mo atom inside the cage.

[2] We have also found that it is favorable to attach a Mo-atom to Ge clusters of all sizes, as the EE turns out to be positive in every case. Clusters containing more than nine Ge atoms are able to absorb Mo atom endohedrally in a

Ge cage, both in pure and cationic states. In all Mo-doped clusters beyond $n > 2$, the spin magnetic moment on the Mo atom is quenched at the expense of stability of the cluster. As measured by the BE, EE, HOMO-LUMO gap, FE, stability and other parameters both for neutral and cationic clusters, it is found that those having 18 valence electrons show enhanced stability which is in agreement with shell model predictions. This also shows up in the IP values of the Ge_nMo clusters, as there is a sharp drop in IP when cluster size changes from $n=12$ to 13. Validity of nearly free-electron shell model is similar to that of transition metal doped silicon clusters. Although the signature of stability is not so sharp in the HOMO-LUMO gaps of these clusters. There is still a local maximum at $n=12$ for the neutral clusters, indicating enhanced stability of an 18-electron cluster, whereas, and this signature is very much clear in cationic Ge_{13}Mo cluster. Variation in HOMO-LUMO gap in different sized clusters could be useful for device applications. The large HOMO-LUMO gap (2.25 eV) of MoGe_{12} could make this cluster as a possible candidate as luminescent material in the blue region.

[3] Major contribution of the charge from the d -orbital of Mo in hybridization and its dominating contribution in DOS indicate that the d -orbitals of Mo atoms are mainly responsible for the hybridization and stability of the cluster. Presence of the dominating contribution of Mo d -orbital close to the Fermi level in DOS is also significant for ligand formation and a strong indication of possibility to make stable cluster assembled materials.

[4] Variation of calculated NICS values with the distance from the center of the cluster clearly indicates that the cluster is aromatic in nature and the aromaticity of the cluster is one of the main reasons for its stability.

Towards the understanding of the growth behavior and superatomic properties of Nb doped Ge nanocluster, we have performed a systematic analysis and results are as follow:

[1] Theoretically study of the electronic properties, vibrational properties and superatomic behavior of Nb doped Ge clusters at different sizes in neutral and cationic states. Different physical and chemical parameters like binding energy (BE), stability, dissociation energy (DE) and HOMO-LUMO gap of the clusters show that neutral NbGe_{12} and cationic NbGe_{16} are the most stable species in the whole range of study. In addition, neutral NbGe_{10} and NbGe_{16} ; and cationic NbGe_{13} also show enhanced stability. Therefore, to identify the most stable behavior, we have further studied NICS and closed shell model in both neutral and cationic state of these clusters. We have found that the NICS behavior of the ground state NbGe_{12} cluster supports the aromatic behavior, whereas, cationic NbGe_{16} follow the closed shell superatomic model.

[2] The large HOMO-LUMO gap of 1.85eV makes this cluster suitable for optoelectronic devices. Further, the absence of any imaginary frequencies in these clusters shows that there is no presence of imaginary bonds in the clusters and clusters can be physically acceptable. The electronic and structural properties of transition metal encapsulated Ge clusters have been studied because these systems have potential application in photonic devices or in optoelectronics application.

Further, it is worth to notice that the ab initio (First principles) electronic simulation can offer great insight into the understanding of the storage of the hydrogen as metal hydrides. In particular, Mg hydride is one of the most prominent materials. For the adsorption and dissociation of hydrogen, metal doped magnesium hydride takes much attention due to their higher diffusivity and high surface to volume ratio. In the last two chapters, a number of useful understandings of hydrogen storage in TM (Co and Rh) doped magnesium nanoclusters are presented. Results of this part of the work can be summarized as follows:

[1] The report presents the use of Mg_nCo as an effective hydrogen storage element in the form of nanoclusters. From the growth pattern of Mg_nCo ($n=1-10$) clusters it is found that Mg_4Co and Mg_6Co both are stable in the series where Co prefers to take peripheral position. From the chemisorptions and physisorptions energies and VIP and VEA parameters, we have found Mg_5Co can only be used as effective hydrogen storage and dissociate element. After the addition of H_2 , H_2-Mg_5Co is appears as an efficient hydrogen catalyst. Together with these two, H_2-Mg_5Co shows highest reaction energy in IRC path and we have found the same activation barrier during the chemical process as we studied in our simulation. The complete study shows that in the Mg_nCo ($n=1-10$) series, Mg_5Co can be selected as an efficient hydrogen storage element.

[2] In the last chapter of the thesis, studies on the adsorption and dissociation behavior of H_2 molecule on Mg_nRh ($n=1-10$) clusters using DFT calculation have been discussed. It is revealed that Mg_6Rh cluster is observed as the most stable species physically as well as chemically in the whole series. In the different optimized adsorption modes, H_2 molecule can be easily adsorbed on the top of the Rh atom. Due to this the H-H bond length increases which is the signature of relaxation of hydrogen bond on the cluster. This is also verified by the study of vibrational frequencies of Mg_nRh-H_2 cluster. Following the calculated IRC path of H_2-Mg_9Rh cluster, it is found that H_2 molecule adsorbs at the Rh atom site in Mg_9Rh with low coordinate number and then it moves to the Mg atom and form Mg-H bonds by overcoming the energy barrier of 15.73 kcal/mol. The maximum chemisorptions energy, low activation barrier and large value of reaction energy indicate that Mg_9Rh cluster is the suitable candidate for adsorption and dissociation of hydrogen; and therefore can be used as an effective hydrogen storage element.

7.2 Future scope

The work done in this thesis will lead to the DFT investigation of other transition metal doped germanium and silicon semiconductor nanocluster. There are many scopes of transition metal doped cluster studies, which are still needed to be understood like magnetic superatom, cluster assemblies and hydrogen storage materials. Materials are now being considered as the building blocks of future modern technologies due to their size dependent electronic properties which can be tuned easily. There are numerous and important applications in the field of electronics, chemistry and biology, which become possible considering these facts. This thesis gives an additional chance to prepare and to apply semiconducting nanocluster in the fields of electronic devices in the near future.

In near future, enormous numbers of hybrid nanoclusters are possible, so it is a research problem to model these types nanoclusters and to understand their physical and chemical properties. On the other side doping of TM in metal clusters like magnesium can be used as an effective hydrogen storage medium for future fuel problem. So the present thesis makes an effort towards an interesting field of research in the cluster science. The future scope of the present research can be summarized as follows:

[1] Investigation of more hybrid TM metal doped Ge, Si, and Sn semiconductor cage cluster. Transition metal doped semiconductor nanoparticles have attracted scientific attention due to their prospective applications in optoelectronic devices or electronic devices. Many other compositions can also form hybrid semiconductor clusters with characteristic physical and chemical properties that will be helpful to understand the superatom building blocks.

[2] Investigation of metal clusters as catalysis and hydrogen storage materials. The interaction of hydrogen with metal clusters and their cations in the gas phase is also enabling the design and synthesis of a new class of hydrogen storage materials.

[3] It is quite important to study of the clusters assembled materials to make nanodevices and quantum dots. Cluster assembled materials are of interest because of their ability to tune component properties. It is one path way towards nanomaterials with controllable band gaps and hence cluster assembled materials. By controlling the cluster assembled building blocks into quantum dots and bulk is the next step towards achieving superatom materials with tunable physical properties. Clusters assembled materials can also be used to make nanotubes and 2D graphene nanosheet having different physical and chemical properties that can be useful for device applications and future building blocks.

[4] Supported clusters these are more nearer to practical application but they need huge computational facilities. Numerous attempts have been made to prepare supported metal clusters with nearly uniform structures. It is a new

class of catalyst made possible by synthesis involving organometallic chemistry in surfaces, gas phase cluster chemistry. The relevance of ligand stabilized metal clusters on support to the supported metal clusters on interest for their role as precursors.

So the studies of clusters have been useful to gain a fundamental understanding of catalysis, magnetism, superatomic and hydrogen storage. It is possible to create a magnetic cluster from nonmagnetic materials by controlling its size and composition. The challenges still remain.....

APPENDIX A

Fig. 3SIA Onsite magnetic moment of low energy neutral and cationic isomers with the bond length and relative energies with respect to the ground state neutral clusters. Dip blue balls are Mo and pink balls are Ge. Onsite magnetic moment is written in green in terms of μ_B

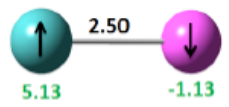
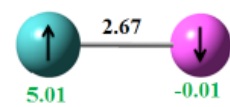

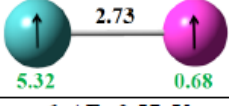
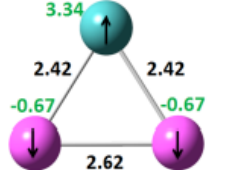


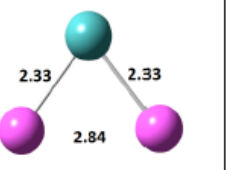
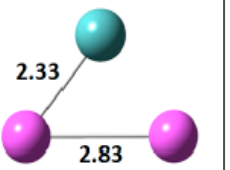
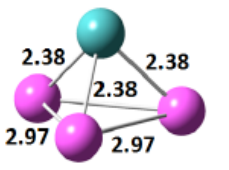
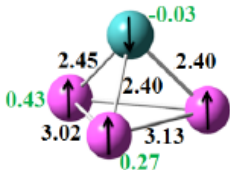
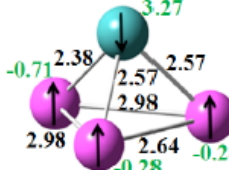
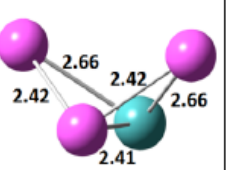
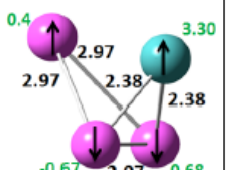
Ground state	Cationic ground state	Nearest spin states of the ground state isomer	Next low energy isomers	
 <p>$\mu_{\text{tot}}=4, \Delta E=0$</p>	 <p>$\mu_{\text{tot}}=5, \Delta E=7.07\text{eV}$</p>	 <p>$\mu_{\text{tot}}=2, \Delta E=0.26\text{eV}$</p>  <p>$\mu_{\text{tot}}=6, \Delta E=0.57\text{eV}$</p>		
 <p>$\mu_{\text{tot}}=2, \Delta E=0$</p>	 <p>$\mu_{\text{tot}}=3, \Delta E=7.26\text{eV}$</p>	 <p>$\mu_{\text{tot}}=4, \Delta E=0.56\text{eV}$</p>	 <p>$\mu_{\text{tot}}=0, \Delta E=0.54\text{eV}$</p>	 <p>$\mu_{\text{tot}}=0, \Delta E=0.53\text{eV}$</p>
 <p>$\mu_{\text{tot}}=0, \Delta E=0$</p>	 <p>$\mu_{\text{tot}}=1, \Delta E=7.62\text{eV}$</p>	 <p>$\mu_{\text{tot}}=2, \Delta E=1.31\text{eV}$</p>	 <p>$\mu_{\text{tot}}=0, \Delta E=0.002\text{eV}$</p>	 <p>$\mu_{\text{tot}}=2, \Delta E=1.36\text{eV}$</p>

Fig. 3SIB Electronic configuration and different valence electron orbitals of small sized Ge-Mo clusters in different spin states. The blue arrows represent the change of electronic state when the cluster shifted from lower level to higher spin state.

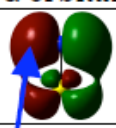
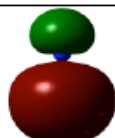
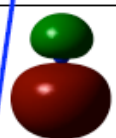
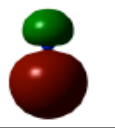
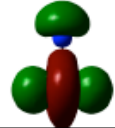
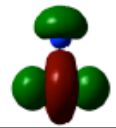
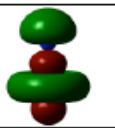


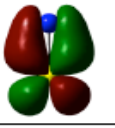
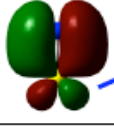

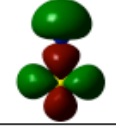
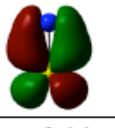
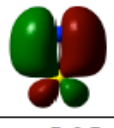
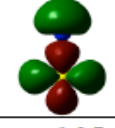
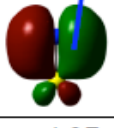
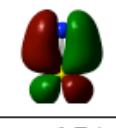
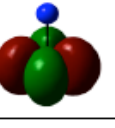
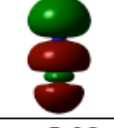
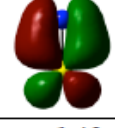
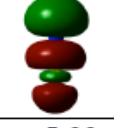
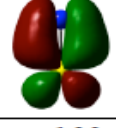
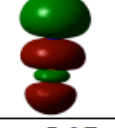
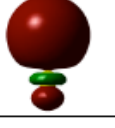
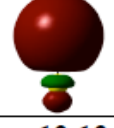
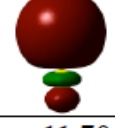
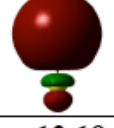
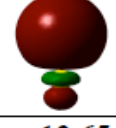
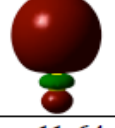
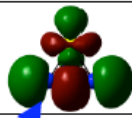
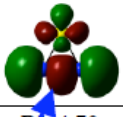
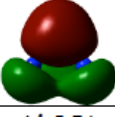
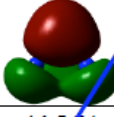
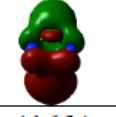
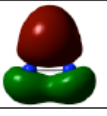
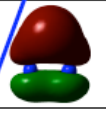
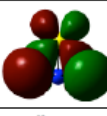
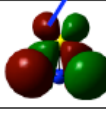
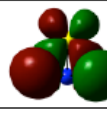
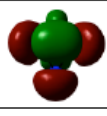
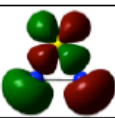
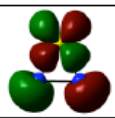


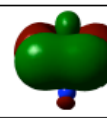
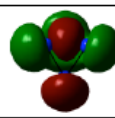
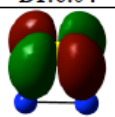
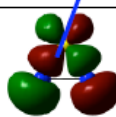
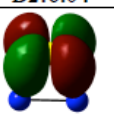
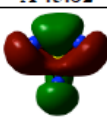
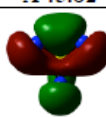
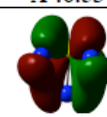

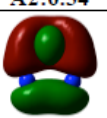
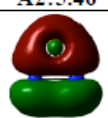
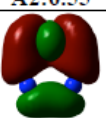
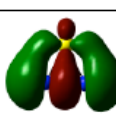
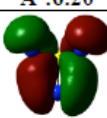
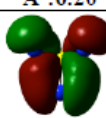
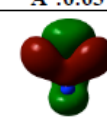
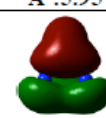
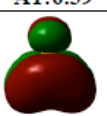
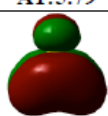
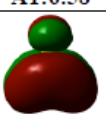
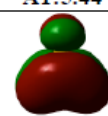
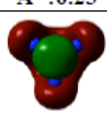
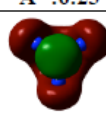
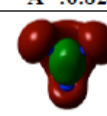
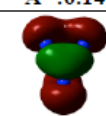
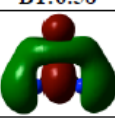
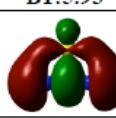
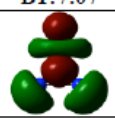
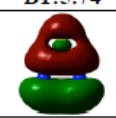
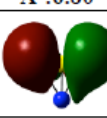
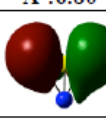
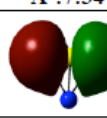
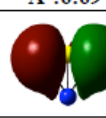
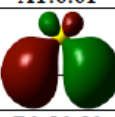
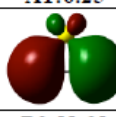
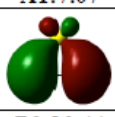

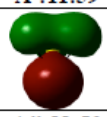
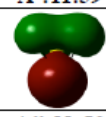
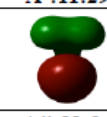
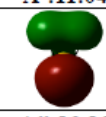




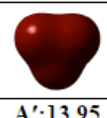



GeMo Triplet		GeMo Quintet		GeMo Septet	
α orbital	β orbital	α orbital	β orbital	α orbital	β orbital
					
				$\pi:4.29$	
					
		$\pi:5.19$		$\pi:5.52$	
					
$\pi:5.27$		$\pi:6.06$		$\pi:6.36$	
					
$\sigma:6.28$		$\sigma:6.09$		$\sigma:6.39$	
					
$\pi:6.44$	$\pi:5.25$	$\pi:6.14$		$\pi:6.58$	
					
$\pi:6.44$	$\pi:5.25$	$\pi:6.25$	$\pi:4.97$	$\pi:6.74$	
					
$\sigma:7.31$	$\sigma:5.38$	$\sigma:6.42$	$\sigma:5.33$	$\sigma:6.93$	$\sigma:5.27$
					
$\sigma:11.21$	$\sigma:12.13$	$\sigma:11.70$	$\sigma:12.19$	$\sigma:12.65$	$\sigma:11.64$

Fig. 3SIC continue

Ge(2)Mo Triplet		Ge(2)Mo Quintet		Ge(3)Mo Singlet		Ge(3)Mo Triplet	
α orbital	β orbital	α orbital	β orbital	α orbital	β orbital	α orbital	β orbital
							
							
		B1:4.70		A':5.74	A':5.74	A':6.14	
							
A1:5.63		A1:4.70		A'':5.79	A'':5.79	A'':6.47	A'':5.68
							
B1:6.04		B2:6.04		A':5.82	A':5.82	A':6.53	A':5.93
							
A2:6.34	A2:5.46	A2:6.55		A':6.20	A':6.20	A':6.63	A':5.95
							
A1:6.39	A1:5.79	A1:6.58	A1:5.44	A'':6.23	A'':6.23	A'':6.82	A'':6.14
							
B1:6.58	B1:5.93	B1:7.07	B1:5.74	A':6.80	A':6.80	A':7.34	A':6.69
							
A1:6.61	A1:6.25	A1:7.07	A1:5.93	A':11.59	A':11.59	A':11.29	A':11.04
							
B2:10.82	B2:11.21	B2:10.44	B2:10.26	A'':11.59	A'':11.59	A'':11.86	A'':12.10
							
A1:13.57	A1:13.93	A1:13.98	A1:15.75	A':13.95	A':13.95	A':14.66	A':14.66

Ge2Mo: Triplet - $3(a_1)^2 2(b_2)^2 4(a_1)^2 2(b_1)^2 5(a_1)^2 1(a_2)^2 3(b_2)^1 6(a_1)^1$
 Quintet - $3(a_1)^2 2(b_2)^2 4(a_1)^2 2(b_1)^2 5(a_1)^2 1(a_2)^1 3(b_2)^1 6(a_1)^1 3(b_1)^1$
 Ge3Mo: Singlet - $1(A')^2 A(A'')^2 2(A')^2 3(A')^2 2(A'')^2 4(A')^2 5(A')^2 3(A'')^2 6(A')^2$
 Triplet - $1(A')^2 A(A'')^2 2(A')^2 3(A')^2 2(A'')^2 4(A')^2 5(A')^2 3(A'')^2 6(A')^1 7(A')^1$

Fig. 3SID Variation of Mullikan charge on Mo atom with the cluster size (n)

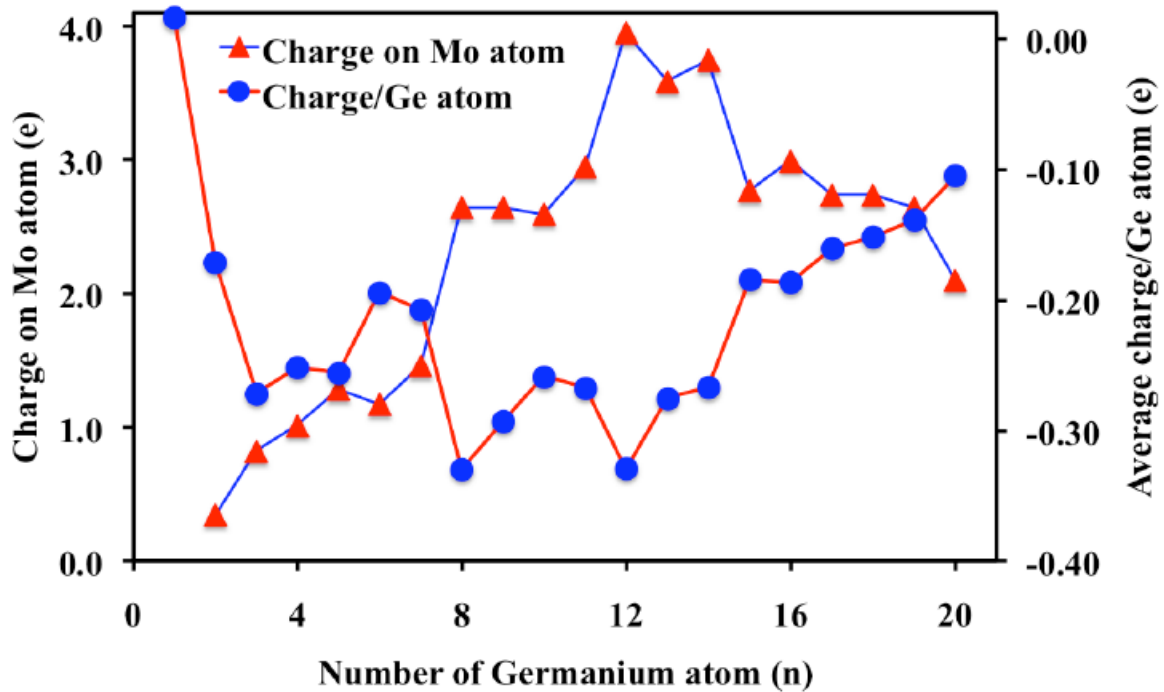


Fig. 3SIE Site projected density of states plot of different MoGe_n clusters with the contribution of Mo d orbital (in red line)

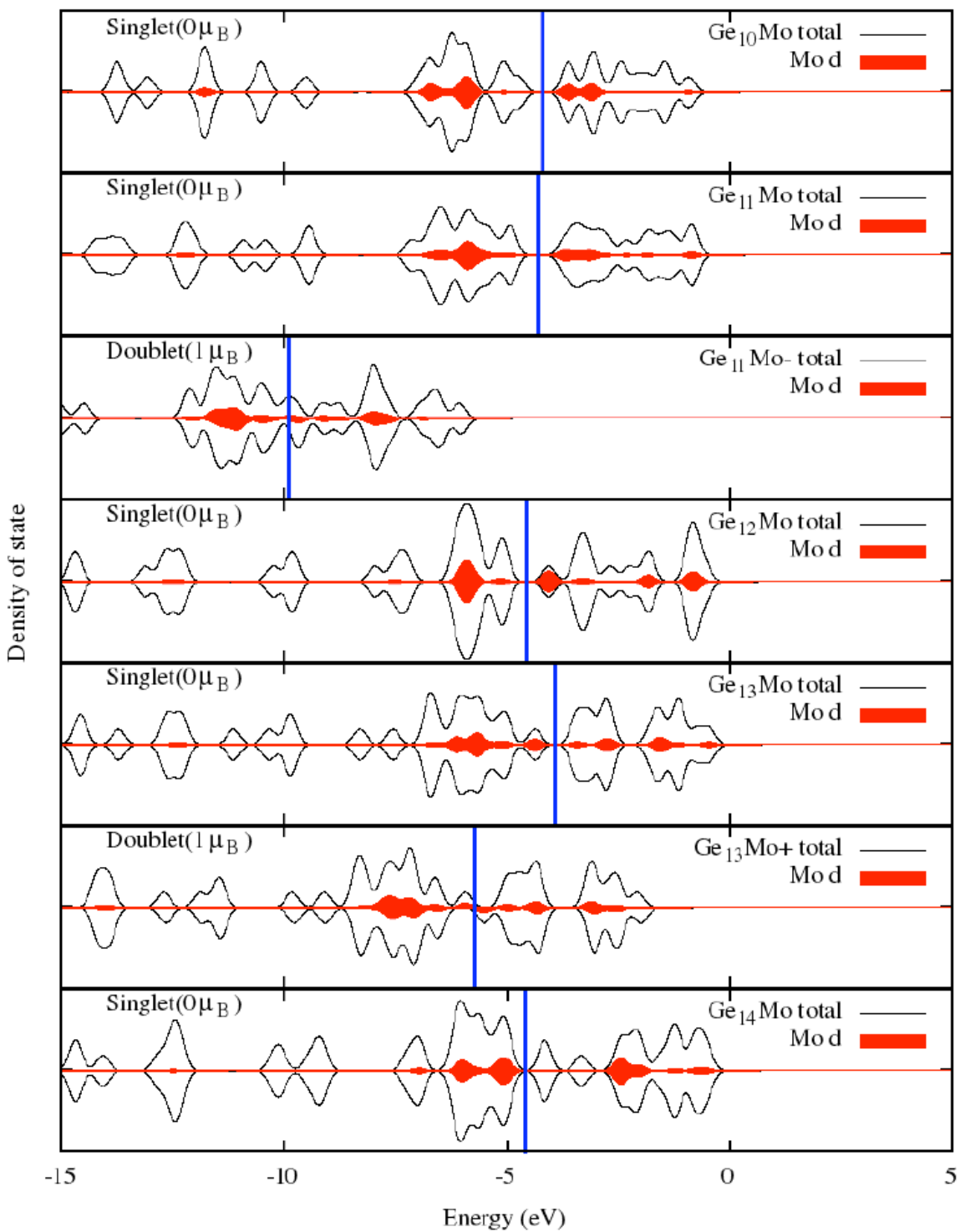


Fig.3IF Variation of HOMO-LUMO gap of neutral and cationic of MoGe_n clusters with the cluster size (n)

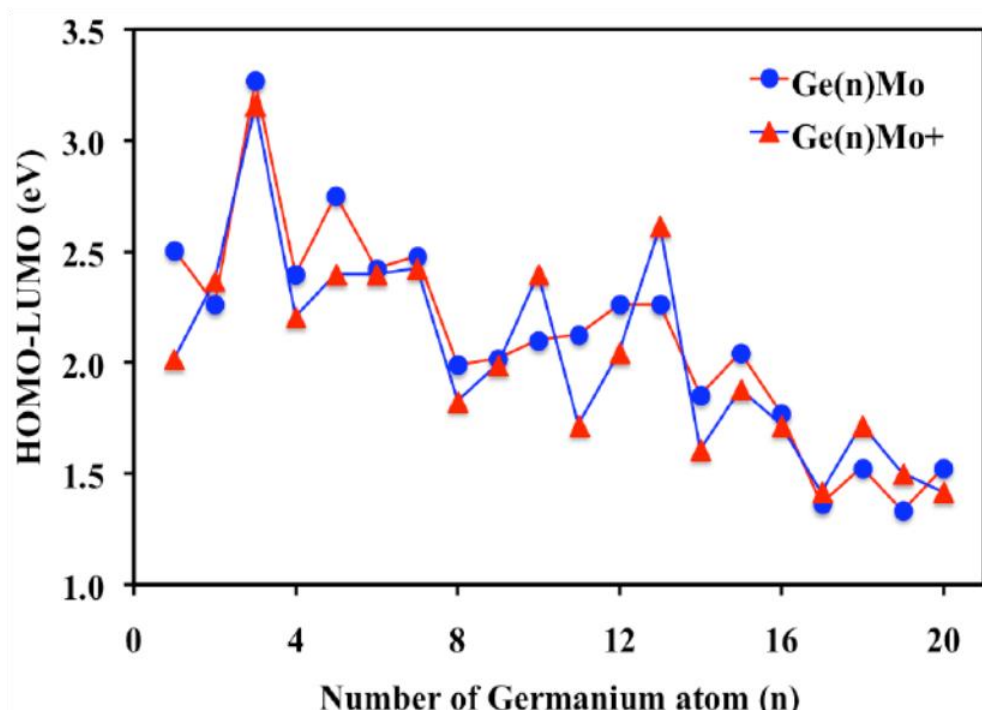
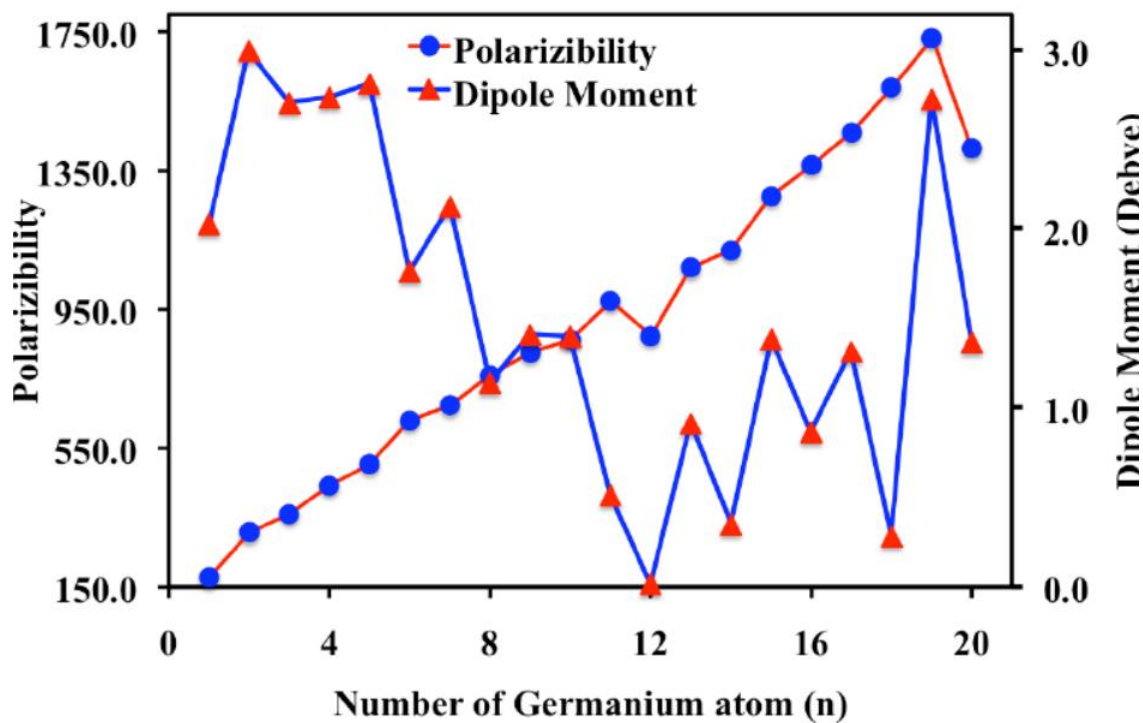


Fig.3SIG Variation of exact polarizability and dipole moment of MoGe_n clusters with cluster size (n)



APPENDIX B

Fig. 4SIA Variation of charge on Nb atom and Dipole moment with the number of germanium atom

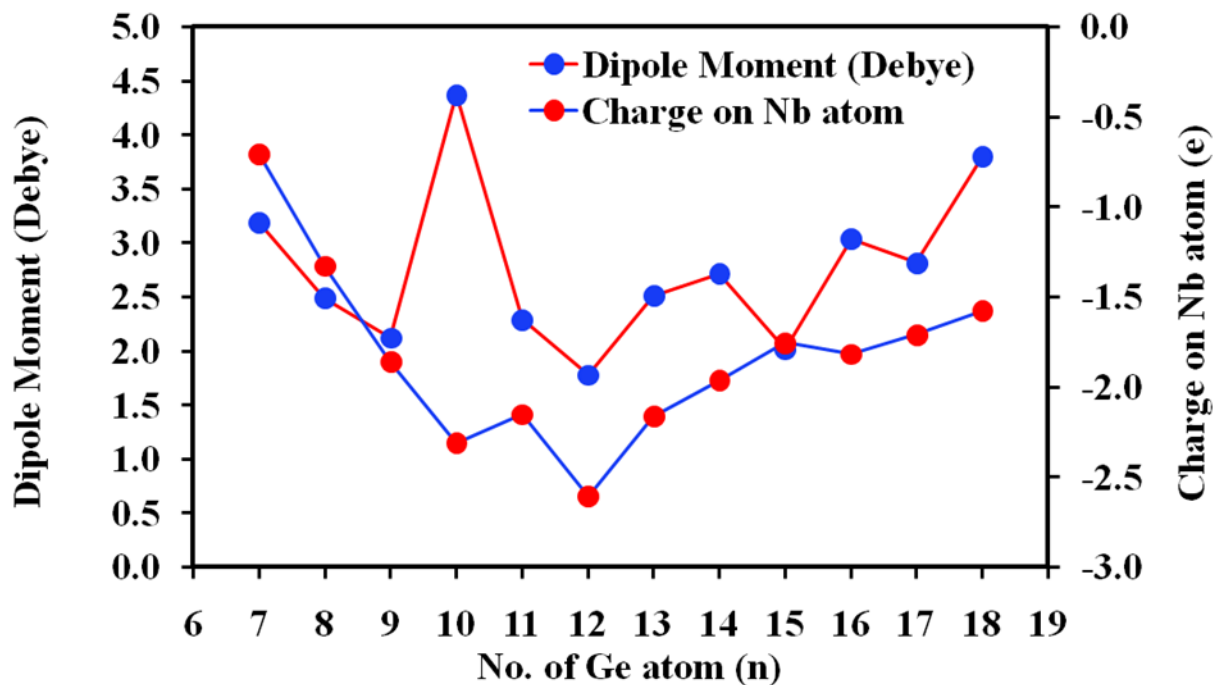


Fig. 4SIB Variation of Bond length with the number of germanium atom showing strong cage structure at n =12

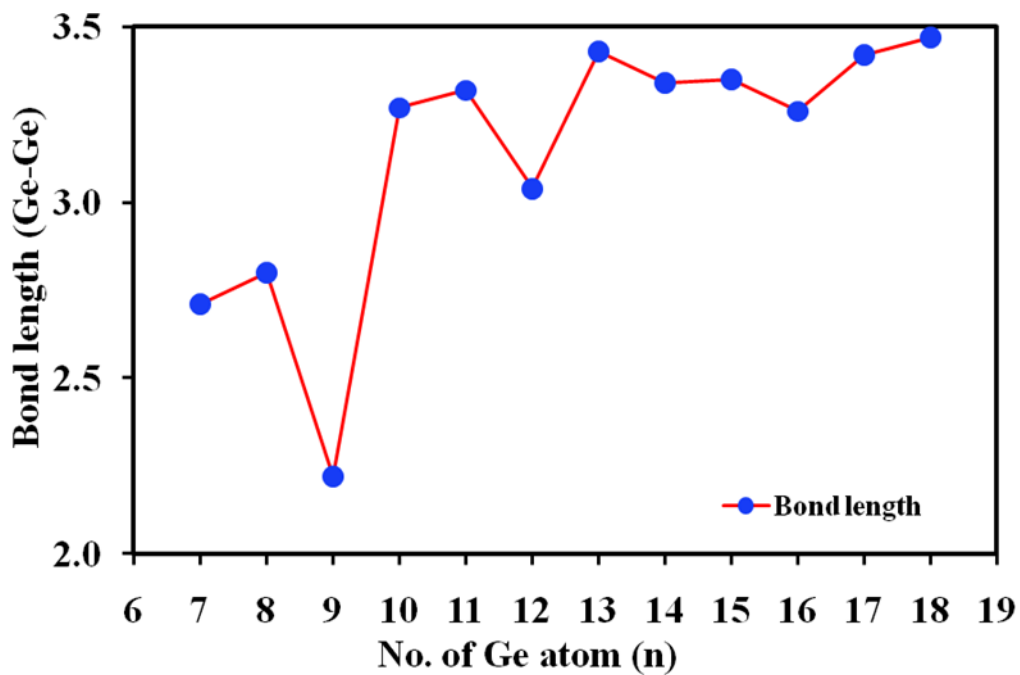


Fig. 4SIC IR and Raman spectra for NbGe_n (n = 10-15) ground states clusters.

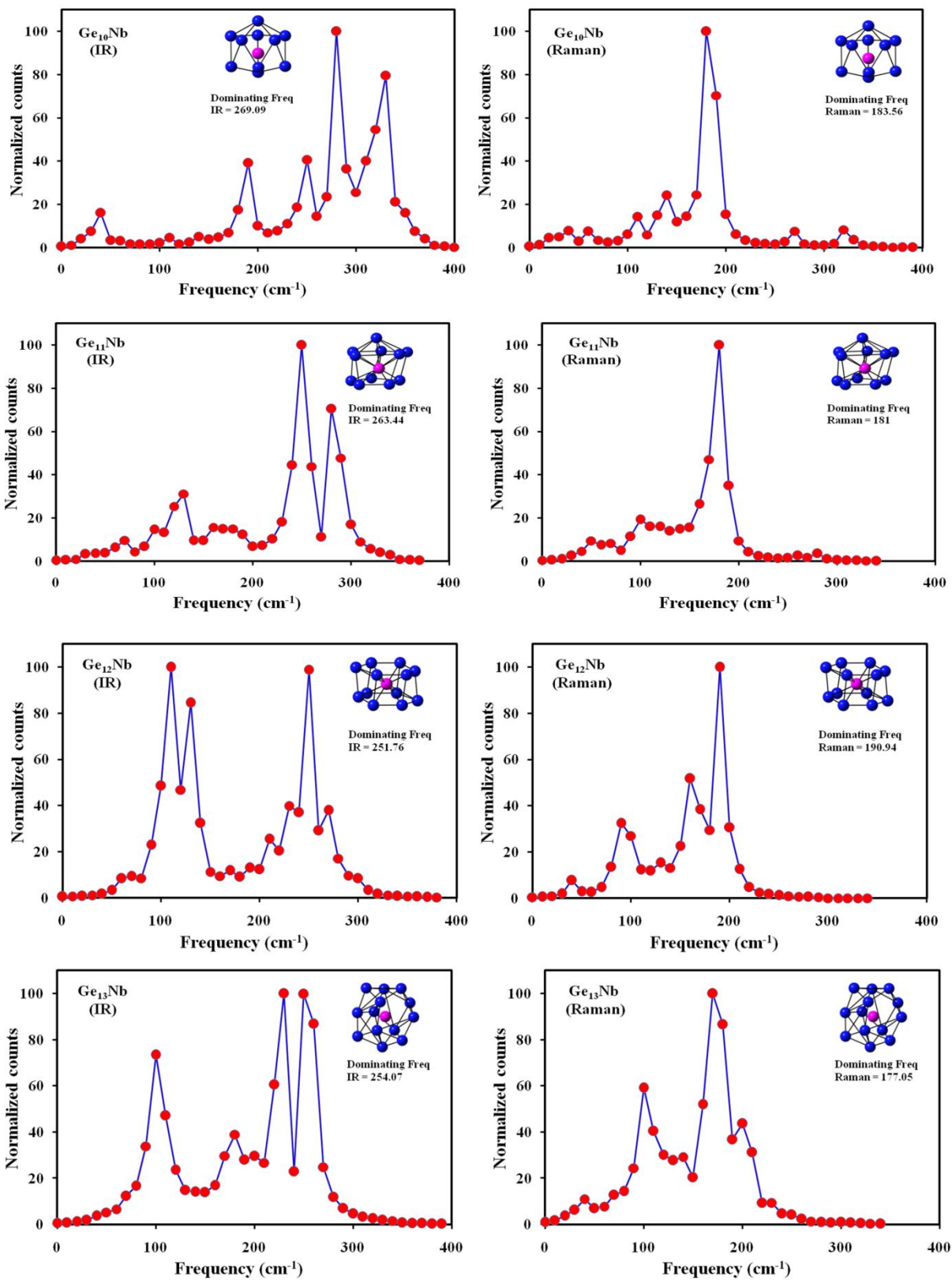
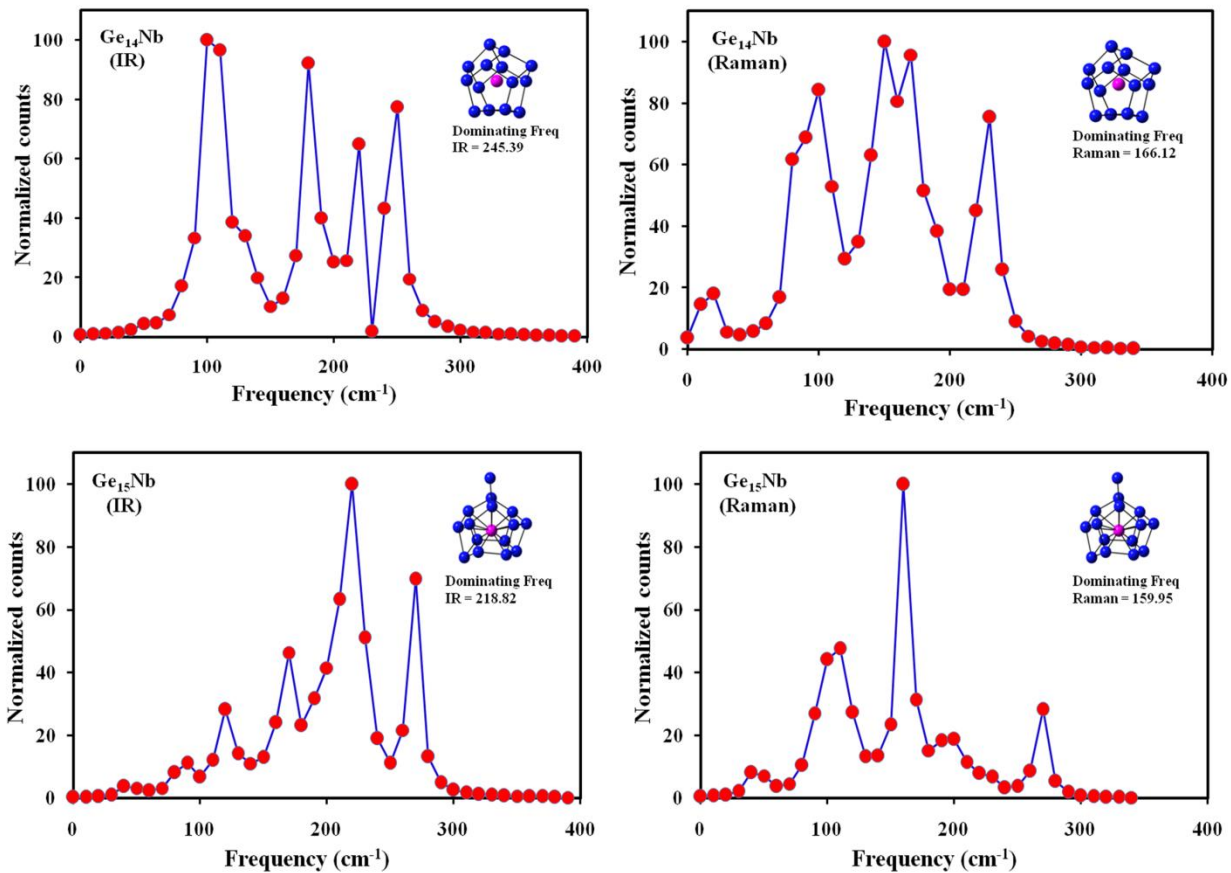


Fig. 4SIC Continue



APPENDIX C

LANL2DZdp ECP basis set for Germanium (Ge)	LANL2DZ ECP basis set for Molybdenum (Mo)
Ge 0 S 2 1.00 0.8935000 -2.1756591 0.4424000 2.4493467 S 1 1.00 0.1162000 1.0000000 P 2 1.00 1.8770000 -0.1006779 0.2623000 1.0306256 P 1 1.00 0.0798000 1.0000000 P 1 1.00 0.0209000 1.0000000 D 1 1.00 0.2460000 1.0000000 GE 0 GE-ECP 3 28 f-ul potential 5 1 318.2167583 -28.0000000 2 61.5370967 -180.9891676 2 13.2986899 -55.0043909 2 3.8985215 -19.7906526 2 1.2137666 -1.8533572 s-ul potential 5 0 205.1886932 3.0000000 1 68.9790278 65.2262558 2 27.9194879 225.2354522 2 8.5481650 94.0125472 2 2.3173734 29.9415005 p-ul potential 5 0 33.2488002 5.0000000 1 15.7777247 23.4778157 2 14.9260722 45.0980414 2 5.8416394 56.3326957 2 1.8349575 16.6058640 d-ul potential 5 0 42.0206343 3.0000000 1 19.2096363 23.7371518 2 9.4133917 56.4792249 2 3.3282907 25.8901835 2 0.8522331 3.0229836	Mo 0 S 3 1.00 2.3610000 -0.9121760 1.3090000 1.1477453 0.4500000 0.6097109 S 4 1.00 2.3610000 0.8139259 1.3090000 -1.1360084 0.4500000 -1.1611592 0.1681000 1.0064786 S 1 1.00 0.0423000 1.0000000 P 3 1.00 4.8950000 -0.0908258 1.0440000 0.7042899 0.3877000 0.3973179 P 2 1.00 0.4995000 -0.1081945 0.0780000 1.0368093 P 1 1.00 0.0247000 1.0000000 D 3 1.00 2.9930000 0.0527063 1.0630000 0.5003907 0.3721000 0.5794024 D 1 1.00 0.1178000 1.0000000 MO 0 MO-ECP 3 28 f-ul potential 5 0 537.9667807 -0.0469492 1 147.8982938 -20.2080084 2 45.7358898 -106.2116302 2 13.2911467 -41.8107368 2 4.7059961 -4.2054103 s-ul potential 3 0 110.2991760 2.8063717 1 23.2014645 44.5162012 2 5.3530131 82.7785227 p-ul potential 4 0 63.2901397 4.9420876 1 23.3315302 25.8604976 2 24.6759423 132.4708742 2 4.6493040 57.3149794 d-ul potential 5 0 104.4839977 3.0054591 1 66.2307245 26.3637851 2 39.1283176 183.3849199 2 13.1164437 98.4453068 2 3.6280263 22.4901377

LANL2DZ ECP basis set for Niobium (Nb)				LANL2DZ ECP basis set for Magnesium (Mg)			
Nb	0			Mg	0		
S	3	1.00		S	2	1.00	
		2.1820000	-0.8846144			0.7250000	-0.4058454
		1.2090000	1.1033775			0.1112000	1.1688704
		0.4165000	0.6298776	S	1	1.00	
S	4	1.00				0.0404000	1.0000000
		2.1820000	0.7790287	P	2	1.00	
		1.2090000	-1.0752788			1.2400000	-0.0749753
		0.4165000	-1.1506014			0.1346000	1.0178183
		0.1454000	0.9969155	P	1	1.00	
S	1	1.00				0.0422000	1.0000000
		0.0392000	1.0000000	MG	0		
P	3	1.00		MG-ECP	2	10	
		4.5190000	-0.0817303	d-ul potential			
		0.9406000	0.6995115	5			
		0.3492000	0.3980996	1	237.5484804		-10.0000000
P	2	1.00		2	47.7520367		-55.8993968
		0.4106000	-0.1212176	2	10.7837852		-20.1391957
		0.0752000	1.0480477	2	3.1992124		-7.0679107
P	1	1.00		2	1.0636953		-0.8133109
		0.0247000	1.0000000	s-ul potential			
D	3	1.00		5			
		3.4660000	0.0315983	0	348.3008631		3.0000000
		0.9938000	0.4834306	1	59.4680133		44.0075660
		0.3350000	0.6164893	2	19.0767582		107.3861344
D	1	1.00		2	5.2965613		35.8289088
		0.1024000	1.0000000	2	1.3867373		10.1143435
NB	0			p-ul potential			
NB-ECP	3	28		6			
f-ul potential				0	1256.8739085		5.0000000
5				1	189.8608839		117.1053672
0	342.9638405		-0.0447401	2	54.6949631		420.5972073
1	139.9308014		-20.0535100	2	13.8990137		107.6122959
2	43.3523405		-103.7244021	2	3.9597181		29.1002576
2	12.4448533		-41.0459165	2	1.2552787		7.0875570
2	4.3204837		-4.2046219				
s-ul potential							
3							
0	112.8630617		2.7964669				
1	22.9678676		42.8845786				
2	4.9340673		75.1876966				
p-ul potential							
4							
0	63.6801963		4.9461846				
1	23.0912429		24.8316376				
2	24.4283647		137.9183292				
2	4.2310090		50.9778471				
d-ul potential							
5							
0	99.3359636		3.0064059				
1	64.0586472		25.5347458				
2	37.0891011		178.9597452				
2	12.0708574		92.9577490				
2	3.1575323		18.4744256				

LANL2DZ ECP basis set for Cobalt (Co)				LANL2DZECP basis set for Rhodium (Rh)			
Co	0			Rh	0		
S	3	1.00		S	3	1.00	
		7.1760000	-0.3856734			2.6460000	-1.3554084
		2.0090000	0.7453116			1.7510000	1.6112233
		0.8055000	0.5091819			0.5713000	0.5893814
S	4	1.00		S	4	1.00	
		7.1760000	0.1736161			2.6460000	1.1472137
		2.0090000	-0.3970442			1.7510000	-1.4943525
		0.8055000	-0.4630622			0.5713000	-0.8589704
		0.1070000	1.0899654			0.1438000	1.0297241
S	1	1.00		S	1	1.00	
		0.0375000	1.0000000			0.0428000	1.0000000
P	3	1.00		P	3	1.00	
		21.3900000	-0.0480413			5.4400000	-0.0987699
		2.6500000	0.6222337			1.3290000	0.7433595
		0.8619000	0.4758042			0.4845000	0.3668462
P	1	1.00		P	2	1.00	
		0.0800000	1.0000000			0.6595000	-0.0838056
P	1	1.00				0.0869000	1.0244841
		0.0230000	1.0000000	P	1	1.00	
D	4	1.00				0.0257000	1.0000000
		39.2500000	0.0361541	D	3	1.00	
		10.7800000	0.1896744			3.6690000	0.0760059
		3.4960000	0.4524981			1.4230000	0.5158852
		1.0660000	0.5710427			0.5091000	0.5436585
D	1	1.00		D	1	1.00	
		0.2606000	1.0000000			0.1610000	1.0000000
CO	0			RH	0		
CO-ECP	2	10		RH-ECP	3	28	
d-ul potential				f-ul potential			
3				5			
1	434.1076104	-10.0000000		0	600.3243032	-0.0538958	
2	78.8402758	-66.7240276		1	157.6910176	-20.1316282	
2	19.6037749	-11.7192243		2	49.8841995	-105.3654121	
s-ul potential				2	15.5966895	-42.3274370	
4				2	5.5099296	-3.6654043	
0	151.2307582	3.0000000		s-ul potential			
1	169.6790026	20.1553110		5			
2	64.9909423	413.3762244		0	59.3442526	2.9753728	
2	12.5076287	133.8727705		1	83.7426061	25.1230306	
p-ul potential				2	18.4530248	626.0926145	
4				2	12.4194606	-812.2549385	
0	92.7319924	5.0000000		2	8.8172913	467.3729340	
1	121.1910183	6.1892353		p-ul potential			
2	48.6265909	326.3215919		5			
2	11.9966971	73.8788970		0	53.4309068	4.9537213	
				1	65.6671843	20.4871116	
				2	16.8369862	598.0120139	
				2	11.3042136	-718.4059028	
				2	8.0312444	382.8173151	
				d-ul potential			
				4			
				0	64.3993653	3.0279532	
				1	43.4625053	24.7526516	
				2	19.4020301	142.6844289	
				2	4.6879328	32.1406857	

Reference

EMSL basis set exchange: <https://bse.pnl.gov/bse/portal>

List of Publications

- Electronic structure and stabilities of Ni- doped germanium nanoclusters: A density functional modeling study, J Mol Model. 2013; 19; 1473-1488
- Magnetic behavior in Cr_2Ge_n ($n= 1-12$) clusters- A density functional investigation, AIP proceedings. 2014; 1591; 1498
- Study of electronic properties, stabilities and magnetic quenching of molybdenum-doped germanium clusters: A density functional investigation, RSC. 2014; 4; 64825-64834
- Hydrogen storage in small size Mg_nCo nanocluster- A density functional investigation, International journal of Hydrogen energy. 2015; 40; 12727-12735
- Role of NIC and shell closing model in the stability of neutral and cationic NbGe_n ($n = 7-18$) clusters :A density functional study **(To be communicated in RSC Advance)**
- Study of adsorption and dissociation pathway oh H_2 molecule on MgnRh ($n = 1-10$) clusters: A density functional investigation **(Communicated in Int. J. of Hydrogen energy)**

List of attended conferences and workshop

- Poster presentation in “international E – Workshop/Conference on Computational Condensed Matter Physics and Material Science (IWCCMP – 2015), ABV – IIITM, Gwalior” Oct. 18-22, 2015
- Oral presentation on " Research Scholar day 2015, BITS- Pilani, Pilani campus" on March 15, 2015
- Oral presentation on “Study of Magnetic Quenching and Aromatic nature of Mo doped germanium cluster – A density functional investigation at IUAC New Delhi during HPC workshop on March 11-13, 2015.
- Poster presentation in “International Conference on Current Trend in Condensed Matter Physcis” (CTCMP-2015), IOP, Bhubaneswar, Feb 19-22, 2015
- Present Oral presentation on Research Scholar day in BITS, Pilani, Pilani campus, March 23, 2014
- Attended “Workshop and Training on current Research trends in Condensed matter- Material Science”, BITS, Pilani, Pilani campus, March 7-8, 2014
- Attended " WORKSHOP ON HIGH PERFORMANCE COMPUTING, Inter University Accelerator Centre, New Delhi" during May 5-6, 2014
- Attended “International symposium on Science of Clusters, Nanoparticles and Nanoscale Materials (SOCNAM)”, Central university of Rajasthan and Virginia commonwealth university, USA, March 4-7, 2013
- Attended “International Conference and Workshop on Nanostructured Ceramics and other Nanomaterials (ICWNCN)”, University of Delhi, March 13-16, 2012

BIOGRAPHY OF THE SUPERVISOR

Professor Debashis Bandyopadhyay is an experimental and theoretical condensed matter physicist. He obtained his Ph.D. from Indian Institute of Technology (I.I.T), Kanpur in the field of experimental condensed matter physics in the year of 1997. After spending a couple of years in IIT Kanpur as post doctoral fellow he joined Emory University, Atlanta, USA for his second post doctoral work. There he worked on the study of reaction kinetics of several proteins at low-temperatures. Then returning to India, he joined the physics department of BITS, Pilani, Pilani campus. He has wide range of research experiences in several fields like low temperature physics, magnetism, industrial material, mineral processing, fuel, alloys phase diagram, reaction kinetics in biological systems etc. Currently his main research focus is DFT based study of magnetic metal nanoclusters, transition metal doped semiconductor nanoclusters, hydrogen storage materials and super atoms which are useful for several applications in recent technologies. He is the author of several research papers published in reputed international journals. At present he is professor in the department of physics in BITS Pilani, Pilani campus, and supervising two Ph.D. students.

BIOGRAPHY OF THE CANDIDATE

Mr. Ravi Kumar Trivedi is a full time research scholar in Department of Physics, BITS, Pilani since August 2011. He holds B.Sc. (Physics, Chemistry and Mathematics) from M. L. B. Government College, Nokha affiliated with M. G. S. University, Bikaner in the year 2006 and Masters Degree in Physics with specialization in laser and electronics in the year 2008 from Dungeer College, Bikaner affiliated with M. G. S. University Bikaner. Later he joined Poornima group of college as a lecturer in 2010. The area of his research are hybrid semiconductor nanoclusters specially germanium nanoclusters and hydrogen storage materials. He is currently pursuing Ph.D. from BITS-Pilani, Pilani campus in computational physics using Density functional study in small hybrid semiconductor nanocluster and hydrogen storage materials. He has published four papers in international journals and presented my work in eight national or international conferences in India.

Following basic grounding in Physics, the duration of his Doctoral work has provided him over five years of experience in computational modeling of nanoclusters, superatom and hydrogen storage materials. This has involved hands on training with DFT (Density Functional Theory) simulation technique using computational software like Gaussian' 03, 09 and VASP. Our work has merited publication in international journal of repute (RSC Advance, Int Journal of Hydrogen energy, AIP Proceedings, J Molecular Modeling).